

Higher-Order Gradient Continuum Analysis of Elastic Fibre-Reinforced Solid Subjected to Flexural and Tensile Loads

by

Seyed Ehsan Seyed Bolouri

A thesis submitted in partial fulfillment of the requirements for the degree of

Master of Science

Department of Mechanical Engineering

University of Alberta

© Seyed Ehsan Seyed Bolouri, 2020

Abstract

Composite is a multiphase material that is artificially made, as opposed to one that occurs or forms naturally. Many composite materials are composed of just two phases; one is termed the matrix, which is continuous and surrounds the other phase, often called the dispersed phase. Composites have endless applications in industries such as biomedical, automotive, and aerospace products. The most distinctive characteristic that made them popular among corporations and factories is that they can be designed to achieve the desired properties. It is worth mentioning that the main objective of obtaining the optimal design by various types of analysis and simulations is avoiding failure and damages subjected to the load and prevent indemnification and outrageous costs in industries.

Continuum mechanics is a universal tool that gained so much attention during recent years due to its ability to formulate mechanical responses of composites. It would eventually lead to a comprehensive analysis of matrix material subject to mechanical loads. In this thesis, a continuum-based model has been developed to predict the behavior of composite material subject to flexural and bias extension loads. Equilibrium equation has been augmented with the concept of incompressibility to start elastic solids analysis. Non-linear formulations, accounting by the second, and third-order gradient methods integrated by principles of virtual work and refined energy density function have been derived analytically. Numerical approaches such as linearization and finite element analysis consisting of higher-order Gateaux derivatives along the

fiber direction have been taken into account to solve the ordinary and partial differential equations.

The FEniCS project open-source finite element package is used to solve the corresponding systems of partial differential equations. Remarkably, The numerical results, such as deformation profiles and shear strain contours, demonstrate a reasonable agreement with the experimental results.

Preface

The materials in this thesis are part of the research project under the supervision of Professor Chun Il Kim.

Chapter 2 of this work has been published as Bolouri, S. E. S., Kim, C. I., Yang, S. (2019). Linear theory for the mechanics of third-gradient continua reinforced with fibers resistance to flexure. *Mathematics and Mechanics of Solids*, 25(4), 937–960. doi: 10.1177/1081286519893408

Chapter 3 of this work has been submitted to *Acta Mechanica* journal entitled "A model for the second strain gradient continua reinforced with extensible fibers in plane elastostatics".

Chapters 4 of this work is based on joint work with Suprabha Islam.

*“ To my dear parents, and sister **Elaheh, Morteza, and Niloofar**”
For their love, endless support, encouragement ,and sacrifices*

We all die. The goal isn't to live forever, the goal is to create something that will.

– Chuck Palahniuk

Acknowledgements

Firstly, I would like to express my very special gratitude to Professor Chun Il Kim for his support, patience, motivation, and in-depth knowledge. His guidance helped me in all the time of M.Sc. research.

Besides my advisor, I would like to thank my thesis committee: Professor Hyo-Jick Choi, Professor Zengtao Chen and Professor Mohtada Sadrzadeh.

Finally, I must express my special gratitude to my parents for providing me continuous encouragement during my graduate studies.

Contents

1	Introduction	1
1.1	Background on Composite Materials	1
1.2	Elastic and Hyperelastic Materials	3
1.3	Stress Measures	4
1.4	Higher-Order Gradient Analysis	6
	1.4.1 Cosserat Theory	8
	1.4.2 Higher-Order Gradient Theory Applications	9
1.5	Experimental Setup Details	11
1.6	Gist and Structure of Thesis	12
2	Linear theory for the mechanics of third-gradient continua reinforced with fibers resistance to flexure	15
2.1	Kinematics	15
2.2	Equilibrium	19
2.3	Boundary conditions	21
2.4	Linear Theory	24
2.5	Solution to the linearized problem	28
	2.5.1 Theoretical results obtained from the 3rd order gradient model	32
	2.5.2 Comparison between experimental results and theoretical predictions	40
2.6	Denouement	42
3	A model for the second strain gradient continua reinforced with extensible fibers in plane elastostatics	45
3.1	Kinematics	45
3.2	Equilibrium	49
3.3	Boundary conditions	52
3.4	Linear Theory	57
	3.4.1 Example: Neo-Hookean type materials	60
3.5	Solution to the linearized problem	61
	3.5.1 Theoretical predictions and experimental comparisons	65
3.6	Denouement	71
4	The second-order finite element analysis of hyper-elastic composites reinforced with fibers subjected to tensile loads	72
4.1	Kinematics	72
4.2	Equilibrium	74
4.3	Composite with exponential Fibre Potential	76
	4.3.1 Finite element analysis of the 4th order coupled PDE	78
4.4	Theoretical predictions and experimental comparisons	79
4.5	Denouement	87

5	Conclusion and Future works	89
5.1	Conclusion	89
5.2	Future Works	91
	References	92

List of Figures

1.1	Unidirectional cloth and bidirectional cloth	2
1.2	Quantities of stress measures	5
1.3	Defections of lipid membrane	7
1.4	Rate of changes in lengths/angles	8
1.5	Rate of changes in length	8
1.6	Distribution of the Cauchy stresses in a cylindrical cartilage	11
2.1	Schematic of the problem	28
2.2	Deformation profiles	31
2.3	Deformed configurations with respect to C/μ	31
2.4	Deformed configurations with respect to A/μ	32
2.5	Deformed configurations with respect to r/μ	33
2.6	Comparison with the existing results	33
2.7	Shear strain gradients with respect to \mathbf{r}	35
2.8	Shear angle contour with respect to \mathbf{r}	36
2.9	Shear angle contour with respect to \mathbf{r}	37
2.10	Shear angle contours with respect to \mathbf{r}	38
2.11	Comparison with the nonlinear solution (Shear angle zone)	39
2.12	Comparison with the nonlinear solution (Shear strain gradient)	39
2.13	Comparison with the CNC fiber composites bending test results	41
2.14	(a) is the three points bending experimental setup for Nylon-6 fiber neoprene rubber composite, and (b) is the numerical comparison with the Nylon-6 fiber neoprene rubber composite bending test results	43
2.15	Maximum error	43
2.16	Comparison with the nonlinear solution	44
3.1	Schematic of the problem	61
3.2	Deformation profiles with respect to the number of iterations N	65
3.3	Deformation mapping	66
3.4	Deformation configurations	66
3.5	Deformation configurations	67
3.6	Comparison with the second gradient model	68
3.7	Shear strain gradient	68
3.8	Shear angle contours	69
3.9	Shear strain gradients	70
3.10	Shear angle contours	70
3.11	Shear angle contours	70
4.1	Theoretical predictions	79
4.2	Deformation contour	80
4.3	Experimental results	80
4.4	Stress-strain	81

4.5	Stress-strain	82
4.6	Stress-strain	83
4.7	Stress-strain	84
4.8	Stress-strain	85
4.9	Stress-strain	85
4.10	Stress-strain	86
4.11	Stress-strain	87

Chapter 1

Introduction

1.1 Background on Composite Materials

In modern society, composites are widely used in daily life. From shower stalls to spacecrafts, composite materials are all around us [1], [2]. Composite structures consist of at least two components with entirely different properties [3]. The primary constituent materials are called matrix and reinforcement. The reinforcement component is generally stiffer and more durable to provide the necessary strength while the composite structure is under the load. The typical reinforcement material is in the form of fibers, which is normally made of glass, carbon, and boron. As a matter of fact, it adds tensile strength to the matrix material, which is designed to bear mostly compression and shear loads [4]. Additionally, the matrix material prevents the fibers from being degraded as a result of mechanical and chemical interactions. The main factors that determine the characteristics of the reinforcement component are geometry, volume, orientation, and packing arrangement [5]. Unidirectional and bidirectional structures are examples of different packing arrangements that are presented in Figure 1.1 [6].

Researchers have been trying to describe the behavior of composites under various types of loads within a wide range of boundary conditions [8], [9]. However, analytical solutions describing the behavior of composites subjected to extension and bending are very few. A mathematical framework integrated with continuum mechanics principles such as employing the virtual work statement and strain energy function to derive the deformation formula-

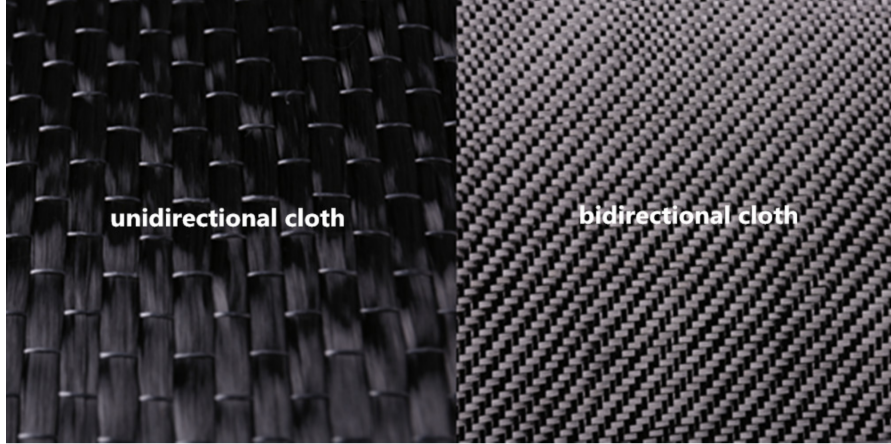


Figure 1.1: the difference between carbon fiber unidirectional cloth and bidirectional cloth [7]

tion is a reasonable approach that helps us anticipate what happens in different conditions and would help us design the structure in a way that satisfies our mechanical requirements [10]. Notably, primary continuum mechanics methods consider composites as anisotropic materials whose response function only depends on the first gradient of deformation [11], [12]. However, the classical theory consisting of only the first gradients of deformation is not always the best method to predict the mechanical response of the solids [13]–[15]. Indeed, Conventional models augmented with bulk incompressibility condition are often so constrained that demonstrate the deformation profile as a function determined only by the kinematics of the structure [16], [17]. Despite the limitations of classic models, the first gradient continuum models have been widely used due to the straightforwardness in the derivation of corresponding mathematical frameworks over the discretized domain [18]–[20].

Classification of composite materials have been tendered in literature at two different stages:

1. The first condition that is investigated is the matrix constituent material. Some of the popular types of matrix composites are encompass organic matrix composites (OMCs), and ceramic matrix composites (CMCs). It is worth noting that, composite materials that have carbon as the pri-

mary component in their chemical compound formula, such as polymer matrix composites (PMCs) are categorized as OMCs [21].

2. The second criterion is based on the reinforcement material. Fiber-reinforced composites (FRCs), and laminar composites are the main subcategories of this type of classification. The main discussion in this thesis is around the first subcategory, which continuous or discontinuous strings of fiber surround the matrix material. In such cases, the radius of fiber is far smaller than the fiber length, and they usually increase the matrix strength while experiencing the bending or twist moment [22], [23].

Fiber-reinforced composites are usually made by cross-linking cellulosic fiber molecules in the material matrix. This method of re-engineering the matrix material by adding a complementary component is very effective in increasing the durability and strength of the material [24]. It is notable that previously mentioned composites can be recycled up to 20 times [24], [25]. This capability decreases the price of production in industries and helps us to maintain the ecological balance. Continuity or discontinuity in the reinforcement phase of the composites is a critical property that determines the mechanical characteristics of the material. For instance, Discontinuous fiber composites are designed to be random in alignment, which significantly decreases their strength [26].

1.2 Elastic and Hyperelastic Materials

Different types of materials and their properties have been studied using continuum mechanics principals. For many cases, a linear relationship between stress and strain is not enough to accurately predict the mechanical behavior, and that is the point where hyperelasticity comes into play [27]. Neo-Hookean and Mooney-Rivlin solids are elastic and hyperelastic materials that have been used widely in continuum mechanics analysis [28], [29].

Neo-Hookean solid inherited its name from Hook's law and is designed

to model the non-linear behavior of stress-strain responses. Ronald Rivlin proposed this model in the 19th century to predict the deformation of plastics and rubber-like substances [30], [31]. It should be stressed that the Neo-Hookean model does not consider the waste of energy during deformation and assumes the perfect elasticity at all stages. It is usually used for small deformations (strains less than 20%) and does not show enough accuracy for large deformations [28], [32]. For compressible solids, the strain energy density function (1.3) is obtained with D_1 as the material constant. By substituting $J = 1$ into the energy equation, (1.1) is derived that is used for incompressible Neo-Hookean solids [33].

$$W = C_1(I_1 - 3) \quad (1.1)$$

$$I_1 = (\lambda_1)^2 + (\lambda_2)^2 + (\lambda_3)^2 \quad (1.2)$$

$$W = C_1(I_1 - 3 - 2 \ln J) + D_1(J - 1)^2; J = \det(\mathbf{F}) = \lambda_1 \lambda_2 \lambda_3 \quad (1.3)$$

In Mooney-Rivlin types of solids, the strain energy density function is presented as a linear combination of two invariants of Cauchy-Green deformation tensor [34]–[36]. It is notable that C_1 and C_2 are material constants, and \mathbf{F} is the deformation gradient tensor. The detailed formulation of Mooney-Rivlin continuum mechanics model is mentioned below:

$$W = C_1(I_1 - 3) + C_2(I_2 - 3) \quad (1.4)$$

$$I_1 = J^{(-2/3)}((\lambda_1)^2 + (\lambda_2)^2 + (\lambda_3)^2) \quad (1.5)$$

$$I_2 = J^{(-4/3)}((\lambda_1 \lambda_2)^2 + (\lambda_1 \lambda_3)^2 + (\lambda_2 \lambda_3)^2); J = \det(\mathbf{F}) = \lambda_1 \lambda_2 \lambda_3 \quad (1.6)$$

1.3 Stress Measures

There are several stress measures in continuum mechanics. Some of the most prominent ones are Cauchy stress tensor, the first, and the second Piola-Kirchhoff stress. They can be useful in different computational contexts. Many parameters are used in defining stress measures that can be found in Figure 1.2.

The Cauchy stress is a symmetric tensor and is defined on an element after deformation. In this formulation \mathbf{t} is the traction vector, \mathbf{n} is the outward normal to a surface, \mathbf{P} is the first Piola-Kirchhoff stress, \mathbf{S} is the second Piola-Kirchhoff stress, \mathbf{T} is the Biot stress, and $d\mathbf{f}$ corresponds to the force vector [37].

$$d\mathbf{f} = \mathbf{t}d\mathbf{T} = \boldsymbol{\sigma}^T \cdot \mathbf{n}d\mathbf{T} \quad (1.7)$$

The first Piola-Kirchhoff stress is an asymmetric tensor. It depends on the reference configuration in addition to the deformed shape. It can be defined as it is shown below:

$$d\mathbf{f} = \mathbf{t}d\mathbf{T} = \mathbf{N}^T \cdot \mathbf{n}_0 d\mathbf{T}_0 = \mathbf{P} \cdot \mathbf{n}_0 d\mathbf{T}_0 \quad (1.8)$$

The second Piola-Kirchhoff stress is defined in a way that is symmetric unlike the first Piola-Kirchhoff stress [28].

$$d\mathbf{f}_0 = \mathbf{S}^T \cdot \mathbf{n}_0 d\mathbf{T}_0 = \mathbf{F}^{-1} \cdot \mathbf{t}_0 d\mathbf{T}_0 \quad (1.9)$$

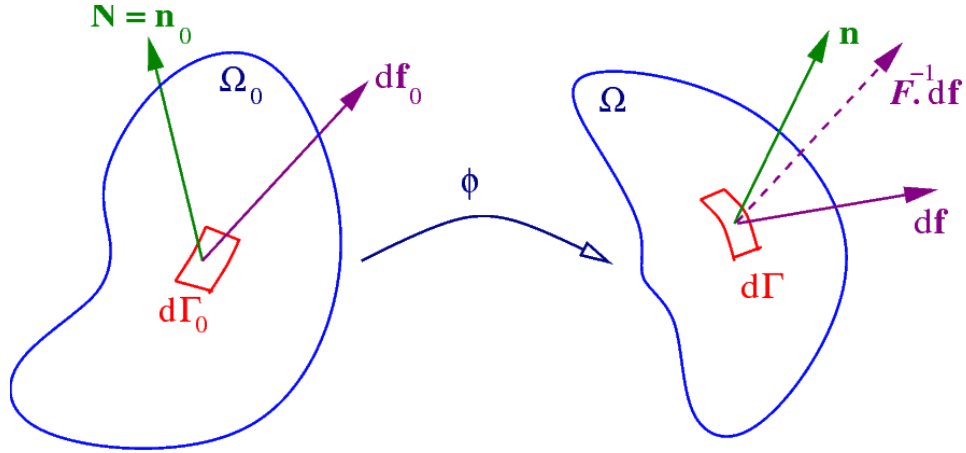


Figure 1.2: Quantities used in the definition of stress measures [38].

It is always essential to use appropriate stress and strain measures when a continuum mechanic problem is subjected to investigation. Consequently, we need to identify the natural reference before starting the analysis and make use of measures that cause conjugate pairing. Using this procedure, the expression for elastic potential is expressed. Mostly we are interested in the rate

of changing quantities for the material rather than their absolute value. Subsequently, the strain-stress measures, which possess an equal rate compared to the rate of deformation, are more appropriate for conventional use [39], [40].

1.4 Higher-Order Gradient Analysis

Continuum theory augmented with microstructural effects of fibers has begun receiving attention in the view of having more reliable estimations compared to the classical theories [8], [41], [42]. Some research projects have been designed to demonstrate the impact of higher-order terms on fracture and fatigue mechanics. As an illustration, some works have been done to provide an analytical model to delineate the failure behavior of very large atomic models of IGF in silicon nitride by adopting the principals of the granular microstructural mechanics and higher-order continuum [43]. Moreover, [44] presented a thorough model using higher-gradient terms to describe the damage evolution in dual-phase steels. They incorporated the rate of change in shear strain to show that strength and ductility of the material is not only the function of plastic strain localization, and material damage evolution plays a deterministic role as well. Lastly, it is worth mentioning that the higher-order gradient analysis is applicable to the continuum analysis of nano-beams [45], [46]. They utilized Euler–Bernoulli theory as the leading equation and correspondingly solved the obtained partial differential equations with the help of numerical approaches such as finite element analysis. Static, buckling, and dynamic responses of nano-beams have been presented in the previously mentioned paper.

Continuum mechanics analysis of fiber-reinforced materials considering the second gradient of deformation to derive the corresponding partial differential equations is the subject of discussion in [9], [47], [48]. The authors of aforementioned papers successfully derived a comprehensive formulation to describe the mechanical behavior of composites and obtained smooth shear strain contours. Recent studies on lipid membranes' morphology with intra-membrane viscous flows indicate the effects of non-linearity followed by the second-order gradient terms the obtain a complete solution [49]–[51]. These ideas seem necessary

and practical to achieve a decent accuracy in biomechanics and mechanics of composites. In detail, the equilibrium state of the purely elastic surface is the base-line to derive the corresponding equations. Additionally, the straining effects of the fluid were accommodated by taking the rate of different properties with respect to time. Finally, the augmentation of linearization and partial differential equations solving algorithms would result in membrane shape evolutions in the presence of intra-membrane and similar deflection contours that can be seen in Figure 1.3.

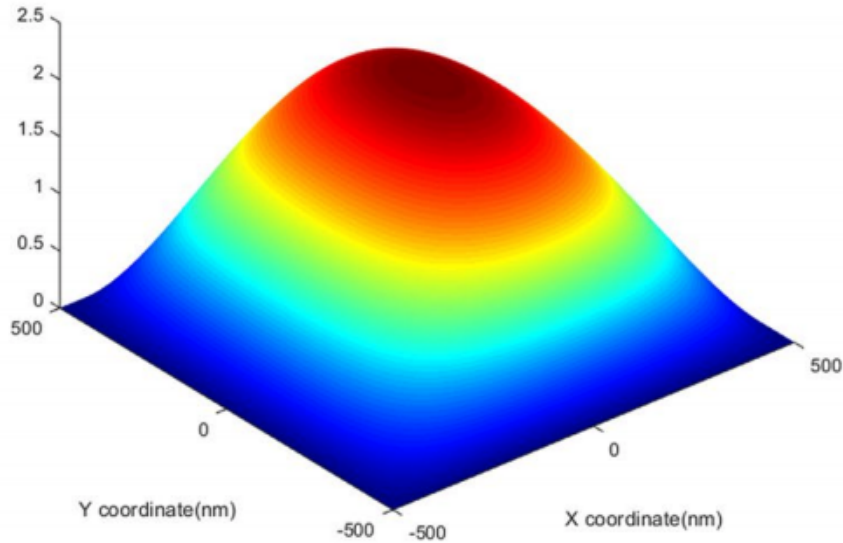


Figure 1.3: Deflections of lipid membrane with respect to intra-membrane viscous flows considering higher-order gradients. [51].

Investigating fiber composites incorporating the effects of bending and tensile resistance of continua that is resulted by microstructure entanglement would cause the higher-order gradients of deformation to appear in the formulations. The previously mentioned analysis can be framed in a mathematical space by integrating non-linear terms into the partial differential equations. It should be emphasized that the computation of gradients of deformation is based on the assumption of having continuous curves along the structure that are depicted in the Cartesian coordinate system [52]. Figure 1.4 and Figure 1.5 are good illustrations of how the first-order and higher-order gradient meth-

ods differ. The relative rotation is considered to be an additional property of the material compared to traditional approaches that significantly affect the shear-strain relation.

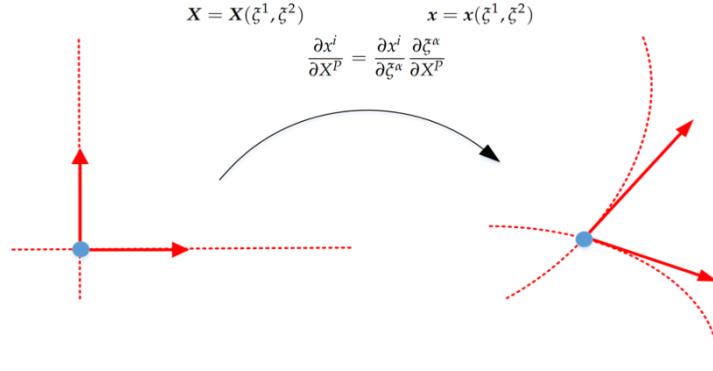


Figure 1.4: Rate of changes in lengths/angles via the first gradient [53].

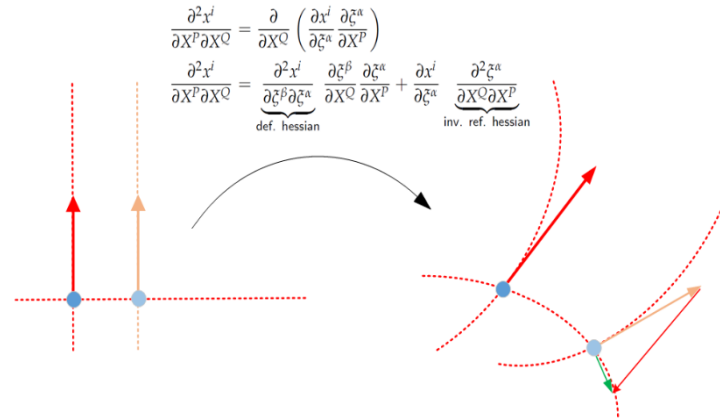


Figure 1.5: Rate of changes in length via the second gradient [53].

1.4.1 Cosserat Theory

The Cosserat theory is a famous micropolar elasticity analysis that, unlike the classical interpretation, takes the local rotation of points into account. The idea of couple stress can be considered as the foundation of this higher-order theory. Cosserat brothers have initiated the early stage of using micro-inertia in modern continuum mechanics [54], [55].

In contrast to two elastic coefficients for materials in the classical continuum mechanics, micropolar elasticity assumes four more constants to investigate the effects of rotation and nonlocality. By adopting micropolar continuum mechanics, strain gradient and other internal properties are affected in composite materials. For instance, the stress concentration factor around the hole or crack in the material is less than classical values. Additionally, in wave propagation analysis, the pace of dilational waves in the Cosserat medium is independent of frequency [56]–[58].

The Cosserat continuum has the equilibrium equations that are mentioned below:

$$\sigma_{ji,j} = 0 \quad (1.10)$$

$$\mu_{ji,j} + \varepsilon_{ijk}\sigma_{jk} = 0; i, j = 1, 2, 3 \quad (1.11)$$

$$\sigma_{ji} = (\mu + \alpha)\gamma_{ji} + (\mu - \alpha)\gamma_{ij} + \lambda\gamma_{kk} \quad (1.12)$$

$$\mu_{ji} = (\gamma + \varepsilon)\kappa_{ji} + (\gamma - \varepsilon)\kappa_{ij} + \beta\kappa_{kk} \quad (1.13)$$

σ_{ij}, μ_{ij} , and ε_{ijk} are stress, moment stress, and the altering tensor [59].

1.4.2 Higher-Order Gradient Theory Applications

Continuum mechanics theories play vital roles in the analysis of solid materials. Detailed and accurate investigation of solid materials is needed in every industry to design most expertly and avoid outrageous costs of maintenance and replacements. Currently, the number of analytical solutions for predicting the response of composite subjected to different types of boundary conditions such as bending and twist is limited. Consequently, numerical approaches augmented with higher-order gradients are commonly stable and precise alternatives that would help industries achieve their desired output. Higher-order gradient analysis is a practical approach in fiber-reinforced composites, biomedical engineering, and crack and fracture analysis [60], [61].

1. Fiber-reinforced composites:

Authors in [9], [47], [48] investigated the effects of second-order terms in shear strain and deformation contour. The corresponding results are

used to design composite materials based on the necessary mechanical expectations. Their numerical methods are fast and stable, which would generate the desired results in the global composite materials market. The composites market, including materials and products, is worth approximately 30 billion dollars in the US as the second-largest market after China [62], [63]. It is worth mentioning that the growing popularity and considerable demands of fiber-reinforced composites have been resulted from low maintenance costs and high durability [64].

2. Tissues in the Human Body:

The human body can be categorized at different levels at scales such as cellular, tissue, and organ levels [65]. The nature of living tissues in the body is so complicated that finding a general formulation to model the mechanical behavior of these structures seems to be very difficult. Considering tissue structures as composites with continuous fibers is a novel idea that is implemented in [66], [67]. In point of fact, the previously mentioned authors superposed the effects of matrix material and statistically oriented fibers to generate a model to describe what happens to biological tissues when they are subjected to mechanical loads. A good illustration of higher-order Cauchy stresses in a cylindrical cartilage is presented in Figure 1.6.

3. Crack and fracture:

Mechanics of fracture and fatigue is a branch that focuses on the propagation of the crack in the solid material [68]. It evaluates the force on the critical points of the structure by utilizing continuum mechanics principals. Classical models fail in some particular cases when mathematical models become ill-posed in accumulated damages [69]. For instance, it has been shown that cracks are one of the main reasons for failure in vehicles [70]. Analyzing the corresponding failures show that cracks undergo an oscillatory instability controlled by elastic nonlinearity [69], [71]. Moreover, regarding the damage analysis, we can mention the works of

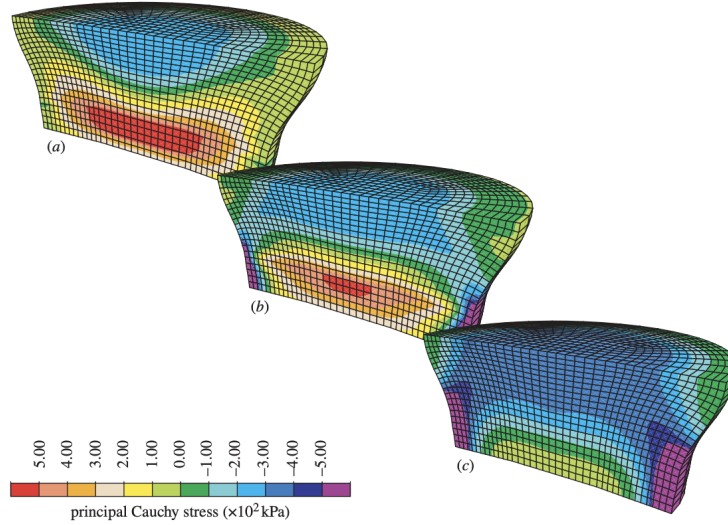


Figure 1.6: Distribution of the (a) first, (b) second and (c) third principal Cauchy stresses in a cylindrical cartilage specimen under unconfined compression [66].

authors in [72] introduced a gradient-enhanced damage model to improve the predictions of the traditional model.

1.5 Experimental Setup Details

In this thesis, two types of experimental tests have been designed to validate the numerical results. To check the quality and the accuracy of analytical and numerical results for the tensile stress, the bias-extension test was done. In fact, the composite sample has been placed between two jaws. One of them was completely fixed, and the other one was moving with the pace of 10mm/min. The X and Y coordinates of the moving jaw have been recorded in a data sheet. Moreover, a three-point bending test was arranged to compare the experimental outcome with the results obtained from the third-order gradient model for the flexural load. The sample has been located between two fixed stands, and the compressive load has been placed in the middle of the sample. The mechanical load gradually produced deformation, and the X, Y coordinates of the moving end were filed. Some details regarding the properties of the corresponding composite materials are mentioned in Table

Table 1.1: Material Properties.

Material	C	μ
Crystalline Nanocellulose (CNC)	150GPa	1GPa
Nylon-6 Fiber Neoprene Rubber Composite	2000MPa	1MPa

Table 1.2: Constituent Materials.

Material	Fiber Percentage	Matrix percentage
nylon/spandex (NSP-8020)	80	20
nylon/spandex (NSP-8515)	85	15

1.1, and Table 1.2.

It is worth mentioning that NSP-8020 and NSP-8515 composites are fabricated in a three-layer procedure. In the first step, Ecoex 0050 elastomer is produced by mixing two components (a base and curing agent) with an equal ratio. Then entrapped bubbles are removed using a vacuum chamber. In the second step, the second layer of fibers is placed on the first layer. Next, gaps between pores are filled using a small amount of elastomer, and the surface is flattened. Lastly, a proper amount of elastomer is poured over the second layer and placed into the film applicator rod to obtain the hyper-elastic composite.

1.6 Gist and Structure of Thesis

This thesis consists of 5 main chapters, including the introduction and the overall conclusion. The primary objective is to investigate the behavior of composite materials subject to mechanical loads such as tensile and flexural forces.

In addition to the introduction, the next two chapters are third-order analysis of reinforced composite material with unidirectional fibers under the flexural and tensile loads. They start with basic formulations of continuum mechanics followed by the bending and tensile energy of fibers introduced by Spencer and Soldatos. As the next step, the Euler equilibrium equation has been taken

into account to complete the analysis and derive the corresponding Piola stress equation. Linearization is also a necessary step to reduce the complexity of the equations. Neo-Hookean type of materials with small deformations are investigated in the following chapters. To find the solutions to the linearized formulations, I have implemented various approaches such as change of variables, separation of variables, and method of characteristics. The analytical solution is derived as a result of the analysis and can be applied to real-world problems by imposing the appropriate boundary conditions. The final results are assessed with the help of a dataset that was collected from the experimental set. The comparison shows us a perfect match between predictions from the model and the experimental data. The results that have been investigated in the previously mentioned chapters are categorized into two different classes. The first class mostly depends on the deformation profile to explain the properties of composite material. Changing the material parameters such as C and E and investigating the effect of these parameters on the deformation contour is the first step in the following analysis. The second step is experimenting with the material's intrinsic properties, such as shear angle and shear strain contours. Augmenting these two aspects give us a comprehensive view regarding the mechanical response expected from the material under the load.

In chapter four, the second-order terms and exponential strain energy function are considered to be investigated, and the procedure is the same to obtain the partial differential equations through using Euler equilibrium formulations and continuum mechanics fundamental concepts. However, the idea of solving the corresponding system of PDE is using the finite element method instead of analytical methods. I used the Galerkin method and integration by parts to derive the weak form that can be analyzed by FEM packages. The Newton non-linear solver solves the system of non-linear partial differential equations and provides us the deformation and shear strain contour. It should be stressed that the most crucial factor that has been analyzed in the fourth chapter is the strain-energy function. In fact, hyperelastic materials can be delineated with the exponential form of the strain energy equation. By having this assumption, the corresponding equation for the finite element analysis was obtained.

The outcome of this numerical approach has been compared with the experimental data collected from NSP-8020 and NSP-8515 tensile tests. Finally, a reasonable agreement has been observed in such hyperelastic cases and the numerical model using the exponential form of the strain energy function.

The conclusion chapter is a wrap-up of all three previous approaches to describe the behavior of fiber-reinforced composite materials. It states the results and the possible future works that can be done in this regard to make the analysis more comprehensive and practical.

Throughout the thesis, we use standard notation such as \mathbf{A}^T , \mathbf{A}^{-1} , \mathbf{A}^* and $tr(\mathbf{A})$. These are the transpose, the inverse, the cofactor and the trace of a tensor \mathbf{A} , respectively. The tensor product of vectors is indicated by interposing the symbol \otimes , and the Euclidian inner product of tensors \mathbf{A} , \mathbf{B} is defined by $\mathbf{A} \cdot \mathbf{B} = tr(\mathbf{A}\mathbf{B}^T)$; the associated norm is $|\mathbf{A}| = \sqrt{\mathbf{A} \cdot \mathbf{A}}$. The symbol $|\ast|$ is also used to denote the usual Euclidian norm of three-vectors. Latin and Greek indices take values in $\{1, 2\}$ and, when repeated, are summed over their ranges. Lastly, the notation $F_{\mathbf{A}}$ stands for the tensor-valued derivatives of a scalar-valued function $F(\mathbf{A})$.

Chapter 2

Linear theory for the mechanics of third-gradient continua reinforced with fibers resistance to flexure

2.1 Kinematics

Let \mathbf{D} denote the unit tangent to the fiber's trajectory so that the orientation of a particular fiber can be written as

$$\lambda = |\mathbf{d}| = \frac{ds}{dS} \text{ and } \boldsymbol{\tau} = \lambda^{-1}\mathbf{d}, \quad (2.1)$$

where

$$\mathbf{d} = \mathbf{F}\mathbf{D}. \quad (2.2)$$

Here, \mathbf{F} is the first gradient of the deformation function ($\chi(\mathbf{X})$) and \mathbf{d} is the unit tangent to the fiber trajectory in the current configuration. Eq. (2.2) can be derived by taking the derivative of $\mathbf{r}(S) = \chi(\mathbf{X}(S))$, upon making the identifications $\mathbf{D} = d\mathbf{X}(S)/dS$ and $\mathbf{d} = d\mathbf{r}(s)/ds$. Thus, from Eq. (2.2), the geodesic curvature of an arc ($\mathbf{r}(S)$) is obtained by

$$\mathbf{g} = \frac{d^2\mathbf{r}(s)}{ds^2} = \frac{d\left(\frac{d\mathbf{r}(s)}{ds}\right)}{dS} = \frac{\partial(\mathbf{F}\mathbf{D})}{\partial\mathbf{X}} \frac{d\mathbf{X}}{dS} = \nabla[\mathbf{F}\mathbf{D}]\mathbf{D}. \quad (2.3)$$

In the present study, we consider the cases of initially straight fibers such that

$$\nabla\mathbf{D} = \mathbf{0}, \quad (2.4)$$

and thereby reduce Eq. (2.3) to

$$\mathbf{g}(\mathbf{G}) = \mathbf{G}(\mathbf{D} \otimes \mathbf{D}), \quad (2.5)$$

where we adopt the conventions of the second gradient of deformations (see, also, [47], [73] and [74])

$$\nabla \mathbf{F} \equiv \mathbf{G}. \quad (2.6)$$

Further, the compatibility condition of \mathbf{G} are given by

$$G_{iAB} = F_{iA,B} = F_{iB,A} = G_{iBA}. \quad (2.7)$$

Based on the above kinematical settings, the authors in [41] proposed that the bending energy of fibers is accounted for by the second gradient of the continuum deformation explicitly such that

$$\widehat{W}(\mathbf{F}) + W(\mathbf{G}) = W(I, \mathbf{g}), \quad W(\mathbf{G}) \equiv \frac{1}{2} C(\mathbf{F}) |\mathbf{g}|^2, \quad (2.8)$$

where $C(\mathbf{F})$ refers to the material properties of fibers and I is the first invariant of the deformation gradient tensor \mathbf{F} , respectively. Also, in general, $C(\mathbf{F})$ is independent of the deformation gradient (i.e. $C(\mathbf{F}) = C$). The above energy density form (Eq. 2.8) has been widely and successfully adopted in the relevant studies (see, for example, [47], [73], [74], [75], and [76]). Within the framework of [41], the following form of the higher-gradient energy function may be considered to achieve a more comprehensive description of the mechanics of the fiber-reinforced composite;

$$\begin{aligned} \widehat{W}(\mathbf{F}) + W(\mathbf{G}) + W(\mathbf{H}) &= W(I, \mathbf{g}, \boldsymbol{\alpha}), \\ W(\mathbf{G}) &\equiv \frac{1}{2} C(\mathbf{F}) |\mathbf{g}|^2, \quad W(\mathbf{H}) \equiv \frac{1}{2} A(\mathbf{F}) |\boldsymbol{\alpha}|^2. \end{aligned} \quad (2.9)$$

In the above, $\boldsymbol{\alpha}$ is designated to accommodate the rate of change in curvature computed at points on the convected curves of fibers as

$$\begin{aligned} \boldsymbol{\alpha} &= \frac{d^3 \mathbf{r}(s)}{ds^3} = \frac{d(\nabla[\mathbf{F}\mathbf{D}]\mathbf{D})}{dS} = \frac{\partial(\nabla[\mathbf{F}\mathbf{D}]\mathbf{D})}{\partial \mathbf{X}} \frac{d\mathbf{X}}{dS} = [\nabla\{\nabla[\mathbf{F}\mathbf{D}]\mathbf{D}\}]\mathbf{D} \\ &= [\nabla\{\nabla[\mathbf{F}\mathbf{D}]\}\mathbf{D} + \nabla[\mathbf{F}\mathbf{D}](\nabla\mathbf{D})]\mathbf{D}. \end{aligned} \quad (2.10)$$

Eq. (2.10) can be further simplified similarly as in Eqs. (2.3)-(2.5) so that

$$\begin{aligned}\boldsymbol{\alpha} &= \nabla(\nabla\mathbf{F})(\mathbf{D} \otimes \mathbf{D} \otimes \mathbf{D}), \\ \nabla(\nabla\mathbf{F}) &= \nabla(\mathbf{G}) \equiv \mathbf{H}, \text{ and} \\ \boldsymbol{\alpha} &= \mathbf{H}(\mathbf{D} \otimes \mathbf{D} \otimes \mathbf{D}) = \boldsymbol{\alpha}(\mathbf{H}, \mathbf{D}),\end{aligned}\tag{2.11}$$

in which we denote \mathbf{H} as the third gradient of deformation; i.e.

$$\nabla\mathbf{G} = \mathbf{H}.\tag{2.12}$$

The phenomenological implications of Eq. (2.9) will be discussed in later sections through selected examples and experiments. In this section, we focus on the mathematical framework and the associated formulations, which will be used in the derivation of a compatible linearized model. Also, in the foregoing analysis, the parameter A is assumed to be independent of the deformation gradient (i.e. $A(\mathbf{F}) = A$), similar to the second gradient parameter. For use in the formulation of the Euler equation, we continue by evaluating the induced energy variation of the response function with respect to I , \mathbf{g} , and $\boldsymbol{\alpha}$ as

$$\dot{W}(I, \mathbf{g}, \boldsymbol{\alpha}) = W_I \cdot \dot{I} + W_{\mathbf{g}} \cdot \dot{\mathbf{g}} + W_{\boldsymbol{\alpha}} \cdot \dot{\boldsymbol{\alpha}},\tag{2.13}$$

where the superposed dot refers to the derivatives with respect to a parameter ϵ at a fixed value (e.g. $\epsilon = 0$ at equilibrium) that labels a one-parameter family of deformations. In particular, the variational derivatives of $W(\mathbf{G})$ and $W(\mathbf{H})$ in the sense of [41] (see, Eq. (2.9)) yield

$$\dot{W}(\mathbf{G}) = C\mathbf{g} \cdot \dot{\mathbf{g}} \text{ and } \dot{W}(\mathbf{H}) = A\boldsymbol{\alpha} \cdot \dot{\boldsymbol{\alpha}}.\tag{2.14}$$

Also, \dot{I} can be equated as

$$\dot{I} = [\text{tr}(\mathbf{F}^T\mathbf{F})] \dot{=} (\mathbf{I} \cdot \mathbf{F}^T\dot{\mathbf{F}}) = \mathbf{I} \cdot (\dot{\mathbf{F}}^T\mathbf{F}) = 2\mathbf{F} \cdot \dot{\mathbf{F}}.\tag{2.15}$$

Now, taking derivatives of Eqs. (2.5) and (2.11)₃ with respect to ϵ (e.g. $\dot{\mathbf{g}} = \dot{\mathbf{G}}(\mathbf{D} \otimes \mathbf{D})$), and substituting them into Eq. (2.14), we find

$$\begin{aligned}\dot{W}(\mathbf{H}) &= A\boldsymbol{\alpha} \cdot \dot{\boldsymbol{\alpha}} = A\alpha_j \mathbf{e}_j \cdot \dot{H}_{iABC} D_A D_B D_C \mathbf{e}_i = A\alpha_i \dot{H}_{iABC} D_A D_B D_C \\ \dot{W}(\mathbf{G}) &= C\mathbf{g} \cdot \dot{\mathbf{g}} = Cg_j \mathbf{e}_j \cdot \dot{G}_{iAB} D_A D_B \mathbf{e}_i = Cg_i \dot{G}_{iAB} D_A D_B\end{aligned}\tag{2.16}$$

Whereas D_A, D_B , and D_C stand for fiber trajectory in different directions. The above are also equivalent to

$$\begin{aligned}
\dot{W}(\mathbf{H}) &= W_{\mathbf{H}} \cdot \dot{\mathbf{H}} = W_{H_{iABC}} (\mathbf{e}_i \otimes \mathbf{E}_A \otimes \mathbf{E}_B \otimes \mathbf{E}_C) \dot{H}_{jDEF} (\mathbf{e}_j \otimes \mathbf{E}_D \otimes \mathbf{E}_E \otimes \mathbf{E}_F) \\
&= W_{H_{iABC}} \dot{H}_{iABC}, \text{ and} \\
\dot{W}(\mathbf{G}) &= W_{\mathbf{G}} \cdot \dot{\mathbf{G}} = W_{G_{iAB}} (\mathbf{e}_i \otimes \mathbf{E}_A \otimes \mathbf{E}_B \otimes) \dot{G}_{jCD} (\mathbf{e}_j \otimes \mathbf{E}_C \otimes \mathbf{E}_D) \\
&= W_{G_{iAB}} \dot{G}_{iAB}
\end{aligned} \tag{2.17}$$

It should be noted that A, B, C, D, E, and F were taken into account to imply Einstein summation notation. Therefore, by comparing Eqs. (2.16)-(2.17) we have

$$\begin{aligned}
\frac{\partial W}{\partial G_{iAB}} &= C g_i D_A D_B \text{ and } \frac{\partial W}{\partial H_{iABC}} = A \alpha_i D_A D_B D_C \\
\leftrightarrow & W_{\mathbf{G}} = C \mathbf{g} \otimes \mathbf{D} \otimes \mathbf{D}, \text{ and } W_{\mathbf{H}} = A \boldsymbol{\alpha} \otimes \mathbf{D} \otimes \mathbf{D} \otimes \mathbf{D}.
\end{aligned} \tag{2.18}$$

In a typical environment, volumetric changes in the materials' deformations are energetically expensive processes (see, also, [28]-[77]). Thus, to reflect the condition of bulk incompressibility, the energy density function Eq. (2.9) is augmented by

$$U(I, \mathbf{g}, \boldsymbol{\alpha}, p) = W(I, \mathbf{g}, \boldsymbol{\alpha}) - p(J - 1), \tag{2.19}$$

where J is determinant of \mathbf{F} and p is a Lagrange-multiplied field. Lastly, by using the identity $\dot{J} = J_{\mathbf{F}} \cdot \dot{\mathbf{F}} = \mathbf{F}^* \cdot \dot{\mathbf{F}}$, together with the results in Eqs. (2.16-2.18), the variational derivative of the above can be formulated as

$$\dot{U} = (2W_I \mathbf{F} - p \mathbf{F}^*) \cdot \dot{\mathbf{F}} + W_{\mathbf{G}} \cdot \dot{\mathbf{G}} + W_{\mathbf{H}} \cdot \dot{\mathbf{H}}, \tag{2.20}$$

or, equivalently,

$$\dot{U} = (2W_I F_{iA} - p F_{iA}^*) \dot{F}_{iA} + W_{G_{iAB}} \dot{G}_{iAB} + W_{H_{iABC}} \dot{H}_{iABC}. \tag{2.21}$$

Clearly, the obtained variational form (2.21) is dependent on both the second and third gradient of deformations, as intended (i.e. $\dot{U} = \dot{U}(\mathbf{F}, \mathbf{G}, \mathbf{H}, p)$).

2.2 Equilibrium

The derivation of the Euler equation and boundary conditions arising in second-gradient elasticity are well-established (see, for example, [52]-[78] and [79] and references therein). These authors formulate the weak form of the equilibrium equations by employing the principles of the virtual work statement,

$$\dot{E} = P, \quad (2.22)$$

where P is the virtual work of the applied load and the superposed dot refers to the variational and/or Gateaux derivative. In this section, by means of iterated integrations by parts [80]-[82], we present the derivation of the Euler equilibrium equations, which will be used to obtain a linear model.

To begin with, the strain energy of the system can be expressed as

$$E = \int_{\Omega} U(\mathbf{F}, \mathbf{G}, \mathbf{H}, p) dA, \quad (2.23)$$

where Ω is the domain occupied by a fiber-matrix material. We note that the conservative loads are characterized by the existence of a potential L such that $P = \dot{L}$. In the present cases, the problem of determining equilibrium deformations of a fiber subjected to a flexural force at the boundaries is then reduced to the problem of minimizing the potential energy $E - L$. Hence we find

$$\dot{E} = \int_{\Omega} \dot{U}(\mathbf{F}, \mathbf{G}, \mathbf{H}, p) dA. \quad (2.24)$$

Also, in view of Eq. (2.17), we rewrite the energy variations with respect to the second and third gradient of deformation (i.e. \mathbf{G} and \mathbf{H}) as

$$\begin{aligned} \frac{\partial W}{\partial G_{iAB}} \dot{G}_{iAB} &= \frac{\partial W}{\partial G_{iAB}} u_{i,AB} \text{ and} \\ \frac{\partial W}{\partial H_{iABC}} \dot{H}_{iABC} &= \frac{\partial W}{\partial H_{iABC}} u_{i,ABC}, \end{aligned} \quad (2.25)$$

where $u_i = \dot{\chi}_i$ denotes the variation of the position field $\boldsymbol{\chi}(\mathbf{X})$. Now, by applying integration by parts, Eq. (2.25) becomes

$$\begin{aligned} \frac{\partial W}{\partial G_{iAB}} u_{i,AB} &= \left(\frac{\partial W}{\partial G_{iAB}} u_{i,A} \right)_{,B} - \left(\frac{\partial W}{\partial G_{iAB}} \right)_{,B} u_{i,A} \text{ and} \\ \frac{\partial W}{\partial H_{iABC}} u_{i,ABC} &= \left(\frac{\partial W}{\partial H_{iABC}} u_{i,AB} \right)_{,C} - \left(\frac{\partial W}{\partial H_{iABC}} \right)_{,C} u_{i,AB}. \end{aligned} \quad (2.26)$$

We then substitute Eqs. (2.21) and (2.26) into Eq. (2.24) and thereby obtain

$$\begin{aligned} \dot{E} &= \int_{\Omega} [(2W_I F_{iA} - pF_{iA}^*) \cdot \dot{F}_{iA} + \left(\frac{\partial W}{\partial G_{iAB}} u_{i,A} \right)_{,B} - \left(\frac{\partial W}{\partial G_{iAB}} \right)_{,B} u_{i,A} \\ &\quad + \left(\frac{\partial W}{\partial H_{iABC}} u_{i,AB} \right)_{,C} - \left(\frac{\partial W}{\partial H_{iABC}} \right)_{,C} u_{i,AB}] dA. \end{aligned} \quad (2.27)$$

The above further reduces to

$$\begin{aligned} \dot{E} &= \int_{\Omega} [2W_I F_{iA} - pF_{iA}^* - \left(\frac{\partial W}{\partial G_{iAB}} \right)_{,B}] u_{i,A} dA - \int_{\Omega} \left(\frac{\partial W}{\partial H_{iABC}} \right)_{,C} u_{i,AB} dA \\ &\quad + \int_{\partial\Omega} \left[\left(\frac{\partial W}{\partial G_{iAB}} u_{i,A} \right) N_B + \left(\frac{\partial W}{\partial H_{iABC}} u_{i,AB} \right) N_C \right] dS, \end{aligned} \quad (2.28)$$

where \mathbf{N} is the rightward unit normal to the boundary $\partial\Omega$ in the sense of Green-Stoke's theorem. The $u_{i,AB}$ terms in Eq. (2.28) are due to the third gradient of deformation and is required to be in the form of the first derivative of the position field (i.e. $u_{i,A}$) for the formulation of the Piola stresses. For this purpose, we perform iterated integrations by parts and successively deliver from the second integral of the Eq. (2.28) that

$$\begin{aligned} \int_{\Omega} \left(\frac{\partial W}{\partial H_{iABC}} \right)_{,C} u_{i,AB} dA &= \int_{\Omega} \left(\left(\frac{\partial W}{\partial H_{iABC}} \right)_{,C} u_{i,A} \right)_{,B} \\ &\quad - \left(\frac{\partial W}{\partial H_{iABC}} \right)_{,CB} u_{i,A} dA. \end{aligned} \quad (2.29)$$

Applying the Green-Stokes theorem on Eq. (2.29) and substituting it into Eq. (2.28) furnishes

$$\begin{aligned} \dot{E} &= \int_{\Omega} [2W_I - pF_{iA}^* - \left(\frac{\partial W}{\partial G_{iAB}} \right)_{,B}] u_{i,A} dA - \left[- \int_{\Omega} \left(\frac{\partial W}{\partial H_{iABC}} \right)_{,CB} u_{i,A} dA \right. \\ &\quad + \int_{\partial\Omega} \left(\left(\frac{\partial W}{\partial H_{iABC}} \right)_{,C} u_{i,A} \right) N_B dS \left. \right] + \int_{\partial\Omega} \left[\left(\frac{\partial W}{\partial G_{iAB}} u_{i,A} \right) N_B \right. \\ &\quad \left. + \left(\frac{\partial W}{\partial H_{iABC}} u_{i,AB} \right) N_C \right] dS \end{aligned} \quad (2.30)$$

Lastly, Eq. (2.30) may be recast to yield

$$\begin{aligned} \dot{E} &= \int_{\Omega} P_{iA} \dot{F}_{iA} dA + \int_{\partial\Omega} \left[\left\{ \frac{\partial W}{\partial G_{iAB}} - \left(\frac{\partial W}{\partial H_{iABC}} \right)_{,C} \right\} u_{i,A} N_B \right. \\ &\quad \left. + \frac{\partial W}{\partial H_{iABC}} u_{i,AB} N_C \right] dS, \end{aligned} \quad (2.31)$$

where

$$P_{iA} = 2W_I F_{iA} - p F_{iA}^* - \left(\frac{\partial W}{\partial G_{iAB}} \right)_{,B} + \left(\frac{\partial W}{\partial H_{iABC}} \right)_{,CB}, \quad (2.32)$$

is the expression of the Piola stress. Clearly, the resulting Piola-type stress is dependent on both the second and third gradient of deformations. In the case of initially straight fibers (i.e. $\nabla \mathbf{D} = \mathbf{0}$), we evaluate from Eq. (2.18) that

$$\left(\frac{\partial W}{\partial G_{iAB}} \right)_{,B} = C g_{i,B} D_A D_B \text{ and } \left(\frac{\partial W}{\partial H_{iABC}} \right)_{,CB} = A \alpha_{i,BC} D_A D_B D_C \quad (2.33)$$

and hence reduce Eq. (2.32) to

$$P_{iA} = 2W_I F_{iA} - p F_{iA}^* - C g_{i,B} D_A D_B + A \alpha_{i,BC} D_A D_B D_C. \quad (2.34)$$

Eq. (2.32) then satisfies

$$P_{iA,A} = 0 \text{ or } Div(\mathbf{P}) = 0, \quad (2.35)$$

which can be used to obtain the linearized Euler equilibrium equation for the reinforced solids occupying the domain of Ω .

2.3 Boundary conditions

In this section, we derive the admissible boundary conditions arising in the third gradient of virtual displacement. For the sake of conciseness, we confine our analysis to the case where fibers are aligned along the directions of either normal and/or tangential to straight (or fairly straight) boundaries (e.g. rectangular boundaries) such that

$$(\mathbf{D} \cdot \mathbf{T})(\mathbf{D} \cdot \mathbf{N}) = 0 \text{ and } \nabla \mathbf{T} = \nabla \mathbf{N} = \mathbf{0}. \quad (2.36)$$

By decomposing $P_{iA} u_{i,A}$, as in Eq. (2.26), we obtain from Eq. (2.31) that

$$\begin{aligned} \dot{E} &= \int_{\partial\Omega} P_{iA} u_i N_A dS - \int_{\Omega} P_{iA,A} u_i dA + \int_{\partial\Omega} \left[\left\{ \frac{\partial W}{\partial G_{iAB}} - \left(\frac{\partial W}{\partial H_{iABC}} \right)_{,C} \right\} u_{i,A} N_B \right. \\ &\quad \left. + \frac{\partial W}{\partial H_{iABC}} u_{i,AB} N_C \right] dS, \end{aligned} \quad (2.37)$$

where, the Green-Stoke's theorem is applied in the first term of Eq. (2.37). Since $P_{iA,A} = 0$ in Ω (see, Eq. (2.26)), the above reduces to

$$\begin{aligned} \dot{E} &= \int_{\partial\Omega} P_{iA} u_i N_A dS + \int_{\partial\Omega} \left[\left\{ \frac{\partial W}{\partial G_{iAB}} - \left(\frac{\partial W}{\partial H_{iABC}} \right)_{,C} \right\} u_{i,A} N_B \right. \\ &\quad \left. + \frac{\partial W}{\partial H_{iABC}} u_{i,AB} N_C \right] dS. \end{aligned} \quad (2.38)$$

In addition, we project $\nabla \mathbf{u}$ onto the normal and tangential direction as

$$\nabla \mathbf{u} = \nabla \mathbf{u}(\mathbf{T} \otimes \mathbf{T}) + \nabla \mathbf{u}(\mathbf{N} \otimes \mathbf{N}) = \mathbf{u}' \otimes \mathbf{T} + \mathbf{u}_{,N} \otimes \mathbf{N}, \quad (2.39)$$

where $\mathbf{T} = \mathbf{X}'(S) = \mathbf{k} \times \mathbf{N}$ is the unit tangent to $\partial\Omega$. \mathbf{u}' and $\mathbf{u}_{,N}$ are the tangential and normal derivatives of \mathbf{u} on $\partial\Omega$, respectively (i.e. $u'_i = u_{i,A} T_A$, $u_{i,N} = u_{i,A} N_A$). Thus, we find

$$u_{i,A} = \frac{\partial u_i}{\partial s} \frac{\partial s}{\partial X_A} + \frac{\partial u_i}{\partial N} \frac{\partial N}{\partial X_A} = u'_i T_A + u_{i,N} N_A, \quad (2.40)$$

$$u_{i,AB} = u''_i T_A T_B + u'_{i,N} (N_A T_B + T_A N_B) + u_{i,NN} N_A N_B, \quad (2.41)$$

where $T'_A = T_{A,N} = N'_A = N_{A,N} = 0$ from Eq. (2.36). We then substitute Eqs. (2.40)-(2.41) into Eq. (2.38) and thereby obtain

$$\begin{aligned} \dot{E} &= \int_{\partial\Omega} P_{iA} u_i N_A dS + \int_{\partial\Omega} \left\{ \left(\frac{\partial W}{\partial G_{iAB}} \right) - \left(\frac{\partial W}{\partial H_{iABC}} \right)_{,C} \right\} \\ &\quad \left(u'_i T_A N_B + u_{i,N} N_A N_B \right) dS + \int_{\partial\Omega} \frac{\partial W}{\partial H_{iABC}} [u''_i T_A T_B + u'_{i,N} (N_A T_B \\ &\quad + T_A N_B) + u_{i,NN} N_A N_B] N_C dS. \end{aligned} \quad (2.42)$$

Now, by decomposing the terms in the above the same as in Eq. (2.26), we find, for example,

$$\frac{\partial W}{\partial G_{iAB}} T_A N_B u'_i = \left(\frac{\partial W}{\partial G_{iAB}} T_A N_B u_i \right)' - \left(\frac{\partial W}{\partial G_{iAB}} T_A N_B \right)' u_i, \quad (2.43)$$

$$\begin{aligned} \frac{\partial W}{\partial H_{iABC}} (N_A T_B N_C + T_A N_B N_C) u'_{i,N} &= \left[\frac{\partial W}{\partial H_{iABC}} (N_A T_B N_C + T_A N_B N_C) u_{i,N} \right]' \\ &\quad - \left[\frac{\partial W}{\partial H_{iABC}} (N_A T_B N_C + T_A N_B N_C) \right]' u_{i,N}, \end{aligned} \quad (2.44)$$

$$\begin{aligned} \frac{\partial W}{\partial H_{iABC}} T_A T_B N_C u''_i &= \left(\frac{\partial W}{\partial H_{iABC}} T_A T_B N_C u_i \right)'' + \left(\frac{\partial W}{\partial H_{iABC}} T_A T_B N_C \right)'' u_i \\ &\quad - 2 \left[\left(\frac{\partial W}{\partial H_{iABC}} T_A T_B N_C \right)' u_i \right]', \end{aligned} \quad (2.45)$$

and similarly for other terms. Therefore, Eq. (2.46) can be rewritten as

$$\begin{aligned}
\dot{E} = & \int_{\partial\Omega} [P_{iA}N_A - \left\{ \frac{\partial W}{\partial G_{iAB}} T_A N_B \right. \\
& - \left. \left(\frac{\partial W}{\partial H_{iABC}} \right)_{,C} T_A N_B \right\}'] u_i dS - \int_{\partial\Omega} \left[\left(\frac{\partial W}{\partial H_{iABC}} T_A T_B N_C \right)'' \right] u_i dS \\
& + \int_{\partial\Omega} \left[\left\{ \frac{\partial W}{\partial G_{iAB}} T_A N_B - \left(\frac{\partial W}{\partial H_{iABC}} \right)_{,C} T_A N_B \right. \right. \\
& - \left. \left. 2 \left(\frac{\partial W}{\partial H_{iABC}} T_A T_B N_C \right)' \right\} u_i \right]' dS \\
& + \int_{\partial\Omega} \left[\frac{\partial W}{\partial H_{iABC}} (N_A T_B N_C + T_A N_B N_C) u_{i,N} \right]' dS \\
& + \int_{\partial\Omega} \left[\left\{ \left(\frac{\partial W}{\partial G_{iAB}} \right) - \left(\frac{\partial W}{\partial H_{iABC}} \right)_{,C} \right\} N_A N_B \right] u_{i,N} dS \\
& - \int_{\partial\Omega} \left[\left\{ \frac{\partial W}{\partial H_{iABC}} (N_A T_B N_C + T_A N_B N_C) \right\}' \right] u_{i,N} dS \\
& + \int_{\partial\Omega} \left(\frac{\partial W}{\partial H_{iABC}} T_A T_B N_C u_i \right)'' dS \\
& + \int_{\partial\Omega} \frac{\partial W}{\partial H_{iABC}} u_{i,NN} N_A N_B N_C dS. \tag{2.46}
\end{aligned}$$

Further, by means of Eqs. (2.18) and (2.33) (e.g. $\frac{\partial W}{\partial G_{iAB}} = C g_i D_A D_B$, $\left(\frac{\partial W}{\partial G_{iAB}} \right)_{,B} = C g_{i,B} D_A D_B$ etc...), (2.46) may be recast as

$$\begin{aligned}
\dot{E} = & \int_{\partial\Omega} [P_{iA}N_A - \{(C g_i \\
& - A \alpha_{i,C} D_C) D_A T_A D_B N_B \}]' u_i dS + \int_{\partial\Omega} [(A \alpha_i D_A T_A D_B T_B D_C N_C)''] u_i dS \\
& + \sum \left\| \left[(C g_i - A \alpha_{i,C} D_C) D_A T_A D_B N_B - 2 (A \alpha_i D_A T_A D_B T_B D_C N_C)' \right] u_i \right\| \\
& + \sum \| A \alpha_i (D_A N_A D_B T_B D_C N_C + D_A T_A D_B N_B D_C N_C) u_{i,N} \| \\
& + \sum \left\| \frac{d}{ds} (A \alpha_i D_A T_A D_B T_B N_C D_C u_i) \right\| \\
& + \int_{\partial\Omega} [(C g_i - A \alpha_{i,C} D_C) D_A N_A D_B N_B] u_{i,N} dS \\
& + \int_{\partial\Omega} [\{ A \alpha_i D_A D_B D_C (N_A T_B N_C + T_A N_B N_C) \}' u_{i,N}] dS \\
& + \int_{\partial\Omega} (A \alpha_i D_A N_A D_B N_B D_C N_C u_{i,NN}) dS \tag{2.47}
\end{aligned}$$

where the double bar symbol refers to the jump across the discontinuities on

the boundary ∂w (i.e. $\|*\| = (*)^+ - (*)^-$), and the sum refers to the collection of all discontinuities. Therefore, using Eq. (2.36)₁, we reduce the above to

$$\begin{aligned} \dot{E} &= \int_{\partial\Omega} [P_{iA}N_A]u_i dS + \int_{\partial\Omega} [(Cg_i - A\alpha_{i,C}D_C)D_A N_A D_B N_B] u_{i,N} dS \\ &+ \int_{\partial\Omega} (A\alpha_i D_A N_A D_B N_B D_C N_C u_{i,NN}) dS. \end{aligned} \quad (2.48)$$

Since the virtual work statement ($\dot{E} = P$) implies that the admissible mechanical powers are expressed in the following form:

$$P = \int_{\partial w_t} t_i u_i dS + \int_{\partial w} m_i u_{i,N} dS + \int_{\partial w} r_i u_{i,NN} dS + \sum f_i u_i. \quad (2.49)$$

We find by comparing Eqs. (2.48) and (2.49) that

$$\begin{aligned} \mathbf{t} &= \mathbf{PN}, \\ \mathbf{m} &= [C\mathbf{g} - A(\nabla\boldsymbol{\alpha})\mathbf{D}](\mathbf{D} \cdot \mathbf{N})^2, \\ \mathbf{r} &= A\boldsymbol{\alpha}(\mathbf{D} \cdot \mathbf{N})^3, \\ \mathbf{f} &= 0, \end{aligned} \quad (2.50)$$

which will be used to extract linearized boundary conditions.

2.4 Linear Theory

The superposed “*small*” incremental deformation is defined by (see, for example, [28] and [77])

$$\boldsymbol{\chi} = \boldsymbol{\chi}_o + \varepsilon \dot{\boldsymbol{\chi}}; |\varepsilon| \ll 1, \quad (2.51)$$

where $(*)_o$ denote the configuration of $*$, evaluated at $\varepsilon = 0$, and $\dot{(*)} = \partial(*)/\partial\varepsilon$. Also, here and henceforth, we denote the induced small variation of deformation as

$$\dot{\boldsymbol{\chi}} = \mathbf{u}. \quad (2.52)$$

In the above, caution needs to be taken that the present notation is not confused with the one used for the variational computation. Thus from Eq. (2.53), the deformation gradient tensor can be approximated as

$$\mathbf{F} = \mathbf{F}_o + \varepsilon \nabla \mathbf{u}, \text{ where } \dot{\mathbf{F}} = \nabla \mathbf{u}. \quad (2.53)$$

In general, the body is initially undeformed and stress free. This can be accommodated by imposing the initial conditions of

$$\mathbf{F}_o = \mathbf{I} \text{ and } \mathbf{P}_o = \mathbf{0}, \text{ at } \varepsilon = 0. \quad (2.54)$$

Accordingly, Eq. (2.53) becomes

$$\mathbf{F} = \mathbf{I} + \varepsilon \nabla \mathbf{u}, \quad (2.55)$$

and subsequently yields

$$\begin{aligned} \mathbf{F}^{-1} &= \mathbf{I} - \varepsilon \nabla \mathbf{u} + o(\varepsilon), \text{ and} \\ J &= \det \mathbf{F} = 1 + \varepsilon \operatorname{div} \mathbf{u} + o(\varepsilon). \end{aligned} \quad (2.56)$$

Further, in view of Eq. (2.51), the Euler equilibrium equation (2.35) can be expanded to

$$\operatorname{Div}(\mathbf{P}) = \operatorname{Div}(\mathbf{P}_o) + \varepsilon \operatorname{Div}(\dot{\mathbf{P}}) + o(\varepsilon) = \mathbf{0}. \quad (2.57)$$

Hence, dividing the above by ε and limiting $\varepsilon \rightarrow 0$, we find

$$\operatorname{Div}(\dot{\mathbf{P}}) = 0, \quad (2.58)$$

which serves as the compatible linearized Euler equation. The expression of the Piola-type stress in Eq. (2.58) can also be obtained by taking variational derivative of Eq. (2.34) with respect to ε as

$$\begin{aligned} \dot{\mathbf{P}} &= 2W_{II}\dot{I}(\mathbf{F})_o + 2(W_I)_o\dot{\mathbf{F}} - \dot{p}\mathbf{F}_o^* - p_o\dot{\mathbf{F}}^* - C\dot{g}_{i,B}D_AD_B(\mathbf{e}_i \otimes \mathbf{E}_A) \\ &+ A\dot{\alpha}_{i,BC}D_AD_B D_C(\mathbf{e}_i \otimes \mathbf{E}_A). \end{aligned} \quad (2.59)$$

For example, the Neo-Hookian type materials can be considered where the energy density function is defined by

$$W(I_1, I_3) = \frac{\mu}{2}(I_1 - 3) - \mu \log I_3 + \frac{\lambda}{2}(\log I_3)^2, \quad (2.60)$$

where μ and λ are the material constants, and I_1 (here denoted as I) and I_3 are respectively the first and third invariant of the deformation gradient tensor. In the case of the incompressible model (i.e. $I_3 = 1$), Eq. (2.60) further reduces to

$$W(I_1) = \frac{\mu}{2}(I_1 - 3). \quad (2.61)$$

Therefore, we evaluate

$$W_{II} = 0 \text{ and } (W_I)_o = \frac{\mu}{2}, \quad (2.62)$$

and thereby obtain from Eq. (2.59) that

$$\dot{\mathbf{P}} = \mu \dot{\mathbf{F}} - \dot{p} \mathbf{F}_o^* - p_o \dot{\mathbf{F}}^* - C \dot{g}_{i,B} D_A D_B (\mathbf{e}_i \otimes \mathbf{E}_A) + A \dot{\alpha}_{i,BC} D_A D_B D_C (\mathbf{e}_i \otimes \mathbf{E}_A). \quad (2.63)$$

In this equation C is the double stress parameter, u corresponds to the deformation, and A is the triple stress parameter. Now, combining Eqs. (2.58) and (2.63) yields

$$\begin{aligned} Div(\mu \dot{\mathbf{F}}) - Div(\dot{p} \mathbf{F}_o^*) - Div(p_o \dot{\mathbf{F}}^*) - Div[C \dot{g}_{i,B} D_A D_B (\mathbf{e}_i \otimes \mathbf{E}_A)] \\ + Div[A \dot{\alpha}_{i,BC} D_A D_B D_C (\mathbf{e}_i \otimes \mathbf{E}_A)] = 0. \end{aligned} \quad (2.64)$$

In view of Eq. (2.51), terms in the above can be simplified as

$$Div(\mu \dot{\mathbf{F}}) = Div(\mu \nabla \mathbf{u}) = \mu u_{i,AA} \mathbf{e}_i, \quad (2.65)$$

$$Div(\dot{p} \mathbf{F}_o^*) = \mathbf{F}_o^* \nabla \dot{p} = \mathbf{I} \nabla \dot{p} = \dot{p}_{,i} \mathbf{e}_i, \quad \because Div(\mathbf{F}^*) = 0, \text{ and} \quad (2.66)$$

$$Div(p_o \dot{\mathbf{F}}^*) = p_o Div(\dot{\mathbf{F}}^*) = 0, \quad (2.67)$$

Here, the unknown constant p_o can be determined such that the Piola-type stress admits the initial stress free state at $\varepsilon = 0$; i.e.

$$\dot{\mathbf{P}}_o = \mu \dot{\mathbf{F}}_o - p_o \dot{\mathbf{F}}_o^* = 0, \quad (2.68)$$

and thus yielding

$$p_o = \mu. \quad (2.69)$$

Also, since $\mathbf{g} = \mathbf{G}(\mathbf{D} \otimes \mathbf{D})$ and $\boldsymbol{\alpha} = \mathbf{H}(\mathbf{D} \otimes \mathbf{D} \otimes \mathbf{D})$ (see, Eqs. (2.5) and (2.11)), we evaluate

$$\begin{aligned} Div[C \dot{g}_{i,B} D_A D_B (\mathbf{e}_i \otimes \mathbf{E}_A)] &= C Div[u_{i,BCD} D_A D_B D_C D_D \mathbf{e}_i \otimes \mathbf{E}_A] \\ &= C u_{i,ABCD} D_A D_B D_C D_D \mathbf{e}_i, \text{ and} \end{aligned} \quad (2.70)$$

$$\begin{aligned} Div[A \dot{\alpha}_{i,BC} D_A D_B D_C (\mathbf{e}_i \otimes \mathbf{E}_A)] &= A Div[u_{i,BCDEF} D_A D_B D_C D_D D_E D_F \\ &(\mathbf{e}_i \otimes \mathbf{E}_A)] = A u_{i,ABCDEF} D_A D_B D_C D_D D_E D_F \mathbf{e}_i, \end{aligned} \quad (2.71)$$

where $\dot{F}_{iA} = u_{i,A}$ and $\dot{G}_{iAB} = u_{i,AB}$ from Eqs. (2.6), (2.11)₂ and (2.53). Therefore, by substituting Eqs (2.65)-(2.71) into Eq. (2.64), we obtain the following linearized Euler equilibrium equation

$$\begin{aligned} & \mu u_{i,AA} - \dot{p}_{,i} - C u_{i,ABCD} D_A D_B D_C D_D \\ & + A u_{i,ABCDEF} D_A D_B D_C D_D D_E D_F = 0, \end{aligned} \quad (2.72)$$

which solves for u_1, u_2 and p .

Similarly, the constraint of bulk incompressibility and the associated boundary conditions (Eq. (2.50)) can be approximated as (e.g. $\mathbf{t} = \mathbf{t}_o + \varepsilon \dot{\mathbf{t}} + o(e)$ etc...)

$$(J - 1) \dot{\cdot} = \mathbf{F}_o^* \cdot \dot{\mathbf{F}} = \text{div } \mathbf{u} = 0, \text{ and} \quad (2.73)$$

$$\begin{aligned} \dot{\mathbf{t}} &= \dot{\mathbf{P}} \mathbf{N}, \\ \dot{\mathbf{m}} &= [C \dot{\mathbf{g}} - A (\nabla \dot{\boldsymbol{\alpha}}) \mathbf{D}] (\mathbf{D} \cdot \mathbf{N})^2, \\ \dot{\mathbf{r}} &= A \dot{\boldsymbol{\alpha}} (\mathbf{D} \cdot \mathbf{N})^3, \\ \dot{\mathbf{f}} &= 0, \end{aligned} \quad (2.74)$$

where

$$\dot{P}_{iA} = \mu \dot{F}_{iA} - \dot{p} (F_{iA}^*)_o - p_o \dot{F}^* - C \dot{g}_{i,B} D_A D_B + A \dot{\alpha}_{i,BC} D_A D_B D_C, \quad (2.75)$$

and

$$(F_{iA}^*)_o = \delta_{iA}, \quad \because (F_{iA})_o = \delta_{iA} \text{ at } \varepsilon = 0. \quad (2.76)$$

Finally, since $J \partial F_{jB}^* / \partial F_{iA} = F_{jB}^* F_{iA}^* - F_{iB}^* F_{jA}^*$, we obtain at $\varepsilon = 0$,

$$(\partial F_{jB}^* / \partial F_{iA})_o = \delta_{jB} \delta_{iA} - \delta_{iB} \delta_{jA} \text{ and } (\mathbf{F}_{\mathbf{F}}^* [\dot{\mathbf{F}}])_{jB} = (\delta_{jB} \delta_{iA} - \delta_{iB} \delta_{jA}) u_{i,A}. \quad (2.77)$$

Hence Eq. (2.76) furnishes

$$\dot{F}_{iA}^* = (\text{Div } \mathbf{u}) \delta_{iA} - u_{A,i} = -u_{A,i}, \quad \because \text{Div } \mathbf{u} = \text{div } \mathbf{u} = 0. \quad (2.78)$$

The boundary conditions $\dot{\mathbf{t}}$, $\dot{\mathbf{m}}$, and $\dot{\mathbf{f}}$ in Eq. (2.74) are the expressions of linearized edge tractions, edge moments and the corner forces, respectively. In particular, an additional boundary condition $\dot{\mathbf{r}}$ is identified as a result of

introducing the third gradient of continuum deformations. This boundary condition $\dot{\mathbf{r}}$ falls into the category of the triple forces which characterizes the mechanical contact interactions on edges and points of Cauchy cuts (see, for example [82]–[84]). In the present case, the letter may be understood as the local interactions between the fibers and the matrix, and are coupled with the Piola-type triple stress exerted by third gradient continua (see, also, [83], [80] and [80]). Further, within the description of the proposed model, the configuration of such local interactions and the associated triple forces may be achieved via the computation of the third gradient of the continuum deformation on the convected curves of fibers. In this regard, a set of selected examples and experiments are considered in the following sections. Further analysis, including a more general class of materials is, however, beyond the scope of the present study due to the paucity of available data, yet certainly deserves for further research.

2.5 Solution to the linearized problem

For the purposes of demonstration, we consider an elastic solid of Neo-Hookean type, which is reinforced with the single family of fibers and subjected to the double force $\dot{\mathbf{m}}$ (bending moment) and triple force $\dot{\mathbf{r}}$ (see, Figure 2.1).

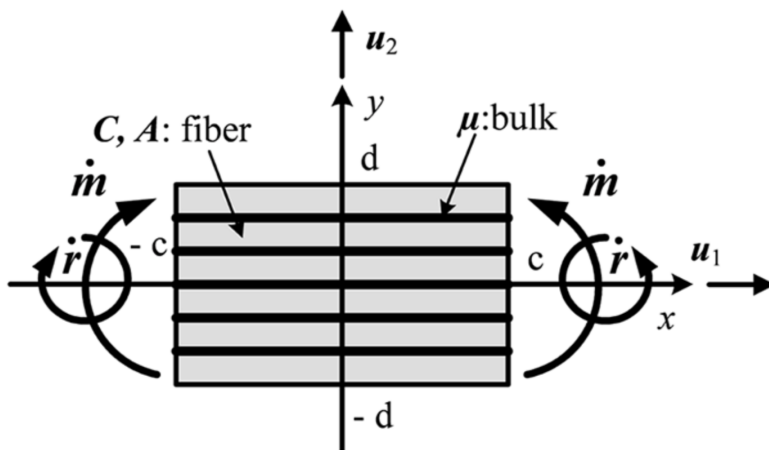


Figure 2.1: Schematic of the problem.

The corresponding director field of the fibers is defined by the unit tangent \mathbf{D} on the convected curve of fibers as

$$\mathbf{D} = \mathbf{E}_1, \quad D_1 = 1, \quad D_2 = 0. \quad (2.79)$$

Therefore, Eq. (2.72) becomes

$$\begin{aligned} \mu(u_{1,11} + u_{1,22}) - \dot{p}_{,1} - Cu_{1,1111} + Au_{1,111111} &= 0 \\ \mu(u_{2,11} + u_{2,22}) - \dot{p}_{,2} - Cu_{2,1111} + Au_{2,111111} &= 0 \\ u_{1,1} + u_{2,2} &= 0, \end{aligned} \quad (2.80)$$

where, the third equation of the above is linearized incompressibility conditions from Eq. (2.73). The systems of equations in (2.80) can be treated by introducing the following scalar field ϕ as

$$\mathbf{u} = \mathbf{k} \times \nabla \phi, \quad \mathbf{k}(\text{unit normal}); \quad u_i = \varepsilon_{\lambda i} \phi_{,\lambda}, \quad (2.81)$$

such that the condition of bulk incompressibility is met (i.e. $u_{1,1} + u_{2,2} = \phi_{,12} - \phi_{,21} = 0$). Hence, invoking Eq. (2.81), Eq. (2.80) may be recast as

$$\begin{aligned} \dot{p}_{,1} &= -\mu(\varphi_{,211} + \varphi_{,222}) + C\varphi_{,21111} - A\varphi_{,2111111}, \\ \dot{p}_{,2} &= \mu(\varphi_{,111} + \varphi_{,122}) - C\varphi_{,11111} + A\varphi_{,1111111}. \end{aligned} \quad (2.82)$$

We now utilize the compatibility condition of p (i.e. $\dot{p}_{,ij} = \dot{p}_{,ji}$) and obtain

$$\mu(\varphi_{,1111} + \varphi_{,2222} + 2\varphi_{,1122}) - C(\varphi_{,111111} + \varphi_{,221111}) + A(\varphi_{,11111111} + \varphi_{,22111111}) = 0, \quad (2.83)$$

which solves unknown function, $\phi(x, y)$. Further, the auxiliary function $H = \Delta\phi$ may be introduced to reduce the above to

$$\mu\Delta H - CH_{,1111} + AH_{,111111} = 0. \quad (2.84)$$

Hence, the general solution of Eq. (2.83) can be found:

$$\begin{aligned} \varphi &= \sum_{m=1}^{\infty} [\{A_m e^{a_m x} + B_m e^{-a_m x} + e^{b_m x} (C_m \sin(c_m x) + D_m \cos(c_m x)) \\ &\quad + e^{-b_m x} (E_m \sin(c_m x) + F_m \cos(c_m x))\} \times \{\sin(my)\}], \end{aligned} \quad (2.85)$$

where

$$\begin{aligned}
a_m &= \sqrt[2]{P^{\frac{1}{3}} - \frac{N}{O} + O}, b_m = \sqrt[2]{\frac{F + \sqrt[2]{F^2 + S^2}}{2}}, c_m = \sqrt[2]{\frac{S^2}{2(F + \sqrt[2]{F^2 + S^2})}}, \\
P &= \frac{C^3}{27A^3}, N = -\frac{C^2}{9A^2} + \frac{\mu}{3A}, S = \frac{1}{2}\left(\frac{N}{O} + O\right)^{\frac{1}{3}}, \\
M &= \left(P - Q + \frac{m^2\mu}{2A}\right)^2, O = \left(\sqrt[2]{M} + \sqrt[2]{(M + N^3)}\right)^{\frac{1}{3}}, F = \frac{N}{2O} + P^{\frac{1}{3}} - \frac{O}{2},
\end{aligned}$$

and

$$m = \frac{n\pi}{2d} \text{ for } n = 1, 3, 5, \dots \quad (2.86)$$

By using Eqs. (2.85)-(2.86) and the admissible boundary conditions (Eq. (2.74)), a_m, b_m and c_m are computed for each m (e.g. $m = \pi/2d$, for $n = 1$ etc...) so that the unknown constant real numbers A_m, B_m, C_m, D_m, E_m , and F_m can be completely determined. In the analysis, the applied double force \dot{m}_1 and \dot{r}_1 triple force are assumed to be 5 which is a constant number that can be approximated by using Fourier series to match the left-hand side of the equation.

$$\begin{aligned}
\dot{\mathbf{m}} &= \dot{m}_1 \mathbf{e}_1 + \dot{m}_2 \mathbf{e}_2, \\
\dot{m}_1 &= Cu_{1,11} - Au_{1,1111} = 5 \simeq \sum_{n=1}^{30} \frac{20}{n\pi} (-1)^{\frac{n-1}{2}} \cos\left(\frac{n\pi}{2d}y\right), \\
\dot{m}_2 &= Cu_{2,11} - Au_{2,1111} = 0, \\
\dot{\mathbf{r}} &= A\dot{\boldsymbol{\alpha}}(\mathbf{D} \cdot \mathbf{N})^3 = \dot{r}_1 \mathbf{e}_1 + \dot{r}_2 \mathbf{e}_2, \dot{r}_1 = Au_{1,111} = 5 \simeq \sum_{n=1}^{30} \frac{20}{n\pi} (-1)^{\frac{n-1}{2}}, \\
\dot{r}_2 &= Au_{2,111} = 0,
\end{aligned} \quad (2.87)$$

which demonstrate fast convergence ranges between 20 and 30 iterations (see, Figure 2.2).

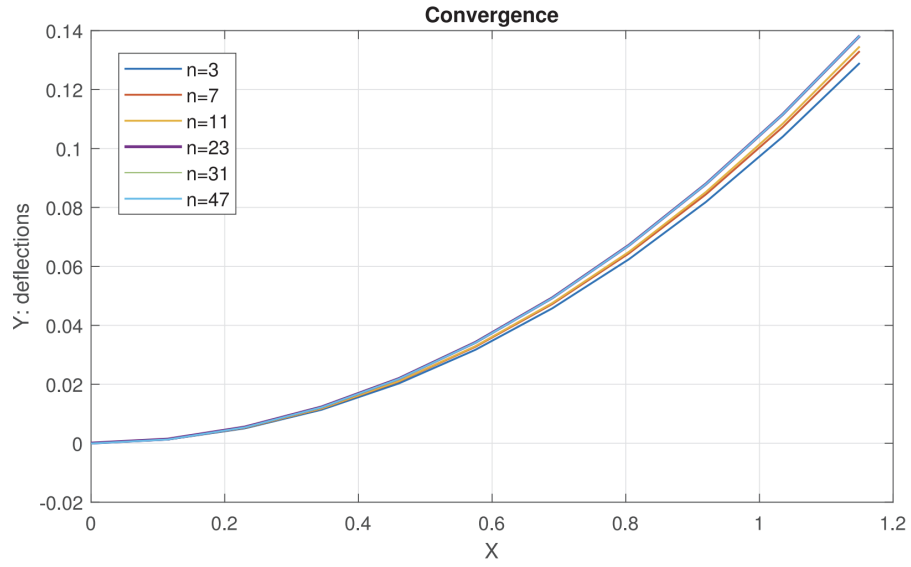


Figure 2.2: Deformation profiles with respect to the number of iterations (N).

Finally, the obtained solution, ϕ , is substituted into the following expression

$$\chi = (X_1 - \phi_{,2})\mathbf{e}_1 + (X_2 + \phi_{,1})\mathbf{e}_2, \quad (2.88)$$

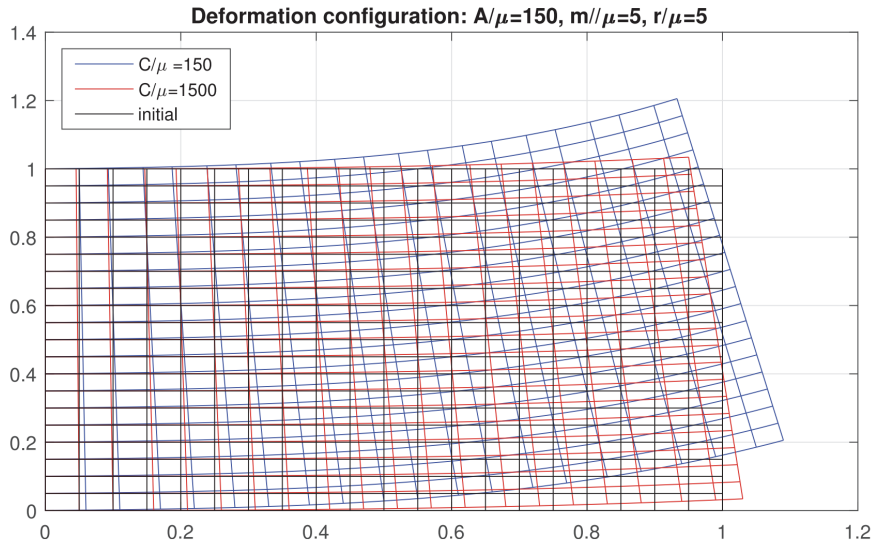


Figure 2.3: Deformed configurations with respect to C/μ .

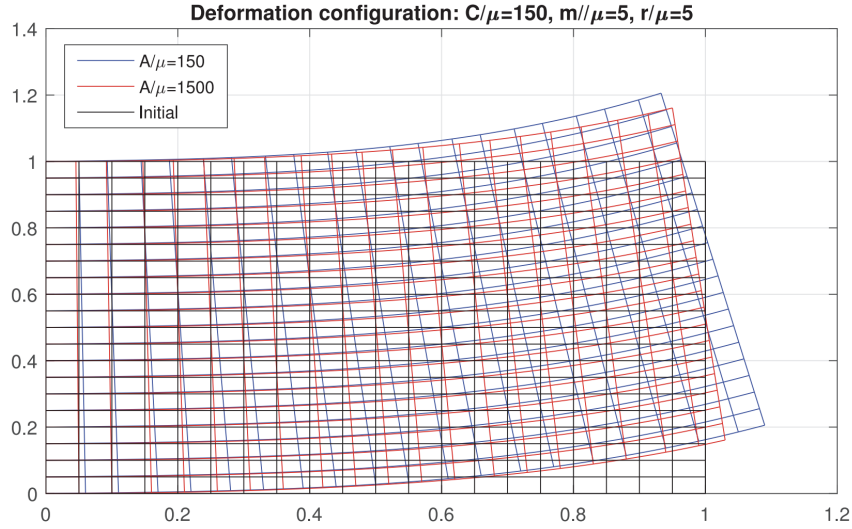


Figure 2.4: Deformed configurations with respect to A/μ .

2.5.1 Theoretical results obtained from the 3rd order gradient model

To configure the deformation map and the corresponding stress field can be computed through Eqs. (2.63), (2.81) and (2.82). It is noted that the corresponding data are obtained under the normalized setting unless otherwise specified (e.g. $C/\mu = 150$, $A/\mu = 100$, etc...). Also, we conveniently denote the material constants pertaining to the Piolar-type double stress and triple stress (i.e. C and A) as the ‘double stress parameter’ and ‘triple stress parameter’, respectively.

It is shown in Figures 2.3-2.5 that the resulting deformation fields are sensitive to both the double stress and triple stress parameters and the applied triple load $\dot{\mathbf{r}}$. For example, gradual decreases in the deformed configuration of the composite are observed with increasing the double stress parameter C which is also aligned with the results in and [9] and [73]. In fact, the obtained results reduce to those obtained from the second gradient model in the limit of the vanishing triple stress parameter and triple stress (i.e. $A = \dot{\mathbf{r}} = 0$, see, Figure 2.6).

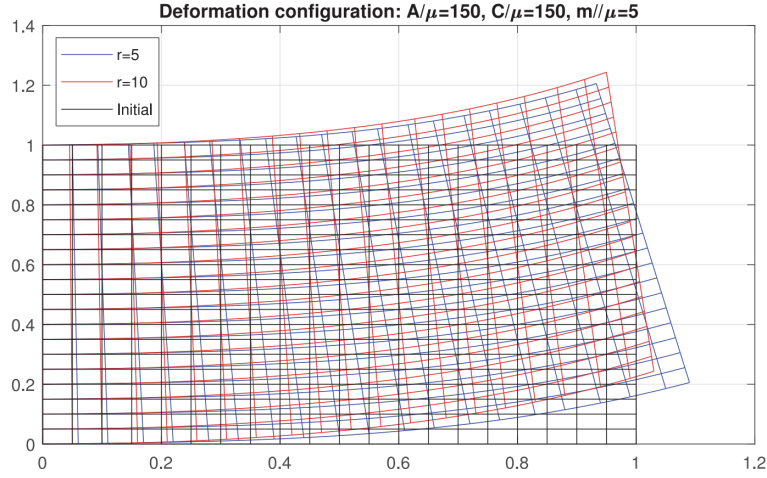


Figure 2.5: Deformed configurations with respect to r/μ .

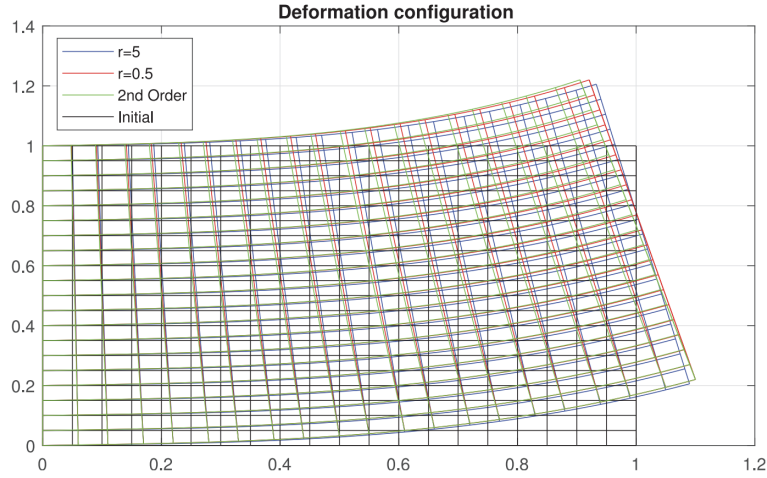


Figure 2.6: Comparison with the existing results in [73].

More importantly, in order to examine the effects of the third gradient of deformations, we compute the shear strain gradients, and the corresponding shear angle fields using, the following relations [85],

$$\phi' = \frac{u_2''(1 + u_1') - u_2' u_1''}{u_2'^2 + (1 + u_1')^2}, \quad (2.89)$$

and

$$\phi = \tan^{-1}\left(\frac{\chi_{2,1} - \chi_{1,1}}{2 + \chi_{1,1} + \chi_{2,1}}\right). \quad (2.90)$$

The results in Figure 2.7 indicate that the shear strain gradually increase with $\mathbf{r} > 0$ and decreases when $\mathbf{r} < 0$. In addition, the continuous shear strain gradient fields give rise to the smooth and dilatational shear angle distributions throughout the domain of interest and the corresponding distribution rates are determined by the applied triple force, $\dot{\mathbf{r}}$ (see, Figure 2.8). This further implies that, with the given double force, $\dot{\mathbf{m}}$, the proposed linear model predicts multiple configurations of shear zones, as opposed to those obtained from the second gradient model where only one configuration (smooth but not dilatational) is possible.

Remark

The presented model accommodates the second gradient-based model as a particular case when the applied triple force $\dot{\mathbf{r}}$ is removed. In other words, the deformation profiles, shear strain distributions and shear angle zones obtained from the second gradient continuum model can be reproduced directly from the proposed model by setting $\dot{\mathbf{r}} = 0$ (see, Figures 2.6, 9b and 10b). This also can be seen from Eqs. (2.74) and (2.80) where the systems of PDEs and the associated boundary conditions yield

$$\begin{aligned} \mu(u_{1,11} + u_{1,22}) - \dot{p}_{,1} - Cu_{1,1111} &= 0 \\ \mu(u_{2,11} + u_{2,22}) - \dot{p}_{,2} - Cu_{2,1111} &= 0 \\ u_{1,1} + u_{2,2} &= 0, \end{aligned} \quad (2.91)$$

and

$$\begin{aligned} \dot{\mathbf{t}} &= \dot{\mathbf{P}}\mathbf{N}, \\ \dot{\mathbf{m}} &= C\dot{\mathbf{g}}(\mathbf{D} \cdot \mathbf{N})^2, \\ \dot{\mathbf{r}} &= 0, \\ \dot{\mathbf{f}} &= 0, \end{aligned} \quad (2.92)$$

when $\dot{\mathbf{r}} = A\dot{\boldsymbol{\alpha}}(\mathbf{D} \cdot \mathbf{N})^3 = 0$. Further, the expression of the corresponding Piola-type stress (Eq. (2.63)) become

$$\dot{\mathbf{P}} = \mu \dot{\mathbf{F}} - \dot{p} \mathbf{F}_o^* - p_o \dot{\mathbf{F}}^* - C \dot{g}_{i,B} D_A D_B (\mathbf{e}_i \otimes \mathbf{E}_A). \quad (2.93)$$

Therefore, the systems of equations and the boundary conditions (Eqs. (2.74) and (2.80)) are now reduced to those formulated from the second gradient continuum model (see, Eqs. (2.69), (2.71), and (2.72))[73].

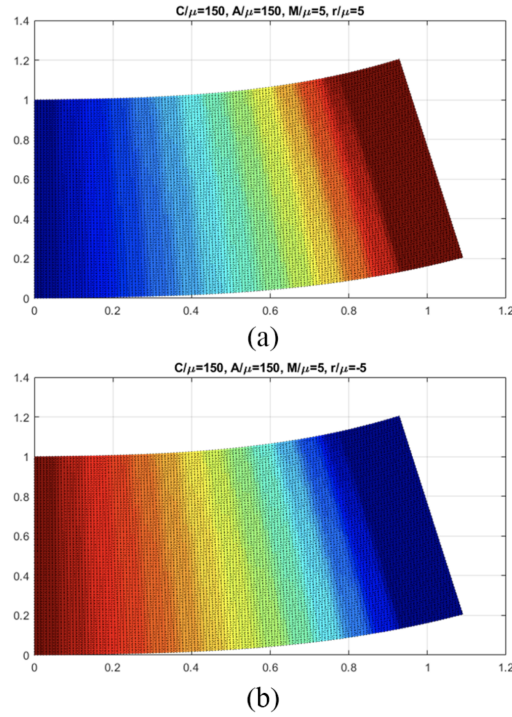


Figure 2.7: Shear strain gradients with respect to \mathbf{r} : $\mathbf{r} > 0$ (a) and $\mathbf{r} < 0$ (b)

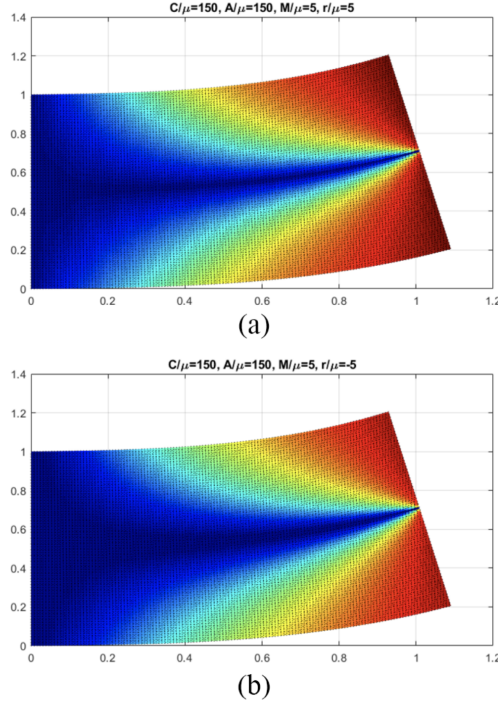
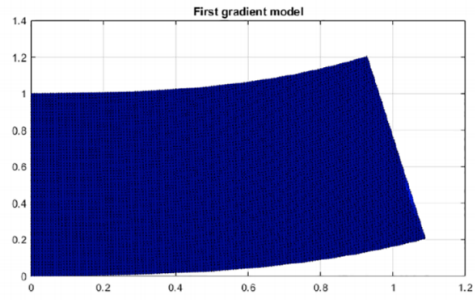
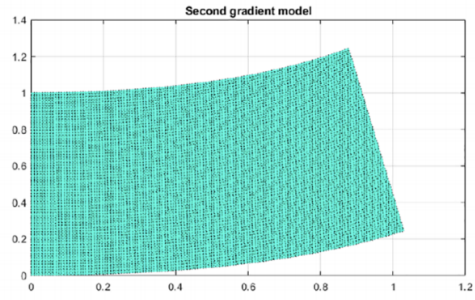


Figure 2.8: Shear angle contours with respect to \mathbf{r} : $\mathbf{r} > 0$ (a) and $\mathbf{r} < 0$ (b)

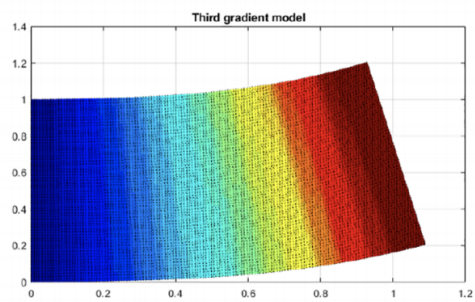
We also plot the shear gradient and shear angle distributions estimated by the first (classical), second and third gradient models in order to examine their capability in prediction ranges. It is clear from Figure 2.9 that the proposed model (third gradient) assimilates gradual changes in shear gradient field whereas the first and second gradient-based model are limited insofar as they estimate either zero or constant strain gradient distributions. As a result, the corresponding shear zones illustrate, discontinued (first gradient), smooth but non-dilatational (second gradient), and smooth and dilatational (third gradient) distributions, respectively (see, Figure 2.10). Lastly, the obtained linear solutions demonstrate reasonable agreement with those from the nonlinear model in the prediction of both the shear angle contours (Figure 2.11), and shear strain gradient fields (Figure 2.12).



(a)



(b)



(c)

Figure 2.9: Shear strain gradients predicted by first gradient (a), second gradient (b), third gradient (c) model.

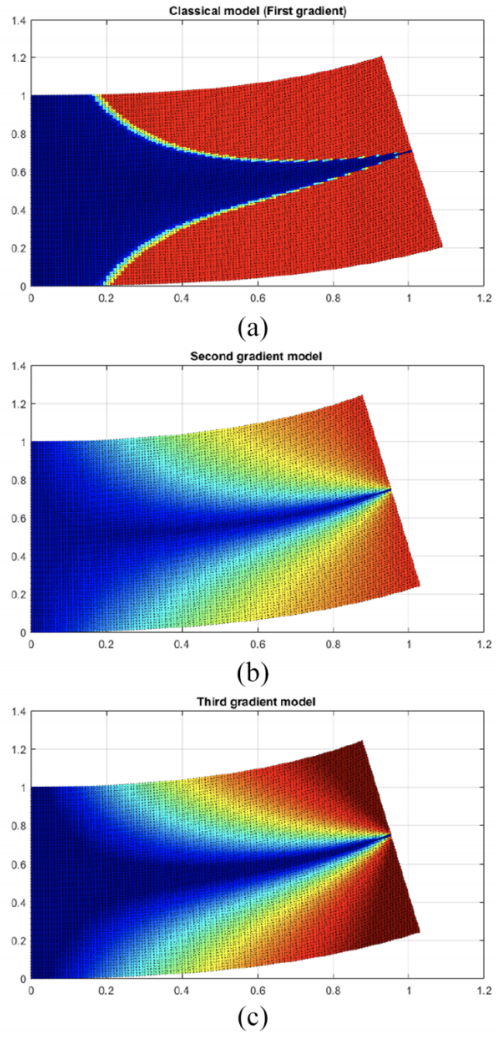
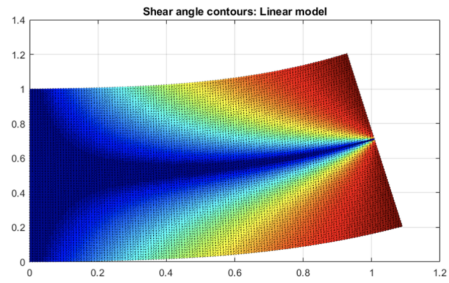
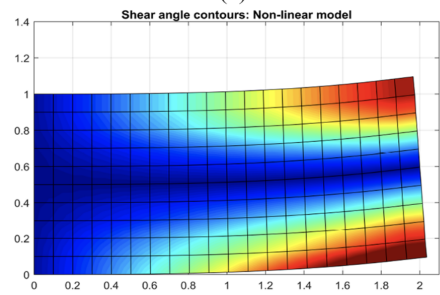


Figure 2.10: Shear angle contours predicted by first gradient (a), second gradient (b), third gradient (c) model.

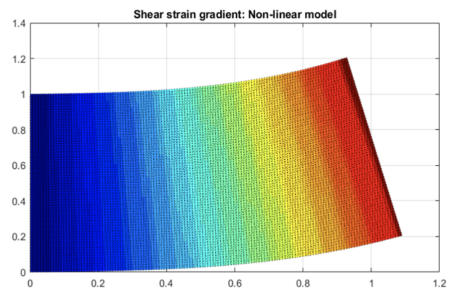


(a)

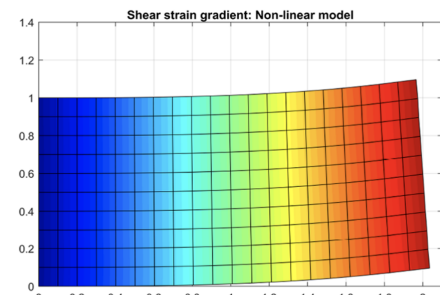


(b)

Figure 2.11: Comparison with the nonlinear solution (Shear angle zone): linear model (a), nonlinear model (b).



(a)



(b)

Figure 2.12: Comparison with the nonlinear solution (Shear strain gradient): linear model (a), nonlinear model (b).

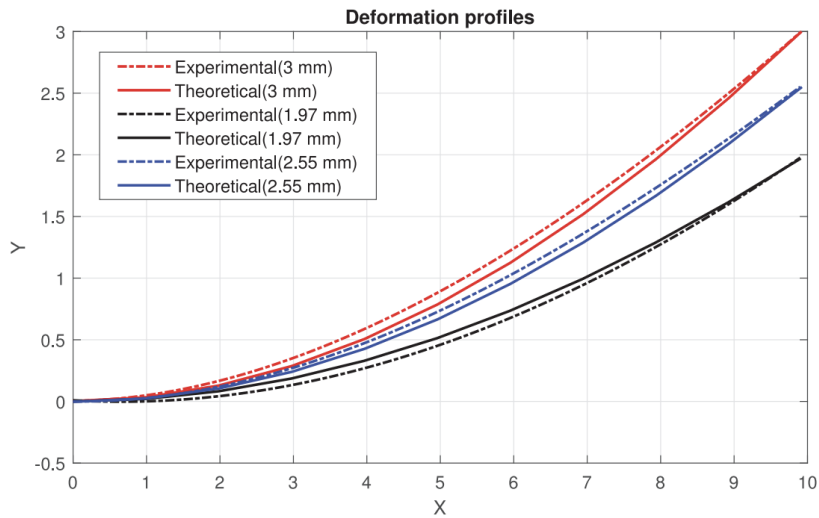
2.5.2 Comparison between experimental results and theoretical predictions

So far, we have shown that the proposed model, based on the third gradient continua, is able to sustain forces, double forces and triple forces to induce dilatational deformations. These forces are coupled, respectively, with the Piola-type stress, double stress, and triple stress through an appropriate material parameter. More precisely, the obtained expression of the Piola-type stress is a combination of the N th order stresses so that the third gradient of the deformation term in Eq. (2.63) can be regarded as the energy couple of the triple force $\dot{\mathbf{r}}$ via the triple stress parameter A . A similar statement can be made for the first and second order stresses where the corresponding parameters C and μ are related to the bending energy of a fiber and the deformation energy of the matrix, respectively. However, little has been studied for parameter A mainly due to the complex nature of mechanical interactions on edges and point of Cauchy cuts [82]–[84].

Here, we present an indirect approach in an effort to estimate the triples stress parameter A through which the accuracy of the proposed model in the deformation analysis of the composites is also examined. For this purpose, two experiments are considered (see, Figures 2.13-14) a three point bending test of Crystalline Nanocellulose (CNC) which is a natural linear biopolymer ($C = 150GPa$, $\mu = 1GPa$) and the bending test of a Nylon-6 Fiber Neoprene Rubber Composites ($C = 2000MPa$, $\mu = 1MPa$) with clamped ends. In the experiments, the out-of-plane direction (x_3) is defined in the parallel direction of either the loading cylinder or the guide clamp so that the corresponding deflections can be estimated by using the proposed model with the setting of $c \gg d$. The resulting deformation profiles are recoded using the MTS load cell and high speed camera.



(a)



(b)

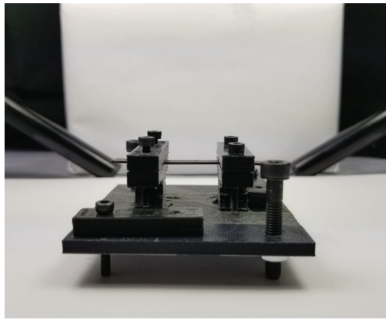
Figure 2.13: (a) is the three points bending test experimental setup for CNC, and (b) is the numerical comparison with the CNC experimental results.

The results in Figures 2.13-14 indicate that the proposed linear model produces reasonably accurate estimations for both the maximum deflections and the deformation profiles of each composite. In particular, we were able to identify a specific range of numbers for A that minimize the prediction errors (see, Figure 2.15). These characteristic numbers turn out to be unique for each material ($A = 208$ for CNC fiber composite and $A = 0.95$ for Nylon rubber composite) and are insensitive to either the magnitude of the applied loadings

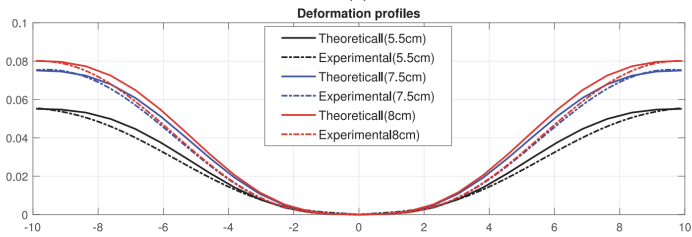
(i.e. \mathbf{r} and \mathbf{m}) or the types of boundary conditions (e.g. simple support, clamped ends). The results are also fairly close to those estimated from the nonlinear model where the A value is found to be 0.825 (see, Figure 2.16). Hence, the estimated values of A may be inferred as the intrinsic properties of the examined composites pertaining the Piola-type triple stress. Further examination regarding the triple stress parameters and the associated triple forces may be of necessary to include more general class of materials, which is beyond the scope of the present study due to the lack of available data. At the same time, progress is being made toward these problems and our intention is to report elsewhere.

2.6 Denouement

In this study, we have presented a complete linear model describing the mechanics of an elastic solid reinforced with a single family of fibers and subjected to both the double force and triple force. The kinematics of fibers have been formulated via the second and third gradient of deformations and subsequently integrated into the model of the continuum deformation. The energy density function of the Spencer and Soldatos type is augmented by the third gradient of deformations in order to accommodate the third gradient continua. Using the virtual work statement and the variational principles arising in the third gradient of virtual displacement, the Euler equation and the associated boundary conditions have also been obtained.

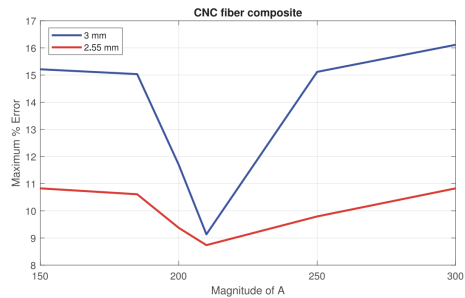


(a)

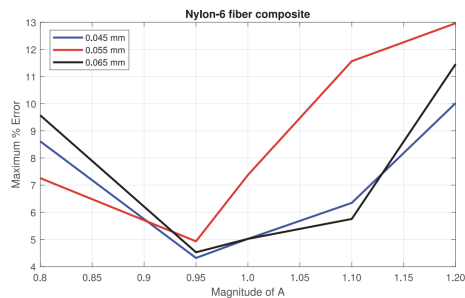


(b)

Figure 2.14: (a) is the bending experimental setup for Nylon-6 fiber neoprene rubber composite, and (b) is the numerical comparison with the Nylon-6 fiber neoprene rubber composites experimental results.



(a)



(b)

Figure 2.15: Maximum error with respect to A: CNC fiber composite (a), Neoprene rubber composite (b).

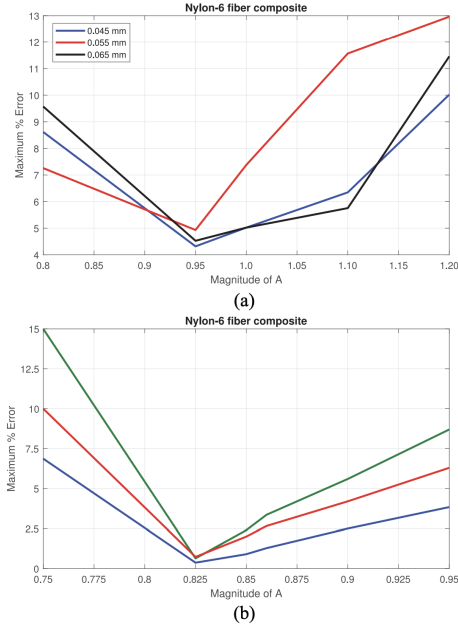


Figure 2.16: Comparison with the nonlinear solution: linear model (a), non-linear model (b).

More importantly, we have derived a compatible linear model from which a complete analytical solution has been obtained for small deformations superposed on large. The obtained solution describes smooth and dilatational shear angle distributions, unlike those predicted by the first and second gradient continuum model where either a sharp variations of the gradient fields or the non-dilatational shear zones are observed. This is due to the smooth transitions in the corresponding shear gradient fields sustained by the third gradient continua. In addition, the obtained solution demonstrates a close correspondence with the experimental results of both the CNC and rubber composites. The proposed model also predicts the intrinsic properties of the composites which may pertain to the Piola-type triple stress. Lastly, the results obtained from the proposed linear model are comparable with those obtained from the nonlinear analysis and, thus, can be employed as an alternative to the nonlinear model for small deformation analyses.

Chapter 3

A model for the second strain gradient continua reinforced with extensible fibers in plane elastostatics

3.1 Kinematics

Let $\boldsymbol{\tau}$ be the unit tangent to the fiber's parametric trajectory of $\mathbf{r}(s)$ in the current configuration and \mathbf{D} and $\mathbf{X}(S)$ are their counterparts in the reference frame. The orientations of a particular fiber are then defined by

$$\lambda = |\mathbf{d}| \text{ and } \lambda\boldsymbol{\tau} = \mathbf{d}; \lambda \equiv \frac{ds}{dS} \text{ and } \boldsymbol{\tau} \equiv \frac{d\mathbf{r}(s)}{ds}, \quad (3.1)$$

where s and S are respectively, the arclength parameters in current and reference configuration and \mathbf{d} is the director field of fibers in the reference frame which can be expressed as

$$\mathbf{d} = \mathbf{F}\mathbf{D}, \mathbf{F} = \lambda\boldsymbol{\tau} \otimes \mathbf{D}, \quad (3.2)$$

and \mathbf{F} is the first gradient of the deformation function ($\boldsymbol{\chi}(X)$). Eq. (3.2) is obtained by taking the derivative of $\mathbf{r}(S) = \boldsymbol{\chi}(X(S))$, upon making the identifications of $\mathbf{D} = dX(S)/dS$ and $\mathbf{d} = d\mathbf{r}(s)/ds$. Here $d(*)/ds$ and $d(*)/dS$ refer to the arclength derivative of $(*)$ along fibers' directions in the deformed and reference configurations, respectively. Therefore, from Eq. (3.2), the geodesic curvature of a parametric curve ($\mathbf{r}(S)$) and the associated rate of changes in

curvature are obtained by following equations

$$\mathbf{g} = \mathbf{r}'' = \frac{d^2 \mathbf{r}(s)}{ds^2} = \frac{\partial(\mathbf{F}\mathbf{D})}{\partial \mathbf{X}} \frac{d\mathbf{X}}{dS} = \nabla[\mathbf{F}\mathbf{D}]\mathbf{D}. \quad (3.3)$$

In a typical environment, most of the fibers are straight prior to deformations. Even slightly curved fibers can be idealized as ‘fairly straight’ fibers, considering their length scales with respect to that of matrix materials. This further leads to the assumption of vanishing gradients fields of \mathbf{D} (i.e. $\nabla\mathbf{D} = \mathbf{0}$). Thus, Eq. (3.3) reduces to

$$\mathbf{g}(\mathbf{G}) = \mathbf{G}(\mathbf{D} \otimes \mathbf{D}), \quad (3.4)$$

where we adopt the commonly used convention of strain gradient tensor:

$$\nabla\mathbf{F} \equiv \mathbf{G}. \quad (3.5)$$

The corresponding strain gradient field is compatible in the sense of Leibniz differentiation which can be seen as

$$G_{iAB} = F_{iA,B} = F_{iB,A} = G_{iBA}. \quad (3.6)$$

Eqs. (3.3)-(3.6) constitute a second gradient-based energy function in the description of an elastic solid reinforced with fibers resistant to flexure

$$W(\mathbf{F}, \mathbf{g}(\mathbf{G})) = W(\mathbf{F}) + \frac{1}{2}C(\mathbf{F}) |\mathbf{g}(\mathbf{G})|^2, \quad (3.7)$$

where $C(\mathbf{F})$ refers to the material parameter associated Piola-type double stress which is, in general, independent of the deformation gradient, i.e.

$$C(\mathbf{F}) = C. \quad (3.8)$$

Eq. (3.7) is based on the kinematic relevance between the bending motions of embedded fibers and the adjoined second gradient fields [41] that has been widely and successfully adopted in the relevant studies (see, for example, [9], [73], [76], and [74]). For the desired applications, the above energy potential is now augmented to accommodate extensible fibers as

$$W(\mathbf{F}, \varepsilon(\mathbf{F}), \mathbf{g}(\mathbf{G})) = W(\mathbf{F}) + \frac{1}{2}E\varepsilon^2 + \frac{1}{2}C |\mathbf{g}(\mathbf{G})|^2, \quad (3.9)$$

where E is a modulus pertaining to the fiber's extension and the expression of ε is given by

$$\varepsilon = \frac{1}{2}(\lambda^2 - 1). \quad (3.10)$$

Further, in view of Eqs. (3.1)-(3.2), λ^2 can be written in terms of the deformation gradient tensor \mathbf{F} and the director field of fibers \mathbf{D} as

$$\lambda^2 = \mathbf{F}\mathbf{D} \cdot \mathbf{F}\mathbf{D} = \mathbf{F}^T\mathbf{F}\mathbf{D} \cdot \mathbf{D} = (\mathbf{F}^T\mathbf{F}) \cdot \mathbf{D} \otimes \mathbf{D}. \quad (3.11)$$

In particular, the third gradient of deformations is introduced into the models of continuum deformation to achieve a more comprehensive description of generalized continua of higher-order. More precisely, we compute the rate of changes in curvature at points of the fibers as

$$\begin{aligned} \boldsymbol{\alpha} = \mathbf{r}''' &= \frac{d(\nabla[\mathbf{F}\mathbf{D}]\mathbf{D})}{dS} = \frac{\partial(\nabla[\mathbf{F}\mathbf{D}]\mathbf{D})}{\partial\mathbf{X}} \frac{d\mathbf{X}}{dS} = [\nabla\{\nabla[\mathbf{F}\mathbf{D}]\mathbf{D}\}]\mathbf{D} \\ &= [\nabla\{\nabla[\mathbf{F}\mathbf{D}]\}\mathbf{D} + \nabla[\mathbf{F}\mathbf{D}](\nabla\mathbf{D})]\mathbf{D}, \end{aligned} \quad (3.12)$$

such that the interactions between the fibers and the surrounding matrix may be characterized. The required third order gradient fields can be formulated in the same spirit as Eqs (3.4)-(3.5) that

$$\begin{aligned} \boldsymbol{\alpha} &= \nabla(\nabla\mathbf{F})(\mathbf{D} \otimes \mathbf{D} \otimes \mathbf{D}), \\ \nabla(\nabla\mathbf{F}) &= \nabla(\mathbf{G}) \equiv \mathbf{H}, \text{ and} \\ \boldsymbol{\alpha} &= \mathbf{H}(\mathbf{D} \otimes \mathbf{D} \otimes \mathbf{D}) = \boldsymbol{\alpha}(\mathbf{H}, \mathbf{D}). \end{aligned} \quad (3.13)$$

Consequently, the energy potential accommodating the third gradient of continuum deformation can be obtained as

$$\begin{aligned} W(\mathbf{F}, \varepsilon(\mathbf{F}), \mathbf{g}(\mathbf{G}), \boldsymbol{\alpha}(\mathbf{H})) &= W(\mathbf{F}) + \frac{1}{2}E\varepsilon^2 + \frac{1}{2}C|\mathbf{g}(\mathbf{G})|^2 \\ &+ \frac{1}{2}A(\mathbf{H})|\boldsymbol{\alpha}(\mathbf{H})|^2. \end{aligned} \quad (3.14)$$

We note here that, similar to Eq. (3.8), $A(\mathbf{H})$ pertaining to the third gradient of continuum deformations is assumed to be constant for the sake of simplicity.

$$A(\mathbf{H}) = A. \quad (3.15)$$

The phenomenological implications vis-a-vis the third gradient of deformations (e.g., interactions between fibers and a matrix material) and the identification of the associated coefficient (here, denoted as A) is addressed in the literature [86], [82], [79], [87], [88], and [89]. In the present study, we place an emphasis on the development of a mathematical framework and the associated analyses in order to promote the implementation of higher-order strain gradient theory in plane elastostatics. For uses in the derivation of Euler equations and the necessary boundary conditions, we continue by evaluating the induced energy variation of the response function with respect to $\mathbf{F}, \varepsilon, \mathbf{g}$, and $\boldsymbol{\alpha}$ as

$$\dot{W}(\mathbf{F}, \varepsilon, \mathbf{g}, \boldsymbol{\alpha}) = W_{\mathbf{F}} \cdot \dot{\mathbf{F}} + W_{\varepsilon} \dot{\varepsilon} + W_{\mathbf{g}} \cdot \dot{\mathbf{g}} + W_{\boldsymbol{\alpha}} \cdot \dot{\boldsymbol{\alpha}}, \quad (3.16)$$

where the superposed dot refers to derivatives with respect to a parameter ϵ at the particular configuration of the composite ($\epsilon = 0$) that labels a one-parameter family of deformations.

The desired expressions for the induced energy variation can be obtained from Eqs. (3.4) and (3.10)-(3.14) that

$$\begin{aligned} \dot{\varepsilon} &= \frac{1}{2}(\lambda^2 - 1) = \frac{1}{2}(\mathbf{FD} \cdot \mathbf{FD} - \mathbf{1}) = \mathbf{FD} \cdot \dot{\mathbf{F}}\mathbf{D} = \mathbf{FD} \otimes \mathbf{D} \cdot \dot{\mathbf{F}}, \quad W_{\varepsilon} \dot{\varepsilon} \\ &= \left(\frac{1}{2}E\varepsilon^2\right) = E\varepsilon \dot{\varepsilon}, \end{aligned} \quad (3.17)$$

$$W_{\mathbf{g}} \cdot \dot{\mathbf{g}} = C\mathbf{g} \cdot \dot{\mathbf{g}} = Cg_j \mathbf{e}_j \cdot \dot{G}_{iAB} D_A D_B \mathbf{e}_i = Cg_i D_A D_B \dot{G}_{iAB}, \quad (3.18)$$

and

$$\dot{W}(\mathbf{H}) = A\boldsymbol{\alpha} \cdot \dot{\boldsymbol{\alpha}} = A\alpha_j \mathbf{e}_j \cdot \dot{H}_{iABC} D_A D_B D_C \mathbf{e}_i = A\alpha_i D_A D_B D_C \dot{H}_{iABC}. \quad (3.19)$$

Hence, from Eqs. (3.16)-(3.19), we find

$$\begin{aligned} \dot{W}(\mathbf{F}, \varepsilon, \mathbf{g}, \boldsymbol{\alpha}) &= W_{F_{iA}} \dot{F}_{iA} + \frac{E}{2}(F_{jC} F_{jD} D_C D_D - 1)(F_{iB} D_B D_A) \dot{F}_{iA} \\ &+ Cg_i D_A D_B \dot{G}_{iAB} + A\alpha_i D_A D_B D_C \dot{H}_{iABC}. \end{aligned} \quad (3.20)$$

Clearly, the resulting energy variation (Eq. (3.20)) is dependent on both the second and third gradients of continuum deformations as intended. It will be seen in the later sections that Eq. (3.20) furnishes the relevant mathematical framework to accommodate the triple force (e.g. interaction forces) and its energy couple (Piola-type triple stress) sustained by the third-gradient continua.

3.2 Equilibrium

The derivation of the Euler equation and boundary conditions arising in second-gradient elasticity is well-established (see, for example, [79], [90] and references therein). In this section, we present a variational formulation arising in the third gradient of the continuum deformation by employing the principles of the virtual work statement and iterated integrations by parts [82], [79]-[88] and [89].

In a typical environment, volumetric changes in materials' deformations are energetically expensive processes and thus are constrained in most of engineering analyses (see, also, [77],[28]). This can be achieved by introducing the weak form of bulk incompressibility condition into the proposed energy potential such that

$$U(\mathbf{F}, \varepsilon, \mathbf{g}, \boldsymbol{\alpha}, p) = W(\mathbf{F}, \varepsilon, \mathbf{g}, \boldsymbol{\alpha}) - p(J - 1), \quad (3.21)$$

J is determinant of \mathbf{F} and p is a constitutively indeterminate scalar field. The strain energy of the system is then expressed as

$$E = \int_{\Omega} U(\mathbf{F}, \mathbf{G}, \mathbf{H}, p) dA, \quad (3.22)$$

where Ω is the referential domain occupied by a fiber-matrix material.

Now, the principle of virtual work states that

$$\dot{E} = P. \quad (3.23)$$

In the above, P is the virtual work of the applied load and the superposed dot refers to the variational and/or Gateaux derivative. Since the conservative loads are characterized by the existence of a potential L such that $P = \dot{L}$, the problem of determining equilibrium deformations is then reduced to the problem of minimizing the potential energy $E - L$. Accordingly, we find

$$\dot{E} = \int_{\Omega} \dot{U}(\mathbf{F}, \mathbf{G}, \mathbf{H}, p) dA. \quad (3.24)$$

Using the identity $\dot{J} = J_{\mathbf{F}}\mathbf{F} \cdot \dot{\mathbf{F}} = \mathbf{F}^* \cdot \dot{\mathbf{F}}$ together with the results in Eqs. (3.20)-(3.21), the variational derivative of the augmented energy potential can be

evaluated as

$$\begin{aligned}\dot{U} &= \dot{W} - p\dot{J} = [W_{F_{iA}}u_{i,A} + \frac{E}{2}(F_{jC}F_{jD}D_C D_D - 1)(F_{iB}D_B D_A)u_{i,A} \\ &+ C(g_i D_A D_B)u_{i,AB} + A(\alpha_i D_A D_B D_C)u_{i,ABC} - pF_{iA}^* u_{iA}],\end{aligned}\quad (3.25)$$

where $u_i = \dot{\chi}_i$ is the variation of the position field. Hence Eqs. (3.24)-(3.25) yield

$$\begin{aligned}\dot{E} &= \int_{\Omega} [W_{F_{iA}}u_{i,A} + \frac{E}{2}(F_{jC}F_{jD}D_C D_D - 1)(F_{iB}D_B D_A)u_{i,A} \\ &+ C(g_i D_A D_B)u_{i,AB} + A(\alpha_i D_A D_B D_C)u_{i,ABC} - pF_{iA}^* u_{iA}]dA.\end{aligned}\quad (3.26)$$

Applying integration by parts on the third and fourth terms in Eq. (3.18), we find

$$\begin{aligned}C(g_i D_A D_B)u_{i,AB} &= C(g_i D_A D_B u_{i,A}),_B - C(g_i D_A D_B),_B u_{i,A}, \text{ and} \\ A(\alpha_i D_A D_B D_C)u_{i,ABC} &= A(\alpha_i D_A D_B D_C u_{i,AB}),_C \\ &- A(\alpha_i D_A D_B D_C),_C u_{i,AB},\end{aligned}\quad (3.27)$$

and thereby obtain

$$\begin{aligned}\dot{E} &= \int_{\Omega} [W_{F_{iA}}u_{i,A} + \frac{E}{2}(F_{jC}F_{jD}D_C D_D - 1)(F_{iB}D_B D_A)u_{i,A} \\ &+ C(g_i D_A D_B u_{i,A}),_B - C(g_i D_A D_B),_B u_{i,A} + A(\alpha_i D_A D_B D_C u_{i,AB}),_C \\ &- A(\alpha_i D_A D_B D_C),_C u_{i,AB} - pF_{iA}^* u_{iA}]dA.\end{aligned}\quad (3.28)$$

Eq. (3.28) may be recast as

$$\begin{aligned}\dot{E} &= \int_{\Omega} [W_{F_{iA}}u_{i,A} - pF_{iA}^* u_{iA} + \frac{E}{2}(F_{jC}F_{jD}D_C D_D - 1)(F_{iB}D_B D_A) \\ &- C(g_i D_A D_B),_B]u_{i,A}dA - \int_{\Omega} [A(\alpha_i D_A D_B D_C),_C u_{i,AB}]dA \\ &+ \int_{\partial\Omega} (Cg_i D_A D_B u_{i,A})N_B dS + \int_{\partial\Omega} (A\alpha_i D_A D_B D_C u_{i,AB})N_C dS,\end{aligned}\quad (3.29)$$

where \mathbf{N} is the rightward unit normal to the boundary $\partial\Omega$ in the sense of Green-Stoke's theorem. To obtain the desired expression, we again apply integration by parts and the Green-Stoke's theorem on the second integral of

the above; i.e.

$$\begin{aligned}
\int_{\Omega} [A(\alpha_i D_A D_B D_C)_{,C} u_{i,AB}] dA &= \int_{\Omega} [\{A(\alpha_i D_A D_B D_C)_{,C} u_{i,A}\}_{,B} \\
&- A(\alpha_i D_A D_B D_C)_{,CB} u_{i,A}] dA = \int_{\partial\Omega} A(\alpha_i D_A D_B D_C)_{,C} u_{i,A} N_B dS \\
&- \int_{\Omega} A(\alpha_i D_A D_B D_C)_{,CB} u_{i,A} dA. \tag{3.30}
\end{aligned}$$

The substitution of Eq. (3.30) into Eq. (3.29) then furnishes

$$\begin{aligned}
\dot{E} &= \int_{\Omega} [W_{F_{iA}} u_{i,A} - p F_{iA}^* u_{iA} + \frac{E}{2} (F_{jC} F_{jD} D_C D_D - 1) (F_{iB} D_B D_A) \\
&- C(g_i D_A D_B)_{,B} + A(\alpha_i D_A D_B D_C)_{,CB}] u_{i,A} dA \int_{\partial\Omega} [\{C g_i D_A D_B \\
&- A(\alpha_i D_A D_B D_C)_{,C}\} u_{i,A} N_B + A \alpha_i D_A D_B D_C u_{i,AB} N_C] dS. \tag{3.31}
\end{aligned}$$

Finally, we obtain

$$\begin{aligned}
\dot{E} &= \int_{\Omega} P_{iA} u_{i,A} dA + \int_{\partial\Omega} [\{C g_i D_A D_B - A(\alpha_i D_A D_B D_C)_{,C}\} u_{i,A} N_B \\
&+ A \alpha_i D_A D_B D_C u_{i,AB} N_C] dS, \tag{3.32}
\end{aligned}$$

where

$$\begin{aligned}
P_{iA} &= W_{F_{iA}} u_{i,A} - p F_{iA}^* u_{iA} + \frac{E}{2} (F_{jC} F_{jD} D_C D_D - 1) (F_{iB} D_B D_A) \\
&- C(g_i D_A D_B)_{,B} + A(\alpha_i D_A D_B D_C)_{,CB}. \tag{3.33}
\end{aligned}$$

Hence, the Euler equation satisfies

$$P_{iA,A} = 0 \text{ or } Div(\mathbf{P}) = 0 \tag{3.34}$$

which holds in Ω . It is also noted here that, for the sake of clarity and completeness, the appropriate tensorial notations of Eqs. (3.32)-(3.33) may be found as

$$\begin{aligned}
\dot{E} &= \int_{\Omega} \mathbf{P} \cdot \dot{\mathbf{F}} dA + \int_{\partial\Omega} [\{C(\mathbf{g} \otimes \mathbf{D} \otimes \mathbf{D})^T - (Div(\boldsymbol{\alpha} \otimes \mathbf{D} \otimes \mathbf{D} \otimes \mathbf{D}))^T\} \mathbf{F}^T \\
&+ (\boldsymbol{\alpha} \otimes \mathbf{D} \otimes \mathbf{D} \otimes \mathbf{D})(\nabla \mathbf{F})^T] \cdot \mathbf{N} dS, \tag{3.35}
\end{aligned}$$

and

$$\begin{aligned}
\mathbf{P} &= W_{\mathbf{F}} - p \mathbf{F}^* + \frac{E}{2} (\mathbf{F} \mathbf{D} \cdot \mathbf{F} \mathbf{D} - 1) \mathbf{F} (\mathbf{D} \otimes \mathbf{D}) \\
&- Div(C \mathbf{g} \otimes \mathbf{D} \otimes \mathbf{D}) + Div(Div(A \boldsymbol{\alpha} \otimes \mathbf{D} \otimes \mathbf{D} \otimes \mathbf{D})), \tag{3.36}
\end{aligned}$$

which clearly meet the basis agreement requirement arising in multilinear transformations of higher-order tensors with mixed bases.

3.3 Boundary conditions

The incorporation of the high order gradient fields into the model of the continuum deformation leads to the necessary existence of their high-order energy conjugate pairs (e.g., triple forces, contact interactions) suitably imposed on the desired boundaries. Although the roles and phenomenological implications regarding these higher-order boundary conditions are discussed in number of studies (see, for example, [82], [87], [88], [91], and [92]), their implementation, particularly those arising in plane elastostatics, in the actual analytical platform has not been well addressed. Throughout the section, we present rigorous derivations vis-a-vis admissible boundary forces of higher-order exerted on the third-gradient continua.

To proceed, we apply integration by parts (i.e. $P_{iA}u_{i,A} = (P_{iA}u_i)_{,A} - P_{iA,A}u_i$) on the first term of Eq. (3.32) and thereby obtain

$$\begin{aligned} \dot{E} = & \int_{\partial\Omega} P_{iA}u_i N_A dS - \int_{\Omega} P_{iA,A}u_i dA + \int_{\partial\Omega} [\{W_{G_{iAB}} - (W_{H_{iABC}})_{,C}\}u_{i,A}N_B \\ & + W_{H_{iABC}}u_{i,AB}N_C]dS, \end{aligned} \quad (3.37a)$$

where we define:

$$W_{G_{iAB}} \equiv Cg_i D_A D_B \text{ and } W_{H_{iABC}} \equiv A\alpha_i D_A D_B D_C, \quad (3.38)$$

for the notational simplicity in the forgoing derivations. Since the Euler equation, $P_{iA,A} = 0$, holds in Ω , the above reduces to

$$\dot{E} = \int_{\partial\Omega} P_{iA}u_i N_A dS + \int_{\partial\Omega} [\{W_{G_{iAB}} - (W_{H_{iABC}})_{,C}\}u_{i,A}N_B + W_{H_{iABC}}u_{i,AB}N_C]dS, \quad (3.39)$$

Now, the projection of onto normal and tangential direction yields

$$\nabla \mathbf{u} = \nabla \mathbf{u}(\mathbf{T} \otimes \mathbf{T}) + \nabla \mathbf{u}(\mathbf{N} \otimes \mathbf{N}) = \mathbf{u}' \otimes \mathbf{T} + \mathbf{u}_{,N} \otimes \mathbf{N}, \quad (3.40a)$$

In the above \mathbf{u}' and $\mathbf{u}_{,N}$ are respectively the tangential and normal derivatives of \mathbf{u} such that

$$u'_i = u_{i,A}T_A, \quad u_{i,N} = u_{i,A}N_A, \quad (3.41)$$

and $\mathbf{T} = \mathbf{X}'(S) = \mathbf{k} \times \mathbf{N}$ is the unit tangent to the boundary ($\partial\Omega$) and \mathbf{N} is the associated unit normal. Hence, invoking Eqs. (3.40a)-(3.41), the projections

of the first and second coordinate derivatives of u_i can be found respectively as

$$u_{i,A} = \frac{du_i}{ds} \frac{ds}{dX_A} + \frac{du_i}{dN} \frac{dN}{dX_A} = u'_i T_A + u_{i,N} N_A, \quad \text{and} \quad (3.42)$$

$$\begin{aligned} u_{i,AB} &= u''_i T_A T_B + u'_i (T'_A T_B + T_{A,N} N_B) + u_{i,N} (N'_A T_B + N_{A,N} N_B) \\ &+ u'_{i,N} (N_A T_B + T_A N_B) + u_{i,NN} N_A N_B. \end{aligned} \quad (3.43)$$

We then substitute Eq. (3.43) into Eq. (3.39) and thereby obtain

$$\begin{aligned} \dot{E} &= \int_{\partial\Omega} P_{iA} u_i N_A dS + \int_{\partial\Omega} [W_{G_{iAB}} - (W_{H_{iABC}})_{,C}] (u'_i T_A + u_{i,N} N_A) N_B dS \\ &+ \int_{\partial\Omega} W_{H_{iABC}} [u''_i T_A T_B + u'_i (T'_A T_B + T_{A,N} N_B) + u_{i,N} (N'_A T_B + N_{A,N} N_B) \\ &+ u'_{i,N} (N_A T_B + T_A N_B) + u_{i,NN} N_A N_B] N_C dS. \end{aligned} \quad (3.44)$$

In order to obtain desired expressions, we apply iterated integration by parts on the tangential derivatives of \mathbf{u} in Eq. (3.44). For example,

$$W_{G_{iAB}} T_A N_B u'_i = (W_{G_{iAB}} T_A N_B u_i)' - (W_{G_{iAB}} T_A N_B)' u_i, \quad (3.45)$$

$$\begin{aligned} W_{H_{iABC}} (N_A T_B N_C + T_A N_B N_C) u'_{i,N} &= [W_{H_{iABC}} (N_A T_B N_C + T_A N_B N_C) u_{i,N}] \\ &' - [W_{H_{iABC}} (N_A T_B N_C + T_A N_B N_C)]' u_{i,N}, \end{aligned} \quad (3.46)$$

$$\begin{aligned} W_{H_{iABC}} T_A T_B N_C u''_i &= (W_{H_{iABC}} T_A T_B N_C u_i)'' + (W_{H_{iABC}} T_A T_B N_C)'' u_i \\ &- 2 \left[(W_{H_{iABC}} T_A T_B N_C)' u_i \right]', \end{aligned} \quad (3.47)$$

and similarly for other terms. Therefore, Eq. (3.44) can be replaced with

$$\begin{aligned}
\dot{E} &= \int_{\partial\Omega} [P_{iA}N_A - \{W_{G_{iAB}}T_A N_B - (W_{H_{iABC}})_{,C}T_A N_B\}'] u_i dS \\
&- \int_{\partial\Omega} [\{W_{H_{iABC}}(T'_A T_B N_C + T_{A,N} N_B N_C)\}' - (W_{H_{iABC}} T_A T_B N_C)''] u_i dS \\
&+ \int_{\partial\Omega} [\{W_{G_{iAB}}T_A N_B - (W_{H_{iABC}})_{,C}T_A N_B - 2(W_{H_{iABC}} T_A T_B N_C)'\} u_i]' dS \\
&+ \int_{\partial\Omega} [W_{H_{iABC}}(T'_A T_B N_C + T_{A,N} N_B N_C) u_i]' dS \\
&+ \int_{\partial\Omega} [W_{H_{iABC}}(N_A T_B N_C + T_A N_B N_C) u_{i,N}]' dS \\
&+ \int_{\partial\Omega} [\{(W_{G_{iAB}}) - (W_{H_{iABC}})_{,C}\} N_A N_B \\
&+ W_{H_{iABC}}(N'_A T_B + N_{A,N} N_B) N_C] u_{i,N} dS \\
&- \int_{\partial\Omega} [\{W_{H_{iABC}}(N_A T_B N_C + T_A N_B N_C)\}'] u_{i,N} dS \\
&+ \int_{\partial\Omega} (W_{H_{iABC}} T_A T_B N_C u_i)'' dS + \int_{\partial\Omega} W_{H_{iABC}} u_{i,NN} N_A N_B N_C dS. \quad (3.48)
\end{aligned}$$

The above may be further recast as

$$\begin{aligned}
\dot{E} &= \int_{\partial\Omega} [P_{iA}N_A - \{(Cg_i - A\alpha_{i,C}D_C)D_A T_A D_B N_B\}' \\
&- \{A\alpha_i D_C N_C (D_A T'_A D_B T_B + D_A T_{A,N} D_B N_B)\}'] u_i dS \\
&+ \int_{\partial\Omega} [(A\alpha_i D_A T_A D_B T_B D_C N_C)''] u_i dS \\
&+ \sum \left\| A\alpha_i (D_A T'_A D_B T_B D_C N_C + D_A T_{A,N} D_B N_B D_C N_C) u_i \right\| \\
&+ \sum \left\| [(Cg_i - A\alpha_{i,C}D_C)D_A T_A D_B N_B - 2(A\alpha_i D_A T_A D_B T_B D_C N_C)'] u_i \right\| \\
&+ \sum \left\| A\alpha_i (D_A N_A D_B T_B D_C N_C + D_A T_A D_B N_B D_C N_C) u_{i,N} \right\| \\
&+ \sum \left\| \frac{d}{ds} (A\alpha_i D_A T_A D_B T_B N_C D_C u_i) \right\| \\
&+ \int_{\partial\Omega} [(Cg_i - A\alpha_{i,C}D_C)D_A N_A D_B N_B] \\
&+ [A\alpha_i D_C N_C (D_A N'_A D_B T_B + D_A N_{A,N} D_B N_B)] u_{i,N} dS \\
&- \int_{\partial\Omega} [\{A\alpha_i D_A D_B D_C (N_A T_B N_C + T_A N_B N_C)\}'] u_{i,N} dS \\
&+ \int_{\partial\Omega} (A\alpha_i D_A N_A D_B N_B D_C N_C u_{i,NN}) dS, \quad (3.49)
\end{aligned}$$

where the double bar symbol refers to the jump across the discontinuities on the boundary $\partial\Omega$ (i.e. $\|*\| = (*)^+ - (*)^-$) and the sum refers to the collection

of all discontinuities. But the virtual work statement for the conservative loads suggest the admissible mechanical powers are of the form

$$P = \int_{\partial w_t} t_i u_i dS + \int_{\partial w} m_i u_{i,N} dS + \int_{\partial w} r_i u_{i,NN} dS + \sum f_i u_i + \sum h_i u_{i,N}, \quad (3.50)$$

Consequently, by comparing Eqs. (3.49) and (3.50), we obtain

$$\begin{aligned} t_i &= P_{iA} N_A + \frac{d^2}{ds^2} (A\alpha_i D_A T_A D_B T_B D_C N_C) \\ &\quad - \frac{d}{ds} [(Cg_i - A\alpha_{i,C} D_C) D_A T_A D_B N_B \\ &\quad - A\alpha_i D_C N_C (D_A T'_A D_B T_B + D_A T_{A,N} D_B N_B)], \\ m_i &= (Cg_i - A\alpha_{i,C} D_C) D_A N_A D_B N_B \\ &\quad + A\alpha_i D_C N_C (D_A N'_A D_B T_B + D_A N_{A,N} D_B N_B) \\ &\quad - \frac{d}{ds} (2A\alpha_i D_A D_B D_C N_A T_B N_C), \\ r_i &= A\alpha_i D_A N_A D_B N_B D_C N_C, \\ f_i &= (Cg_i - A\alpha_{i,C} D_C) D_A T_A D_B N_B - \frac{d}{ds} (2A\alpha_i D_A T_A D_B T_B D_C N_C) \\ &\quad + A\alpha_i (D_A T'_A D_B T_B D_C N_C + D_A T_{A,N} D_B N_B D_C N_C), \\ \frac{d(f_i)}{ds} &= \frac{d}{ds} (A\alpha_i D_A T_A D_B T_B N_C D_C), \\ h_i &= 2A\alpha_i D_A N_A D_B T_B D_C N_C, \end{aligned} \quad (3.51)$$

In the above t_i , m_i and f_i are, respectively, the expressions of edge tractions, edge moments and the corner forces. But more importantly, additional interaction boundary conditions (i.e. r_i , $d(f_i)/ds$, h_i) are obtained via the introduction of the third gradient of deformations. These boundary conditions can be understood as the set of admissible contact interactions suitably sustained by the third-gradient continua (see, for example, [79], [82] and [89]). Moreover, the induced interaction forces are, in turn, coupled with the Piola-type triple stress and thus fall into the category of triple forces that characterize the mechanical contacts on the edges and points of Cauchy cuts [91], [82] and [87]. In the present case, the latter would mean the effects of local interactions between the fiber and matrix which are assimilated via the computation of the third gradient of the continuum deformation on the convected curves of fibers.

We remark here that the obtained triple forces are meaningful only if there exist their conjugate pairs (a class of Piolar-type triple stress) and are necessary to capture the internal energy contributions to the mechanical contact interactions induced on the adjoined boundary. In fact, such necessary mutual existence arising in the third gradient of continuum deformation is equally valid to a class of forces and stresses exerted by lower-order continua. For example, the prescribed double force m_i is the energy pair to the Piolar-type double stress $(Cg_{i,B}D_AD_B)$.

If fibers are aligned along the directions of either normal and/or tangential (such cases are commonly observed in meshed composites, fabric composites and particulate composites produced under controlled environment), we find

$$D_AT_AD_BN_B = 0 \text{ and } T_{A,N} = T'_A = N_{A,N} = N'_A 0, \quad (3.52)$$

and thus Eq. (3.51) reduces to

$$\begin{aligned} t_i &= P_{iA}N_A \\ m_i &= (Cg_i - A\alpha_{i,C}D_C)D_AN_AD_BN_B \\ r_i &= A\alpha_iD_AN_AD_BN_BD_CN_C, \\ f_i &= 0, \\ \frac{d(f_i)}{ds} &= 0, \\ h_i &= 0. \end{aligned} \quad (3.53)$$

Further, the expression of the associated Piolar-stress now becomes

$$\begin{aligned} P_{iA} &= W_{F_{iA}}u_{i,A} - pF_{iA}^*u_{iA} + \frac{E}{2}(F_{jC}F_{jD}D_CD_D - 1)(F_{iB}D_BD_A) \\ &\quad - Cg_{i,B}D_AD_B + A\alpha_{i,BC}D_AD_BD_C, \\ g_i &= F_{iA,B}D_AD_B \text{ and } \alpha_i = F_{iA,BC}D_AD_BD_C. \end{aligned} \quad (3.54)$$

It is clear from Eq. (3.54) that, in the cases of aligned fibers, r_i is the only meaningful boundary conditions due to the third gradient of continuum deformations (i.e. f_i , $d(f_i)/ds$ and h_i are vanished identically). We also note that the imposition of r_i is necessary to determine a unique solution when solving the associated Euler equation (i.e. Eq. (3.51)). The classifications of the

obtained triple forces and boundary conditions may be of practical interest. In this respect, a number of cases are investigated under the prescription of superposed incremental deformations in the foregoing sections.

3.4 Linear Theory

Based on the constitutive formulations presented in the previous sections, we develop a compatible linear model which describes the mechanical responses of an elastic solid reinforced with fiber's resistance to extension and flexure.

For this purpose, we consider, superposed '*small*' deformations defined by

$$\boldsymbol{\chi} = \boldsymbol{\chi}_o + \epsilon \dot{\boldsymbol{\chi}} ; |\epsilon| \ll 1, \quad (3.55)$$

where $(\dot{*}) = \partial(*)/\partial\epsilon$, $\dot{\boldsymbol{\chi}} = \mathbf{u}$ and $(*)_o$ denote configuration of $*$ evaluated at $\epsilon = 0$, $(\dot{*}) = \partial(*)/\partial\epsilon$. Here caution needs to be taken that the present notation is not confused with the one used for the variational computation. Therefore, the deformation gradient tensor can be approximated as

$$\mathbf{F} = \mathbf{F}_o + \epsilon \nabla \mathbf{u}, \text{ where } \dot{\mathbf{F}} = \nabla \mathbf{u}. \quad (3.56)$$

In a typical environment, the body is initially undeformed and stress-free. This can be accommodated by imposing the initial conditions of

$$\mathbf{F}_o = \mathbf{I} \text{ and } \mathbf{P}_o = \mathbf{0}, \text{ at } \epsilon = 0, \quad (3.57)$$

from which we subsequently reduce Eq. (3.56) to

$$\mathbf{F} = \mathbf{I} + \epsilon \nabla \mathbf{u}. \quad (3.58)$$

Eq. (3.58) further leads to

$$\mathbf{F}^{-1} = \mathbf{I} - \epsilon \nabla \mathbf{u} + o(\epsilon) \text{ and } J = \det \mathbf{F} = 1 + \epsilon \operatorname{div} \mathbf{u} + o(\epsilon), \quad (3.59a)$$

which are the linearized expressions of the inverse and determinant of deformation gradient tensor \mathbf{F} . Similarly, the constraint of bulk incompressibility can be approximated as

$$(J - 1) \dot{} = \mathbf{F}_o^* \cdot \dot{\mathbf{F}} = \operatorname{div} \mathbf{u} = 0. \quad (3.60)$$

Now, using Eq. (3.55), the Euler equation (Eq. (3.30)) can be expanded as

$$Div(\mathbf{P}) = Div(\mathbf{P}_o) + \epsilon Div(\dot{\mathbf{P}}) + o(\epsilon) = \mathbf{0}. \quad (3.61)$$

Dividing the above by ϵ and limiting $\epsilon \rightarrow 0$, we obtain

$$Div(\dot{\mathbf{P}}) = 0 \text{ or } \dot{P}_{iA,A} = 0, \quad (3.62)$$

For the use in Eq. (3.62), the expression of \dot{P}_{iA} can be obtained from Eq. (3.29) that

$$\begin{aligned} \dot{P}_{iA} &= (W_{F_{iA}}) - \dot{p}(F_{iA}^*)_o - p\dot{F}_{iA}^* + E[\dot{F}_{jC}(F_{jD})_o D_C D_D][(F_{iB})_o D_B D_A] \\ &+ \frac{E}{2}[(F_{jC})_o (F_{jD})_o D_C D_D - 1](\dot{F}_{iB} D_B D_A) - C\dot{g}_{i,B} D_A D_B \\ &+ A(\alpha_i D_A D_B D_C)_{,CB}. \end{aligned} \quad (3.63)$$

Also, evaluating at $\epsilon = 0$ (e.g. $(F_{jD})_o = \delta_{jD}$, $(F_{iA}^*)_o = \delta_{iA}$), we reduce Eq. (3.63) to

$$\begin{aligned} \dot{P}_{iA} &= (W_{F_{iA}}) + E u_{j,B} D_A D_B D_i D_j - \dot{p}\delta_{iA} - p_o \dot{F}_{iA}^* - C u_{i,BCD} D_C D_D D_A D_B \\ &+ A[(u_{i,EFG} D_E D_F D_G) D_A D_B D_C]_{,CB}, \end{aligned} \quad (3.64)$$

where:

$$\delta_{jC} \delta_{jD} D_C D_D = D_C D_C = 1, \quad \dot{g}_{i,B} = \dot{F}_{iC,BD} D_C D_D \text{ and } \alpha_i = u_{i,EFG} D_E D_F D_G.$$

It is noted that the reference and current bases are now merged so that the initial director field \mathbf{D} is represented by the current basis (i.e. $D_i \mathbf{e}_i$) not by the reference frame (i.e. $D_A \mathbf{E}_A$). This can be explained by the collapse of the two different bases dictated by the linear theory of elasticity (i.e. $\mathbf{e}_i \equiv \mathbf{E}_A$; see, also, [77] and [28]). Hence, From Eqs. (3.62) and (3.64), the linearized Euler equations can be obtained as

$$\begin{aligned} \dot{P}_{iA,A} &= (W_{F_{iA}})_{,A} + E(u_{j,B} D_A D_B D_i D_j)_{,A} - \dot{p}_{,i} - C(u_{i,BCD} D_C D_D D_A D_B)_{,A} \\ &+ A[(u_{i,EFG} D_E D_F D_G) D_A D_B D_C]_{,CBA}, \end{aligned} \quad (3.65)$$

where $\dot{F}_{iA,A}^* = 0$ (Piola's identity) and $(\dot{p}\delta_{iA})_{,A} = \dot{p}_{,A}\delta_{iA} = \dot{p}_{,i}$.

In the case of initially straight fibers (i.e. $\nabla \mathbf{D} = 0$), the above further reduces to

$$\begin{aligned} \dot{P}_{iA,A} &= (W_{F_{iA}})_{,A} + E u_{j,AB} D_A D_B D_i D_j - \dot{p}_{,i} - C u_{i,ABCD} D_C D_D D_A D_B \\ &+ A u_{i,ABCEFG} D_A D_B D_C D_E D_F D_G = 0. \end{aligned} \quad (3.66)$$

Lastly, the boundary conditions in Eq. (3.51) can be approximated similarly as in the above (e.g. $\mathbf{t} = \mathbf{t}_o + \varepsilon \dot{\mathbf{t}} + o(\varepsilon)$ etc...)

$$\begin{aligned}
\dot{t}_i &= \dot{P}_{iA} N_A + \frac{d^2}{ds^2} (A \dot{\alpha}_i D_A T_A D_B T_B D_C N_C) \\
&\quad - \frac{d}{ds} [(C \dot{g}_i - A \dot{\alpha}_{i,C} D_C) D_A T_A D_B N_B \\
&\quad - A \dot{\alpha}_i D_C N_C (D_A T'_A D_B T_B + D_A T_{A,N} D_B N_B)], \\
\dot{m}_i &= (C \dot{g}_i - A \dot{\alpha}_{i,C} D_C) D_A N_A D_B N_B \\
&\quad + A \dot{\alpha}_i D_C N_C (D_A N'_A D_B T_B + D_A N_{A,N} D_B N_B) \\
&\quad - \frac{d}{ds} (2A \dot{\alpha}_i D_A D_B D_C N_A T_B N_C), \\
\dot{r}_i &= A \dot{\alpha}_i D_A N_A D_B N_B D_C N_C, \\
\dot{f}_i &= (C \dot{g}_i - A \dot{\alpha}_{i,C} D_C) D_A T_A D_B N_B - \frac{d}{ds} (2A \dot{\alpha}_i D_A T_A D_B T_B D_C N_C) \\
&\quad + A \dot{\alpha}_i (D_A T'_A D_B T_B D_C N_C + D_A T_{A,N} D_B N_B D_C N_C), \\
\frac{d(\dot{f}_i)}{ds} &= \frac{d}{ds} (A \dot{\alpha}_i D_A T_A D_B T_B N_C D_C), \\
\dot{h}_i &= 2A \dot{\alpha}_i D_A N_A D_B T_B D_C N_C.
\end{aligned} \tag{3.67}$$

Hence, Eqs. (3.60), (3.66) and (3.67) determine the deformed configurations of fiber composites for small deformations superposed on large. In particular, if the fiber's directions are either normal or tangential to the boundary (see, Eq. (3.52)), the above becomes

$$\begin{aligned}
\dot{t}_i &= \dot{P}_{iA} N_A \\
\dot{m}_i &= (C \dot{g}_i - A \dot{\alpha}_{i,C} D_C) D_A N_A D_B N_B \\
\dot{r}_i &= A \dot{\alpha}_i D_A N_A D_B N_B D_C N_C, \\
\dot{f}_i &= 0, \\
\frac{d(\dot{f}_i)}{ds} &= 0, \\
\dot{h}_i &= 0.
\end{aligned} \tag{3.68}$$

The imposition of the above boundary conditions will be further discussed in the following section.

3.4.1 Example: Neo-Hookean type materials

For the implementation of the obtained linear theory, we consider an elastic solid of Neo Hookean type reinforced with a single family of fibers subjected to plane bias extension. In the foregoing analysis, we confine our analysis to the case where fibers are initially straight and aligned along the directions of either normal or tangential to the boundaries (i.e. $\mathbf{D} = \mathbf{E}_1$, $D_1 = 1$, $D_2 = 0$, see, Figure 3.1) such that

$$(\mathbf{D} \cdot \mathbf{T})(\mathbf{D} \cdot \mathbf{N}) = 0 \text{ and } \nabla \mathbf{D} = \nabla \mathbf{T} = \nabla \mathbf{N} = \mathbf{0}. \quad (3.69)$$

We also note here that different types of boundaries and fibers alignments can be readily accommodated by modifying Eq. (3.69) (e.g. $\mathbf{D} = \mathbf{E}_2$, $D_1 = 0$, $D_2 = 1$ and $\mathbf{D} \cdot \mathbf{N} = \mathbf{1}$, etc...).

Accordingly, Eqs. (3.64) and (3.66) becomes

$$\begin{aligned} \dot{P}_{iA} &= (W_{F_{iA}})_{,A} + Eu_{1,1}D_A D_i - \dot{p}\delta_{iA} - p_o \dot{F}_{iA}^* - Cu_{i,111}D_A + A(u_{i,11111})D_A, \\ \dot{P}_{iA,A} &= (W_{F_{iA}})_{,A,A} + Eu_{1,11}D_i - \dot{p}_{,i} - Cu_{i,1111} + Au_{i,11111} = 0. \end{aligned} \quad (3.70)$$

Now, the Neo Hookean strain energy function is given by

$$W(I_1, I_3) = \frac{\mu}{2}(I_1 - 3) - \mu \log I_3 + \frac{\lambda}{2}(\log I_3)^2, \quad (3.71)$$

where μ and λ are the material constants, and $I_1 = tr(\mathbf{F}^T \mathbf{F})$ and $I_3 = \det(\mathbf{F}^T \mathbf{F})$ are respectively the first and third invariant of the deformation gradient tensor. In the case of incompressible materials (i.e. $I_3 = 1$), Eq. (3.71) further reduces to

$$W(\mathbf{F}) = \frac{\mu}{2}(\mathbf{F} \cdot \mathbf{F} - 3). \quad (3.72)$$

Thus, we evaluate $W_{F_{iA}} = \mu F_{iA}$ and thereby obtain from Eq. (3.70) that

$$\dot{P}_{iA} = \mu u_{i,A} + Eu_{1,1}D_A D_i - \dot{p}\delta_{iA} - p_o \dot{F}_{iA}^* - Cu_{i,111}D_A + A(u_{i,11111})D_A, \text{ and} \quad (3.73)$$

$$\dot{P}_{iA,A} = \mu u_{i,AA} + Eu_{1,11}D_i - \dot{p}_{,i} - Cu_{i,1111} + Au_{i,11111} = 0. \quad (3.74)$$

In the above, the unknown constant p_o can be chosen such that the Piola-type stress admits the initial stress free state at $\varepsilon = 0$; i.e.

$$\dot{\mathbf{P}}_o = \mu \dot{\mathbf{F}}_o - p_o \dot{\mathbf{F}}_o^* = 0, \quad (3.75)$$

and thus yielding

$$p_o = \mu. \quad (3.76)$$

In addition, since $J\partial F_{jB}^*/\partial F_{iA} = F_{jB}^*F_{iA}^* - F_{iB}^*F_{jA}^*$, we evaluate at $\varepsilon = 0$ as

$$(\partial F_{jB}^*/\partial F_{iA})_o = \delta_{jB}\delta_{iA} - \delta_{iB}\delta_{jA}, \quad (3.77)$$

and thus find

$$\begin{aligned} \dot{F}_{iA}^* &= (\partial F_{jB}^*/\partial F_{iA})\dot{F}_{jB} = (\delta_{jB}\delta_{iA} - \delta_{iB}\delta_{jA})u_{j,B} \\ &= u_{B,B}\delta_{iA} - u_{A,i} = -u_{A,i}, \end{aligned} \quad (3.78)$$

where $u_{B,B} = 0$ from Eq. (3.60).

Consequently, Eq. (3.74) together with the constraint of bulk incompressibility (Eq. (3.60)) determines the deformed configuration of composites.

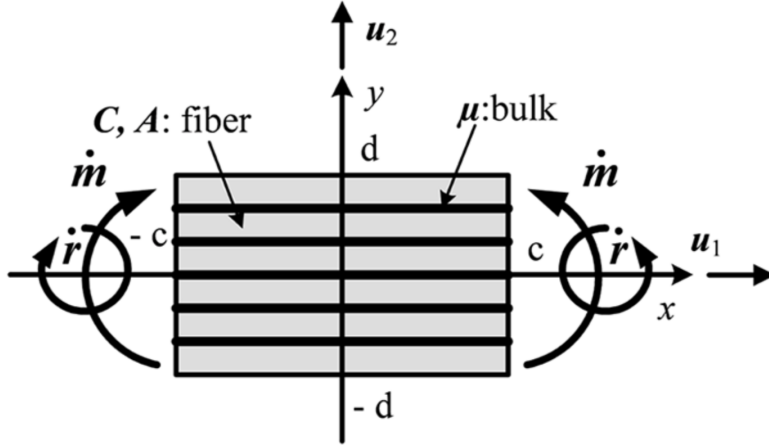


Figure 3.1: Schematic of the problem.

3.5 Solution to the linearized problem

For the purpose of illustration, we consider an elastic solid of Neo-Hookean type reinforced with the single family of fibers and subjected to the double force t_i (extension) and triple force r_i (see, Figure 3.1). Accordingly, we find

from Eqs. (3.60) and (3.74) that

$$\begin{aligned}
\mu(u_{1,11} + u_{1,22}) + Eu_{1,11} - Cu_{1,1111} + Au_{1,111111} - \dot{p}_{,1} &= 0, \\
\mu(u_{2,11} + u_{2,22}) - C_{2,1111} + Au_{2,111111} - \dot{p}_{,2} &= 0, \\
u_{1,1} + u_{2,2} &= 0. \quad (3.79)
\end{aligned}$$

Let us now introduce scalar field, ϕ , as

$$\mathbf{u} = \mathbf{k} \times \nabla\phi, \quad \mathbf{k}(\text{unit normal}); \quad u_i = \varepsilon_{\lambda i} \dot{\phi}_{,\lambda},$$

so that the third equation of Eq. (3.79) can be satisfied (i.e. $\phi_{,12} - \phi_{,21} = 0$).

Hence, Eq. (3.79) becomes

$$\begin{aligned}
\dot{p}_{,1} &= -\mu(\varphi_{,211} + \varphi_{,222}) + C\varphi_{,21111} - A\varphi_{,2111111}, \\
\dot{p}_{,2} &= \mu(\varphi_{,111} + \varphi_{,122}) - C\varphi_{,11111} + A\varphi_{,1111111}. \quad (3.80)
\end{aligned}$$

In addition, we use the compatibility condition of p (i.e. $\dot{p}_{,ij} = \dot{p}_{,ji}$) and thereby reduce Eq. (3.80) to

$$\mu(\varphi_{,1111} + \varphi_{,2222} + 2\varphi_{,1122}) - C(\varphi_{,111111} + \varphi_{,221111}) + A(\varphi_{,11111111} + \varphi_{,22111111}) = 0. \quad (3.81)$$

The above may be reacted into the following compact form

$$\Delta(\Delta\phi - \frac{C}{\mu}\phi_{,1111}) + \frac{E}{\mu}\phi_{,1122} + \frac{A}{\mu}\Delta(\phi_{,111111}) = 0, \quad (3.82)$$

which solves the unknown mapping function, $\phi(x, y)$.

It is noted here that the solution of Eq. (3.82) is not accommodated by conventional methods such as the Fourier transform or the separation of variables. Instead, we adopt the methods of iterative reduction and the principle of eigenfunction expansion [93], [94] to yield

$$\phi(x, y) = X(x)\sin(my), \quad (3.83)$$

and subsequently obtain from Eq. (3.82) that

$$\begin{aligned}
[AX_{,11111111} - (C + Am^2)X_{,111111} + (1 + Cm^2)X_{,1111} - m^2(2 + E)X_{,1111} \\
+ m^4X] \sin my = 0. \quad (3.84)
\end{aligned}$$

Hence the general solution of ϕ can be found as

$$\begin{aligned}
\phi(x, y) &= \sum_{m=1}^{\infty} [\{e^{a_m x} (A_m \sin(b_m x) + B_m \cos(b_m x)) \\
&+ e^{-a_m x} (C_m \sin(b_m x) + D_m \cos(b_m x)) \\
&+ (E_m \sin(c_m x) + F_m \cos(c_m x)) + G_m e^{d_m x} + H_m e^{-d_m x}\} \\
&\times \{\sin(my)\}]. \tag{3.85}
\end{aligned}$$

The expressions of a_m, b_m, c_m and d_m can then be obtained via the simple algebraic procedures:

$$\begin{aligned}
a_m &= \frac{(T_2 + T_1)}{2}, b_m = \frac{(T_2 - T_1)}{2i}, c_m = \frac{T_3}{i}, d_m = T_4, \\
m &= \frac{n\pi}{2d} (n = 1, 3, 5, \text{etc...}), T_1 = \left[\frac{T_{24}}{4A} - T_5 - \{-T_8(T_{18})^2 - 9T_8(T_{10})^{\frac{2}{3}} \right. \\
&+ \left. 12T_{17}T_8 - T_6 + \frac{12(T_{10})^{\frac{1}{3}}T_8T_{18}}{T_7} \}^{0.5} \right]^{0.5}, \\
T_2 &= \left[\frac{T_{24}}{4A} - T_5 + \{-T_8(T_{18})^2 - 9T_8(T_{10})^{\frac{2}{3}} + 12T_{17}T_8 - T_6 \right. \\
&+ \left. \frac{12(T_{10})^{\frac{1}{3}}T_8T_{18}}{T_7} \}^{0.5} \right]^{0.5}, \\
T_3 &= \left[\frac{T_{24}}{4A} + T_5 - \{-T_8(T_{18})^2 - 9T_8(T_{10})^{\frac{2}{3}} + 12T_{17}T_8 + T_6 \right. \\
&+ \left. \frac{12(T_{10})^{\frac{1}{3}}T_8T_{18}}{T_7} \}^{0.5} \right]^{0.5}, \\
T_4 &= \left[\frac{T_{24}}{4A} + T_5 + \{-T_8(T_{18})^2 - 9T_8(T_{10})^{\frac{2}{3}} + 12T_{17}T_8 + T_6 \right. \\
&+ \left. \frac{12(T_{10})^{\frac{1}{3}}T_8T_{18}}{T_7} \}^{0.5} \right]^{0.5}, \\
T_5 &= \frac{T_8}{6(T_9)^{\frac{1}{6}}}, T_6 = 3\sqrt{6}T_{19}[27(T_{19})^2 + 3\sqrt{3}T_{15} - 72T_{17}T_{18} - 2(T_{18})^3]^{0.5}, \\
T_7 &= 6(T_9)^{\frac{1}{6}}[6T_{18}(T_9)^{\frac{1}{3}} + 9(T_9)^{\frac{2}{3}} - T_{12} + \frac{12m^4}{A} + (T_{18})^2 + T_{11} - \frac{3T_{24}T_{16}}{A^2}]^{\frac{1}{4}}, \\
T_8 &= [6T_{18}(T_{10})^{\frac{1}{3}} + 9(T_{10})^{\frac{2}{3}} - T_{12} + \frac{12m^4}{A} + (T_{18})^2 - \frac{3T_{24}T_{22}}{A^2} + T_{11}]^{\frac{1}{2}}, \\
T_9 &= \frac{(T_{14})^2}{2} - \frac{4T_{18}T_{13}}{3} + \left(\frac{\sqrt{3}}{18}\right)[12(T_{18})^2(T_{13})^2 + 27(T_{14})^4 + 16(T_{18})^4T_{13} \\
&+ 256(T_{13})^3 - 4(T_{18})^3(T_{14})^2 - 144T_{18}(T_{14})^2T_{13} - \frac{(T_{18})^3}{27}]^{0.5},
\end{aligned}$$

$$\begin{aligned}
T_{10} &= \frac{(T_{19})^2}{2} + \frac{\sqrt{3}T_{15}}{18} - \frac{4T_{18}T_{17}}{3} - \frac{(T_{18})^3}{27}, T_{11} = \frac{3(T_{24})^2T_{23}}{4A^3}, T_{12} = \frac{9(T_{24})^4}{64A^4}, \\
T_{13} &= T_{21} - \frac{m^4}{A} - T_{20} + \frac{T_{24}T_{16}}{4A^2}, T_{14} = \frac{(T_{24})^3}{8A^3} + \frac{T_{16}}{A} - \frac{T_{24}T_{23}}{2A^2}, \\
T_{15} &= [27(T_{19})^4 + T_{16}T_{17}(T_{18})^4 + 256(T_{17})^3 - 4(T_{18})^3(T_{19})^2, \\
&\quad + 128(T_{18})^2(T_{17})^2 - 144T_{18}(T_{19})^2T_{17}]^{0.5}, \\
T_{16} &= (2 + E)m^2, T_{17} = T_{21} - \frac{m^4}{A} + \frac{T_{24}T_{22}}{4A^2} - T_{20}, \\
T_{18} &= \frac{3(T_{24})^2}{8A^2} - \frac{T_{23}}{A}, T_{19} = \frac{(T_{24})^3}{8A^3} + \frac{T_{22}}{A} + \frac{T_{24}T_{23}}{2A^2}, \\
T_{20} &= \frac{(T_{24})^2T_{23}}{16A^3}, T_{21} = \frac{3(T_{24})^4}{256A^4}, \\
T_{22} &= (2 + E)m^2, T_{23} = Cm^2 + 1 \text{ and } T_{24} = Am^2 + C. \tag{3.86}
\end{aligned}$$

Lastly, the unknown constant real numbers $A_m, B_m, C_m, D_m, E_m, F_m, G_m$ and H_m can be completely determined by imposing the admissible boundary conditions depicted in Eq. (3.68). In the assimilation, the applied forces and triple forces are approximated using Fourier series expansion. For example,

$$\begin{aligned}
t_1 &= \dot{P}_{11}N_1 = \mu(u_{1,1} - u_{2,2}) + Eu_{1,1} - \dot{p} - Cu_{1,111} + Au_{1,11111} \\
&= 5 \simeq \sum_{n=1}^{30} \frac{20}{n\pi} (-1)^{\frac{n-1}{2}} \cos\left(\frac{n\pi}{2d}y\right), \\
\dot{r}_i &= A\dot{\alpha}_i D_A N_A D_B N_B D_C N_C, \dot{r}_1 \\
&= Au_{1,111} = 5 \simeq \sum_{n=1}^{30} \frac{20}{n\pi} (-1)^{\frac{n-1}{2}} \cos\left(\frac{n\pi}{2d}y\right), \\
\dot{r}_2 &= Au_{2,111} = 0. \tag{3.87}
\end{aligned}$$

The obtained solution ϕ is then substituted into the following expression to configure the deformation maps and the corresponding stress fields.

$$\boldsymbol{\chi} = (X_1 - \phi_{,2})\mathbf{E}_1 + (X_2 + \phi_{,1})\mathbf{E}_2. \tag{3.88}$$

We also remark that the required computational cost is minimum (far less expansive than pure numerical approaches) even with the presence of heavy expressions (Eq. (3.63), since the Eq. (3.63) are merely in algebraic structures once implemented. This is also evidenced by the fast convergence rate of the obtained solutions, as illustrated in Figure 3.2 (within 30 iterations).

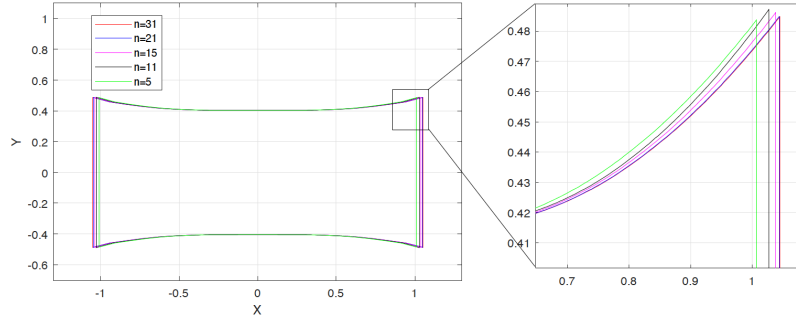


Figure 3.2: Deformation profiles with respect to the number of iterations N .

3.5.1 Theoretical predictions and experimental comparisons

In this section, we simulate the responses of fiber-reinforced composite subjected to plane deformations using the obtained linear model. Emphasis is placed on the assimilation of the deformation profiles, strain field distributions and, in particular, the sensitivity analyses of the proposed linear model with respect to the applied loads and the parameters associated with the Piola-type stresses and triple stresses. It is noted that the data are obtained under the normalized setting unless otherwise specified (e.g. $C/\mu = 20$, $A/\mu = 50$ etc...). Figure 3.3 illustrate the post-processed deformation mapping for a composite with fibers axial, bending and triple force moduli of $E/\mu = 150$, $C/\mu = 150$, and $A/\mu = 150$ when the composite is subjected to axial extension load of $t_1/\mu = 20$. The deformation mapping predicted by the proposed linear solution demonstrates smooth profiles on the boundaries and within the domain of interest (Figure 3.3).

Further, it is shown in Figs. 4-5 that the corresponding deformation configurations are sensitive to both the first and triple stress moduli of Piola-type (i.e. E and A). More precisely, the axial elongation of the composite gradually decreases with increasing the first stress modulus (E). The deformation configuration is also affected by the varying triple stress modulus (A). In this case, the gradients of deformation profiles at each material points become steeper as

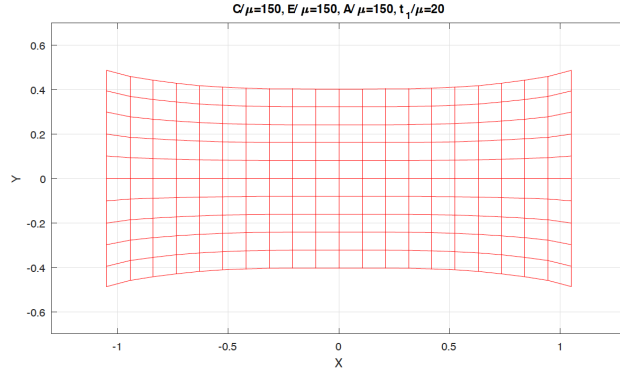


Figure 3.3: Deformation mapping when $t_1/\mu = 20$, $E/\mu = 150$, $C/\mu = 150$, and $A/\mu = 150$.

the triple stress modulus decreases. These results are also closely aligned with the observations in [95], [9] and [96]. In fact, the obtained solution accommodates the deformation configurations predicted by the second gradient theory in the limit of the vanishing triple stress modulus (i.e. $A = 0$, see, Figure 3.6).

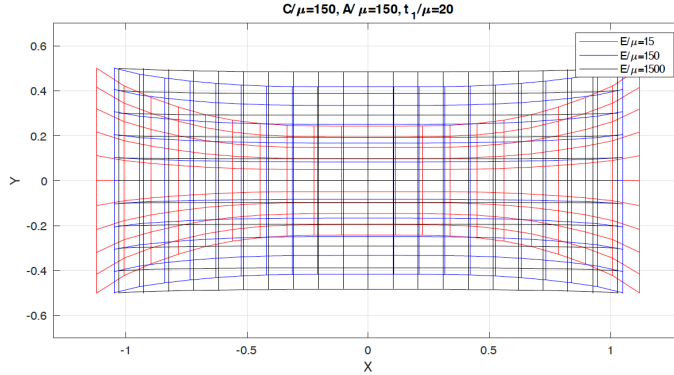


Figure 3.4: Deformation configurations with respect to E/μ when $t_1/\mu = 20$, $C/\mu = 150$, and $A/\mu = 150$.

In particular, utilizing the following relations [85], we evaluate the shear strain gradients and the associated shear angle contours to examine the effects of the third gradient of deformations on the resulting deformation fields,

$$\phi' = \frac{u_2''(1 + u_1') - u_2' u_1''}{u_2'^2 + (1 + u_1')^2}, \quad (3.89)$$

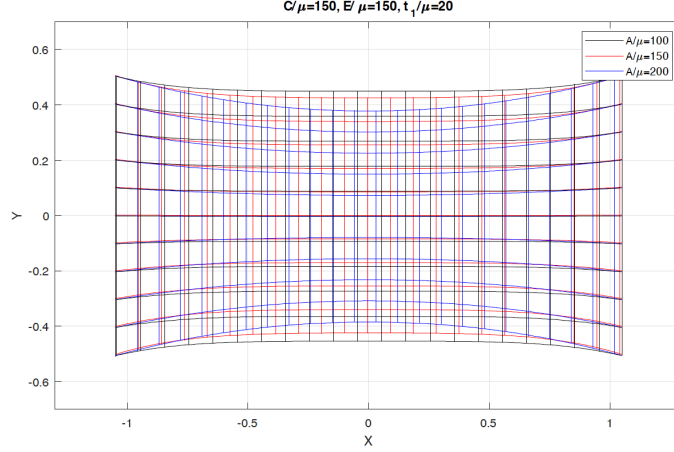


Figure 3.5: Deformation configurations with respect to A/μ when $t_1/\mu = 20$, $E/\mu = 135$, and $C/\mu = 150$.

and

$$\phi = \tan^{-1}\left(\frac{\chi_{2,1} - \chi_{1,1}}{2 + \chi_{1,1} + \chi_{2,1}}\right). \quad (3.90)$$

Figure 3.7 clearly indicate that the magnitude of shear strain gradually increases as approach the right and left boundaries when positive triple force is applied (i.e. $\dot{r}_i > 0$) and vice versa in the case of negative triple force (i.e. $\dot{r}_i < 0$). The continuous shear strain fields give rise to the smooth and dilatational shear strain distributions where the rate of dilatation is dependent on the applied triple force \dot{r}_i (see Figure 3.8). This, in turn suggests that the proposed linear model is capable of predicting multiple configurations of shear angle distributions given the single configuration of the applied force \dot{t}_i and double force \dot{m}_i , whereas only one configuration is possible within the description of the second gradient based models (see, [95], [85], [83] and [9]). In fact, the shear angle field estimated by the second gradient continuum model is one of the particular configurations predicted by the proposed model in the limit of vanishing triple force (i.e. $\dot{r}_i = 0$, see, also, Figure 3.6). This also can be seen by setting Eq. (3.68) as

$$\dot{r}_i = A\dot{\alpha}_i D_A N_A D_B N_B D_C N_C = 0. \quad (3.91)$$

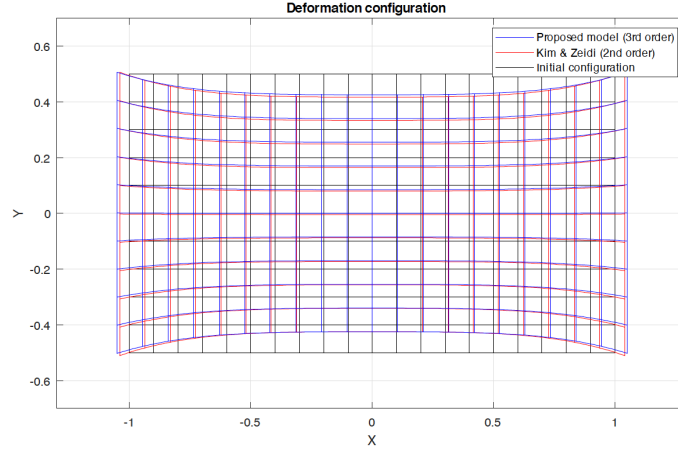


Figure 3.6: Comparison with the second gradient model.

Hence, the expressions of force and double force (Eq. (3.68)) and the associated Piola-type stress (Eq. (3.73)) become

$$\dot{t}_i = \dot{P}_{iA}N_A, \quad \dot{m}_i = C\dot{g}_iD_A N_A D_B N_B, \quad \text{and}$$

$$\dot{P}_{iA} = \mu u_{i,A} + E u_{1,1} D_A D_i - \dot{p}\delta_{iA} - p_o \dot{F}_{iA}^* - C u_{i,111} D_A,$$

which recover the results in [9] (see Eqs. (61)-(62) therein).

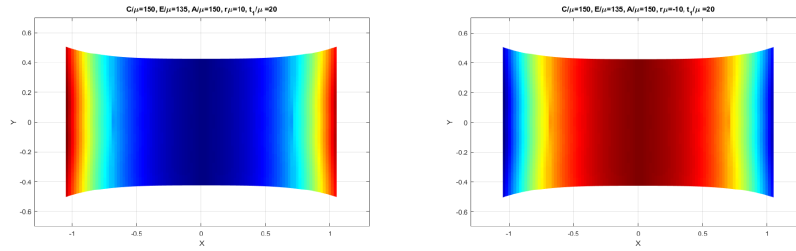


Figure 3.7: Shear strain gradient with respect to \dot{r}_i , $\dot{r}_i > 0$ (Left), and $\dot{r}_i < 0$ (Right).

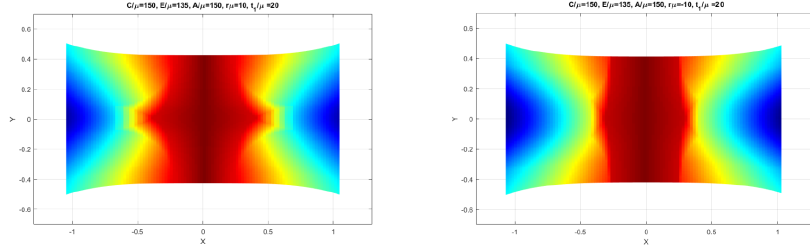


Figure 3.8: Shear angle contours with respect to \dot{r}_i , $\dot{r}_i > 0$ (a), and $\dot{r}_i < 0$ (b).

We also summarize the shear strain gradients and the associated shear angle contours computed, respectively by the first, second and third gradient continuum models for the purpose of further clarification. It is evident from Figure 3.9 that the proposed model (third gradient) predicts smooth and continuous shear strain gradient fields as opposed to those obtained from the first and second gradient models where the corresponding strain gradient fields display either zero or constant distributions (see, Figure 3.9). In results, a comprehensive description of smooth and dilatational shear angle distributions is assimilated by the proposed linear model (see, Figure 3.10). On the other hand, conventional lower-order models produce limited predictions of either discontinued (first gradient model) or non-dilatational (second gradient model) field distributions (Figure 3.10). The obtained results are also aligned with the earlier discussions regarding higher-order continua that N th-order continua can sustain continuous and smooth deformation gradient fields up to $(N - 1)$ th order [82]-[91] and [92].

Lastly, we compare the predicted shear angle distributions with those obtained from the plane extension test of polymeric composites (PES) (see, Figure 3. 11 (Right)). Although the proposed linear model is not intended for relatively large deformation analyses, it produces reasonably good prediction results for both deformation profiles and shear angle distributions of PES composites at 20% and 50% elongations (see, Figure 3.11). We also note that the obtained model may be further extended to include practically more important problems such as determination of the triple force moduli and analyses of the residual triple stress on the mechanical responses of higher-order continua.

Researches on these subjects certainly deserve further attention, which, however, are beyond the scope of the present study due to the paucity of available experimental resources and data sets (especially with the current outbreak).

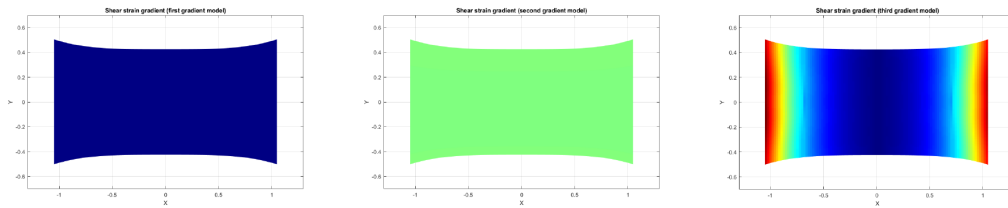


Figure 3.9: Shear strain gradients predicted by the first gradient (Left), second gradient (Middle) and third gradient (Right) models.

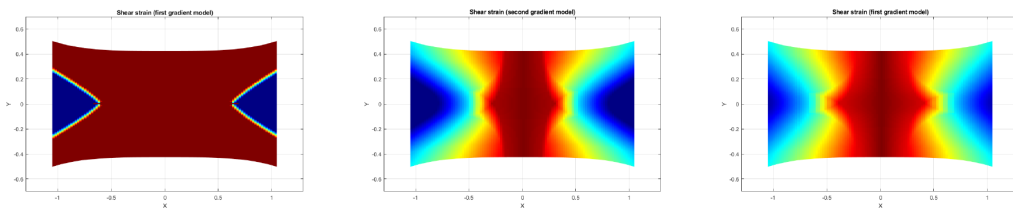


Figure 3.10: Shear angle contours predicted by the first gradient (Left), second gradient (Middle) and third gradient (Right) models.

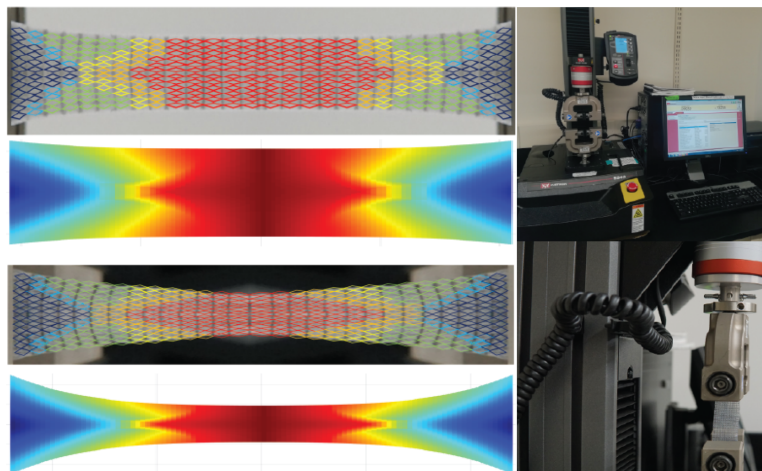


Figure 3.11: Shear angle distributions: PES at 20% (top left) and 50%(bottom left) elongation.

3.6 Denouement

In this study, we present a second gradient-based continuum model for the mechanics of an elastic solid reinforced with extensible fibers and subjected to plane deformations. The fibers are presumed as continuously distributed spatial rods of Kirchhoff type, under which the kinematics of fibers has been formulated via the second and third gradient of continuum deformations. By means of the variational principles and the virtual work statement, the Euler equations and the associated necessary boundary conditions are obtained. The energy density function of Spencer and Soldatos type is augmented by the third gradient of deformations to accommodate the third gradient continua and the associated bulk incompressibility.

More importantly, we formulate a complete linear model within the prescription of superposed incremental deformations from which a complete analytical solution has been obtained. The presented linear model predicts smooth deformations profiles and, in particular, assimilates gradual and dilatational shear angle distributions of the composite subjected to plane bias extension. This is due to the sufficient continuity of the resulting deformation fields suitably sustained by the third gradient of continua, unlike those of lower-order continua where sharp variations are present on the corresponding shear zones. Lastly, we note that the proposed linear model demonstrates reasonably accurate predictions in the deformation and shear angle analyses of polymeric composites.

Chapter 4

The second-order finite element analysis of hyper-elastic composites reinforced with fibers subjected to tensile loads

4.1 Kinematics

The following model has been developed to describe the behavior of solids reinforced with fibers resistance to extension. We propose that the mechanical response of the hyper-elastic fiber material is governed by the following strain energy function:

$$W(\mathbf{F}, \mathbf{G}) = \widehat{W}(\mathbf{F}) + W(\mathbf{G}), \quad W(\mathbf{G}) \equiv \frac{1}{2}C(\mathbf{F})|\mathbf{g}|^2, \quad (4.1)$$

where \mathbf{F} is the first gradient of the deformation function ($\boldsymbol{\chi}(\mathbf{X})$) and \mathbf{G} is the second gradient of the deformation (i.e. $\mathbf{G} = \nabla\mathbf{F}$). The conventional strain energy function in the Eq. (4.1) has been borrowed from [41] by Spencer and Soldatos.

$$\lambda = |\mathbf{d}| \quad \text{and} \quad \lambda\boldsymbol{\tau} = \mathbf{d}; \quad \lambda \equiv \frac{ds}{dS} \quad \text{and} \quad \boldsymbol{\tau} \equiv \frac{d\mathbf{r}(s)}{ds}, \quad (4.2)$$

where

$$\mathbf{d} = \mathbf{F}\mathbf{D}, \quad (4.3)$$

in which \mathbf{D} is the unit tangent to the fiber trajectory in the reference configuration. Eq. (4.3) can be derived by taking the derivative of $\mathbf{r}(s) = \boldsymbol{\chi}(\mathbf{X}(s))$, and correspondingly utilizing $\mathbf{D} = \mathbf{X}'(s)$ and $\mathbf{d} = \mathbf{r}'(s)$. Derivatives respect to

arclength parameter along the fiber in the initial configuration are presented with primes(i.e. $(*)' = d(*)/dS$).

The geodesic curvature of an arc is demonstrated as $(\mathbf{r}(s))$ is derived from Eq. (4.3) and is presented below:

$$\mathbf{g} \equiv \mathbf{r}'' = (\mathbf{F}\mathbf{D})' = \mathbf{F}'\mathbf{D} + \mathbf{F}\mathbf{D}' = \mathbf{F}'\mathbf{D} = \frac{d\mathbf{F}}{d\mathbf{X}}\left(\frac{d\mathbf{X}}{ds} \otimes \mathbf{D}\right) = \mathbf{G}(\mathbf{D} \otimes \mathbf{D}), \quad (4.4)$$

for initially straight fibers (i.e. $\mathbf{D}' = 0$). Also, Eqs. (4.2-4.3) result in:

$$\lambda^2 = \mathbf{F}\mathbf{D} \cdot \mathbf{F}\mathbf{D} = \mathbf{F}^T \mathbf{F}\mathbf{D} \cdot \mathbf{D} = \mathbf{C}\mathbf{D} \cdot \mathbf{D} = \mathbf{C} \cdot \mathbf{D} \otimes \mathbf{D}. \quad (4.5)$$

The compatibility condition is one of the principal equations in the kinematic of fibers and is demonstrated below:

$$G_{iAB} = F_{iA,B} = F_{iB,A} = G_{iBA}. \quad (4.6)$$

We can consider $C(\mathbf{F}) = C$ and thereby conclude:

$$\begin{aligned} \widehat{W}(\mathbf{F}) &= W(I_1, I_2, \varepsilon), \text{ where } I_1 = \text{tr}\mathbf{C} = \lambda_1^2 + \lambda_2^2, I_2 = \frac{1}{2}[\text{tr}(C)^2 - \text{tr}(C^2)], \\ C &= \mathbf{F}^T \mathbf{F} \text{ and } \varepsilon = \frac{1}{2}(\lambda^2 - 1) = \frac{1}{2}(\mathbf{C} \cdot \mathbf{D} \otimes \mathbf{D} - 1). \end{aligned} \quad (4.7)$$

We then have

$$W(I_1, I_2, \varepsilon, \mathbf{g}) = W(I_1, I_2, \varepsilon) + \frac{1}{2}C|\mathbf{g}|^2 = W(\mathbf{F}, \mathbf{G}) \quad (4.8)$$

Correspondingly, by taking the derivative, Eq. (4.8) can be shown in the below format:

$$\dot{W} = \dot{W}(I_1, I_2, \varepsilon, \mathbf{g}) = W_F \dot{F} + W_\varepsilon \dot{\varepsilon} + W_{\mathbf{g}} \cdot \dot{\mathbf{g}}, \quad (4.9)$$

It should be noted that the energy function W is a function of I_1 , I_2 , \mathbf{g} , and ε . \mathbf{G} . To derive the required expressions, we use the principals of continuum mechanics and obtain:

$$\begin{aligned} \dot{I}_1 &= [\text{tr}(\mathbf{C})] = (\mathbf{I} \cdot \mathbf{C}) = \mathbf{I} \cdot \dot{\mathbf{C}} = 2\mathbf{F} \cdot \dot{\mathbf{F}}, \\ \dot{I}_2 &= 2\mathbf{F}[\{(\mathbf{F} \cdot \mathbf{F})\mathbf{I} - \mathbf{F}^T \mathbf{F}\}] \cdot \dot{\mathbf{F}}. \end{aligned} \quad (4.10)$$

and $(\lambda^2) = (\mathbf{F}\mathbf{D} \cdot \mathbf{F}\mathbf{D})$ then

$$\dot{\varepsilon} = \dot{\lambda}\lambda = \mathbf{F}\mathbf{D} \cdot \dot{\mathbf{F}}\mathbf{D} = \text{tr}(\mathbf{F}\mathbf{D} \otimes \dot{\mathbf{F}}\mathbf{D}) = \text{tr}((\mathbf{F}\mathbf{D} \otimes \mathbf{D})\dot{\mathbf{F}}^T) = \mathbf{F}\mathbf{D} \otimes \mathbf{D} \cdot \dot{\mathbf{F}}. \quad (4.11)$$

by substituting Eqs. (4.9), and (4.10) into Eq. (4.11):

$$\begin{aligned}\dot{W} &= W_F \cdot \dot{\mathbf{F}} + W_\varepsilon \dot{\lambda} \lambda + C \mathbf{g} \cdot \dot{\mathbf{g}} \\ &= W_F \cdot \dot{\mathbf{F}} + W_\varepsilon \mathbf{F} \mathbf{D} \otimes \mathbf{D} \cdot \dot{\mathbf{F}} + C \mathbf{g} \cdot \dot{\mathbf{g}}.\end{aligned}\quad (4.12)$$

In order to accommodate bulk incompressibility, we augment the concept of Lagrange multiplier into the original energy function:

$$U(I_1, I_2, \varepsilon, \mathbf{g}, p) = W(I, \varepsilon, \mathbf{g}) - p(J - 1). \quad (4.13)$$

Then

$$\dot{U} = \dot{W} - \dot{p}(J - 1) - p\dot{J} = \dot{W} - p\dot{J}, \quad \because \dot{p}(J - 1) = 0 \text{ for } J = 1. \quad (4.14)$$

Further, since $\dot{J} = \frac{\partial J}{\partial \mathbf{F}} \cdot \dot{\mathbf{F}} = J(\mathbf{F}^{-1})^T \cdot \dot{\mathbf{F}} = \mathbf{F}^* \cdot \dot{\mathbf{F}}$, augmenting (2.13) and (2.19) furnishes to:

$$\dot{U} = (W_F + W_\varepsilon \mathbf{F} \mathbf{D} \otimes \mathbf{D} - p \mathbf{F}^*) \cdot \dot{\mathbf{F}} + W_G \cdot \dot{\mathbf{G}}, \quad (4.15)$$

which considers bulk incompressibility in addition to fibers resistant to extension and flexure .

4.2 Equilibrium

Derivation of Euler equation and corresponding boundary conditions up the second gradient order are owed to the efforts of authors in [52], [82]. The relation between the mechanical loads, and the deformation can be derived by using previously mentioned mathematical formulations and consequently, the weak form of equilibrium equation is presented below:

$$\dot{E} = P, \quad (4.16)$$

where P is the virtual work of the applied loads and the superposed dot refers to the variational derivative;

$$E = \int_{\Omega} U(\mathbf{F}, \mathbf{G}) dA \quad (4.17)$$

The procedure of finding the intended loads depends on the existence of potential L such that $P = \dot{L}$. It can be concluded that, the problem of determining equilibrium deformations can be simplified as a local minima search of energy potential function $E - L$.

Thus, We have

$$\dot{E} = \int_{\Omega} \dot{U}(\mathbf{F}, \mathbf{G}) dA, \quad (4.18)$$

where \dot{U} is taken from (2.21). By substituting the corresponding values we then have:

$$\begin{aligned} W_{\mathbf{G}} \cdot \dot{\mathbf{G}} &= \frac{\partial W}{\partial G_{iAB}} \dot{G}_{iAB} = \frac{\partial W}{\partial G_{iAB}} \dot{F}_{iA,B} = \frac{\partial W}{\partial G_{iAB}} u_{i,AB}; \quad u_i \equiv \dot{r}_i = \dot{\chi}_i, \text{ and} \\ \frac{\partial W}{\partial G_{iAB}} u_{i,AB} &= \left(\frac{\partial W}{\partial G_{iAB}} u_{i,A} \right)_{,B} - \left(\frac{\partial W}{\partial G_{iAB}} \right)_{,B} u_{i,A}, \end{aligned} \quad (4.19)$$

,and

$$\int_{\Omega} W_{\mathbf{G}} \cdot \dot{\mathbf{G}} dA = \int_{\Omega} \left(\frac{\partial W}{\partial G_{iAB}} u_{i,A} \right)_{,B} dA - \int_{\Omega} \left(\frac{\partial W}{\partial G_{iAB}} \right)_{,B} u_{i,A} dA. \quad (4.20)$$

By taking the Green-Stokes theorem into consideration, (2.26) can be reworked as

$$\int_{\Omega} W_{\mathbf{G}} \cdot \dot{\mathbf{G}} dA = \int_{\partial\Omega} \frac{\partial W}{\partial G_{iAB}} u_{i,A} N_B dS - \int_{\Omega} \left(\frac{\partial W}{\partial G_{iAB}} \right)_{,B} u_{i,A} dA, \quad (4.21)$$

where \mathbf{N} is the rightward unit normal to $\partial\Omega$. Additionally, from (2.21)

$$\begin{aligned} \int_{\Omega} W_{\mathbf{G}} \cdot \dot{\mathbf{G}} dA &= \int_{\partial\Omega} \frac{\partial W}{\partial G_{iAB}} u_{i,A} N_B dS - \int_{\Omega} C g_{i,B} D_A D_B \dot{F}_{iA} dA, \\ &= - \int_{\Omega} C \nabla \mathbf{g}(\mathbf{D} \otimes \mathbf{D}) \cdot \dot{\mathbf{F}} dA + \int_{\partial\Omega} W_{\mathbf{G}}^T [\dot{\mathbf{F}}]^T \cdot \mathbf{N} dS. \end{aligned} \quad (4.22)$$

By combining (2.21), (2.24), and (2.28), we deduce

$$\dot{E} = \int_{\Omega} \mathbf{P} \cdot \dot{\mathbf{F}} dA + \int_{\partial\Omega} W_{\mathbf{G}}^T [\dot{\mathbf{F}}]^T \cdot \mathbf{N} dS, \quad (4.23)$$

where

$$\mathbf{P} = W_F + W_{\varepsilon} \mathbf{F}(\mathbf{D} \otimes \mathbf{D}) - p \mathbf{F}^* - C \nabla \mathbf{g}(\mathbf{D} \otimes \mathbf{D}), \quad (4.24)$$

and hence the Euler equation

$$Div(\mathbf{P}) = 0, \quad (4.25)$$

which holds in Ω .

4.3 Composite with exponential Fibre Potential

Hyper-elastic materials are conventionally considered to be soft-material composites such as carbon rubber-fiber composites and polymer composites. There should be some modifications in the energy density function to describe their behavior as it is presented below:

$$W(\mathbf{F}, \varepsilon) = W(\mathbf{F}) + W(\varepsilon) = W(\mathbf{F}) + Ae^{B\varepsilon}. \quad (4.26)$$

In order to proceed we consider the following equations:

$$\varepsilon = \frac{1}{2}(\lambda^2 - 1) = \frac{1}{2}(\mathbf{FD} \cdot \mathbf{FD} - 1), \quad (4.27)$$

$$\dot{\varepsilon} = \lambda\dot{\lambda} = \mathbf{FD} \cdot \dot{\mathbf{F}}\mathbf{D} = \text{tr}(\mathbf{FD} \otimes \dot{\mathbf{F}}\mathbf{D}) = \text{tr}((\mathbf{FD} \otimes \mathbf{D})\dot{\mathbf{F}}^T) \quad (4.28)$$

$$= \mathbf{F}(\mathbf{D} \otimes \mathbf{D}) \cdot \dot{\mathbf{F}}. \quad (4.29)$$

By substituting the above equations in Eq. (4.12), we would obtain:

$$W(\mathbf{F}, \varepsilon) = W(\mathbf{F}) + W(\varepsilon) = W(\mathbf{F}) + Ae^{\frac{B}{2}(\mathbf{FD} \cdot \mathbf{FD} - 1)}. \quad (4.30)$$

while:

$$W(\mathbf{F}) = \frac{\mu}{2}(I_1 - 3); \quad \mu > 0. \quad (4.31)$$

Variational computation of Eq. (4.12) yields to:

$$\dot{W}(\mathbf{F}, \varepsilon) = W_{\mathbf{F}} \cdot \dot{\mathbf{F}} + W_{\varepsilon} \dot{\varepsilon} = W_{\mathbf{F}} \cdot \dot{\mathbf{F}} + W_{\varepsilon} \cdot \dot{\mathbf{F}} \quad (4.32)$$

$$W_{\varepsilon} \cdot \dot{\varepsilon} = \mathbf{A} B e^{\frac{B}{2}(\mathbf{FD} \cdot \mathbf{FD} - 1)} \mathbf{F}(\mathbf{D} \otimes \mathbf{D}) \cdot \dot{\mathbf{F}} \quad (4.33)$$

$$W_{\mathbf{F}} \cdot \dot{\mathbf{F}} = [\mu F_{iA} + \lambda F_{iB}(F_{jC}F_{jC}\delta_{AB} - F_{jA}F_{jB})](\mathbf{e}_i \otimes \mathbf{E}_A) \cdot \dot{F}_{kC}(\mathbf{e}_k \otimes \mathbf{E}_C) \quad (4.34)$$

For desired applications, the above energy variation form can be employed. For example, in the case of unidirectional and inextensible fibers, we combine Eqs. (4.15), (4.18), (4.24), and (4.34). In conclusion, we derive the leading equilibrium equation:

$$\begin{aligned} 0 &= P_{iA,A} = \mu F_{iA,A} + \lambda F_{iB,A}(F_{jC}F_{jC}\delta_{AB} - F_{jA}F_{jB}) + \lambda F_{iB}(2F_{jC,A}F_{jC}\delta_{AB} \\ &- F_{jA,A}F_{jB} - F_{jA}F_{jB,A}) + (\mathbf{A} B e^{\frac{B}{2}(F_{j1}F_{j1} - 1)})[BF_{j1,A}F_{j1}F_{i1}D_A - F_{i1,A}D_A] \\ &- p_{,A}F_{iA,A}^* - CF_{i1,11A}D_A \end{aligned} \quad (4.35)$$

We need to substitute F in Eq. (4. 35) as it mentioned below:

$$F_{iA} = \chi_{i,A} = \frac{\partial \chi_i}{\partial X_A} \quad (4.36)$$

Now, If we expand the equations for $A, B, C = 1, 2$, and $D_1 = 1, D_2 = 0$, and also expand the summations for $j = 1, 2$ we would finally obtain:

$$\begin{aligned}
0 &= \mu(\chi_{i,11} + \chi_{i,22}) + \lambda(\chi_{i,11} + \chi_{i,22})(\chi_{1,1}\chi_{1,1} + \chi_{1,2}\chi_{1,2} + \chi_{2,1}\chi_{2,1} + \chi_{2,2}\chi_{2,2}) \\
&- \lambda(\chi_{i,11} + \chi_{i,12} + \chi_{i,21} + \chi_{i,22})(\chi_{1,1}\chi_{1,1} + \chi_{1,1}\chi_{1,2} + \chi_{1,2}\chi_{1,1} + \chi_{1,2}\chi_{1,2} \\
&+ \chi_{2,1}\chi_{2,1} + \chi_{2,1}\chi_{2,2} + \chi_{2,2}\chi_{2,1} + \chi_{2,2}\chi_{2,2}) + \lambda(\chi_{i,1} + \chi_{i,2})(2\chi_{1,11}\chi_{1,1} \\
&+ 2\chi_{1,21}\chi_{1,2} + 2\chi_{1,12}\chi_{1,1} + 2\chi_{1,22}\chi_{1,2} - \chi_{1,11}\chi_{1,1} - \chi_{1,11}\chi_{1,2} - \chi_{1,22}\chi_{1,1} \\
&- \chi_{1,22}\chi_{1,2} - \chi_{1,1}\chi_{1,11} - \chi_{1,1}\chi_{1,21} - \chi_{1,2}\chi_{1,12} - \chi_{1,2}\chi_{1,22} + 2\chi_{2,11}\chi_{2,1} \\
&+ 2\chi_{2,21}\chi_{2,2} + 2\chi_{2,12}\chi_{2,1} + 2\chi_{2,22}\chi_{2,2} - \chi_{2,11}\chi_{2,1} - \chi_{2,11}\chi_{2,2} - \chi_{2,22}\chi_{2,1} \\
&- \chi_{2,22}\chi_{2,2} - \chi_{2,1}\chi_{2,11} - \chi_{2,1}\chi_{2,21} - \chi_{2,2}\chi_{2,12} - \chi_{2,2}\chi_{2,22}) \\
&+ AB e^{\frac{B}{2}[(\chi_{1,1}\chi_{1,1} + \chi_{2,1}\chi_{2,1})^{-1}]} [B(\chi_{1,11}\chi_{1,1} + \chi_{2,11}\chi_{2,1})\chi_{i,1} - \chi_{i,11}] \\
&- p_{,1}\varepsilon_{ij}\varepsilon_{12}\chi_{j,2} - p_{,2}\varepsilon_{ij}\varepsilon_{21}\chi_{j,1} - C\chi_{i,1111} \quad (4.37)
\end{aligned}$$

Now plugging in $i = 1, 2$ would give us the following equilibrium equations:

$$\begin{aligned}
0 &= \mu(\chi_{1,11} + \chi_{1,22}) + \lambda(\chi_{1,11} + \chi_{1,22})(\chi_{1,1}\chi_{1,1} + \chi_{1,2}\chi_{1,2} + \chi_{2,1}\chi_{2,1} \\
&+ \chi_{2,2}\chi_{2,2}) - \lambda(\chi_{1,11} + \chi_{1,12} + \chi_{1,21} + \chi_{1,22})(\chi_{1,1}\chi_{1,1} + \chi_{1,1}\chi_{1,2} + \chi_{1,2}\chi_{1,1} \\
&+ \chi_{1,2}\chi_{1,2} + \chi_{2,1}\chi_{2,1} + \chi_{2,1}\chi_{2,2} + \chi_{2,2}\chi_{2,1} + \chi_{2,2}\chi_{2,2}) + \lambda(\chi_{1,1} + \chi_{1,2}) \\
&(2\chi_{1,11}\chi_{1,1} + 2\chi_{1,21}\chi_{1,2} + 2\chi_{1,12}\chi_{1,1} + 2\chi_{1,22}\chi_{1,2} - \chi_{1,11}\chi_{1,1} - \chi_{1,11}\chi_{1,2} \\
&- \chi_{1,22}\chi_{1,1} - \chi_{1,22}\chi_{1,2} - \chi_{1,1}\chi_{1,11} - \chi_{1,1}\chi_{1,21} - \chi_{1,2}\chi_{1,12} \\
&- \chi_{1,2}\chi_{1,22} 2\chi_{2,11}\chi_{2,1} + 2\chi_{2,21}\chi_{2,2} + 2\chi_{2,12}\chi_{2,1} + 2\chi_{2,22}\chi_{2,2} - \chi_{2,11}\chi_{2,1} \\
&- \chi_{2,11}\chi_{2,2} - \chi_{2,22}\chi_{2,1} - \chi_{2,22}\chi_{2,2} - \chi_{2,1}\chi_{2,11} - \chi_{2,1}\chi_{2,21} - \chi_{2,2}\chi_{2,12} \\
&- \chi_{2,2}\chi_{2,22}) + AB e^{\frac{B}{2}[(\chi_{1,1}\chi_{1,1} + \chi_{2,1}\chi_{2,1})^{-1}]} [B(\chi_{1,11}\chi_{1,1} + \chi_{2,11}\chi_{2,1})\chi_{1,1} \\
&- \chi_{1,11}] - p_{,1}\chi_{2,2} + p_{,2}\chi_{2,1} - C\chi_{1,1111} \quad (4.38)
\end{aligned}$$

$$\begin{aligned}
0 &= \mu(\chi_{2,11} + \chi_{2,22}) + \lambda(\chi_{2,11} + \chi_{2,22})(\chi_{1,1}\chi_{1,1} + \chi_{1,2}\chi_{1,2} + \chi_{2,1}\chi_{2,1} \\
&+ \chi_{2,2}\chi_{2,2}) - \lambda(\chi_{2,11} + \chi_{2,12} + \chi_{2,21} + \chi_{2,22})(\chi_{1,1}\chi_{1,1} + \chi_{1,1}\chi_{1,2} + \chi_{1,2}\chi_{1,1} \\
&+ \chi_{1,2}\chi_{1,2} + \chi_{2,1}\chi_{2,1} + \chi_{2,1}\chi_{2,2} + \chi_{2,2}\chi_{2,1} + \chi_{2,2}\chi_{2,2}) + \lambda(\chi_{2,1} + \chi_{2,2}) \\
&(2\chi_{1,11}\chi_{1,1} + 2\chi_{1,21}\chi_{1,2} + 2\chi_{1,12}\chi_{1,1} + 2\chi_{1,22}\chi_{1,2} - \chi_{1,11}\chi_{1,1} - \chi_{1,11}\chi_{1,2} \\
&- \chi_{1,22}\chi_{1,1} - \chi_{1,22}\chi_{1,2} - \chi_{1,1}\chi_{1,11} - \chi_{1,1}\chi_{1,21} - \chi_{1,2}\chi_{1,12} \\
&- \chi_{1,2}\chi_{1,22} - 2\chi_{2,11}\chi_{2,1} + 2\chi_{2,21}\chi_{2,2} + 2\chi_{2,12}\chi_{2,1} + 2\chi_{2,22}\chi_{2,2} - \chi_{2,11}\chi_{2,1} \\
&- \chi_{2,11}\chi_{2,2} - \chi_{2,22}\chi_{2,1} - \chi_{2,22}\chi_{2,2} - \chi_{2,1}\chi_{2,11} - \chi_{2,1}\chi_{2,21} - \chi_{2,2}\chi_{2,12} \\
&- \chi_{2,2}\chi_{2,22}) + AB e^{\frac{B}{2}[(\chi_{1,1}\chi_{1,1} + \chi_{2,1}\chi_{2,1})^{-1}]} [B(\chi_{1,11}\chi_{1,1} + \chi_{2,11}\chi_{2,1})\chi_{2,1} - \chi_{2,11}] \\
&+ p_{,1}\chi_{1,2} - p_{,2}\chi_{1,1} - C\chi_{2,1111} \tag{4.39}
\end{aligned}$$

4.3.1 Finite element analysis of the 4th order coupled PDE

The weak form of Eqs. (4.38), and (4.39) are the first two equations in implementing the FEM procedure for the corresponding system of partial differential equations. For the sake of conciseness, we would not go through their weak form expansions in this manuscript. However, the necessary u-substitutions to reduce the order of previously mentioned PDEs are presented below:

$$0 = Q - \chi_{1,11}, \tag{4.40}$$

$$0 = R - \chi_{2,11}, \tag{4.41}$$

$$0 = C - \chi_{1,1}, \tag{4.42}$$

$$0 = D - \chi_{2,1}, \tag{4.43}$$

$$0 = A - \mu(Q + \chi_{1,22}) - CQ_{,11}, \tag{4.44}$$

$$0 = B - \mu(R + \chi_{2,22}) - CR_{,11}, \tag{4.45}$$

In order to simplify the nonlinearities that have been arisen in the original equations, we make use of the Picard iterative method that is described below. In fact, the non-linear terms in the original equations can be replaced by their

corresponding constants and get updated after each iteration

$$-A\chi_{2,2} + B\chi_{2,1} \implies -A_0\chi_{2,2} + B_0\chi_{2,1} \quad (4.46)$$

$$A\chi_{1,2} - B\chi_{1,1} \implies A_0\chi_{1,2} - B_0\chi_{1,1} \quad (4.47)$$

4.4 Theoretical predictions and experimental comparisons

The first step corresponding to the investigation of how the model performs in the real-life application is visualizing the deformation contour. In order to assess the results that have been obtained from the numerical model, [8], [53], [96] seem to be appropriate references. The schematic shape of deformation contours can be visualized in Figure 4.1.

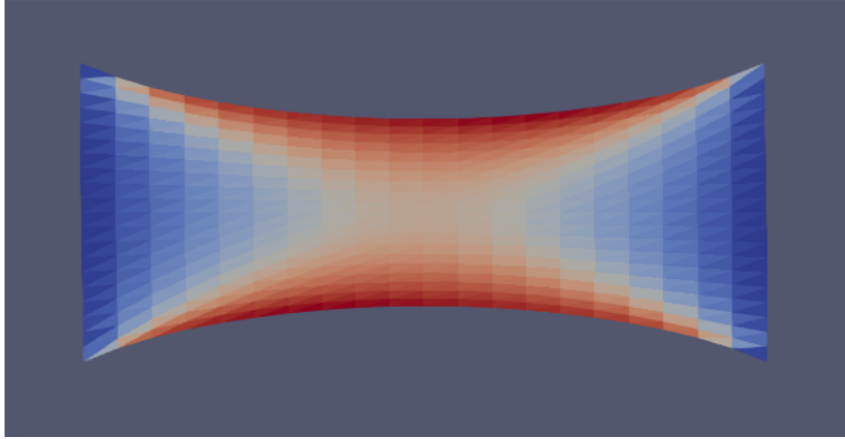


Figure 4.1: Deformation contour for $E1/\mu = 150$, and $P/\mu = 200$.

In terms of schematic deformation contour, It seems to show a reasonable agreement with the experimental results. Some more experiments with the fiber coefficients have been done that are shown in Figure 4.2, and Figure 4.3. In the following cases, all the coefficients except one have been kept the same for both cases.

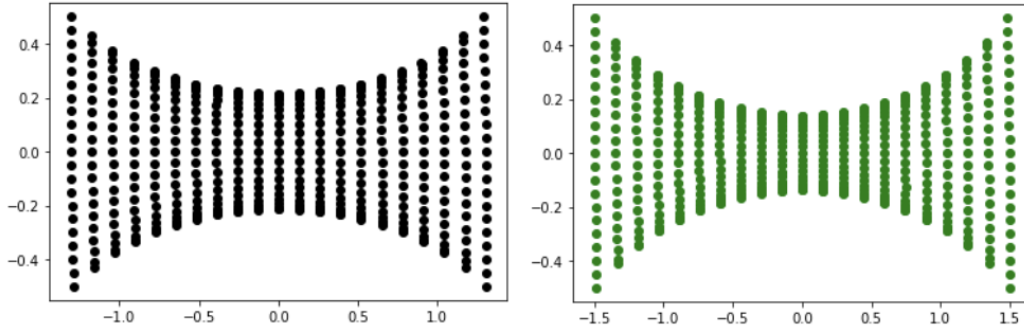


Figure 4.2: Node-based deformation contours comparison for $P/\mu = 150$ (left), and $P/\mu = 230$ (right).

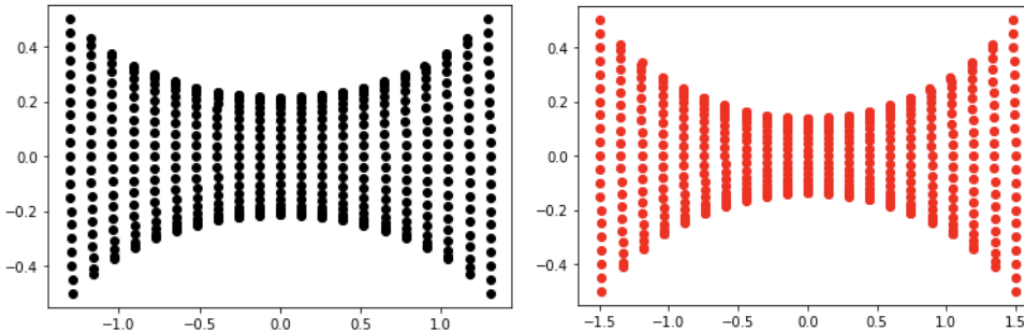


Figure 4.3: Node-based deformation contours comparison for $E/\mu = 200$ (left), and $E/\mu = 150$ (right).

In the first figure having different tensile force causes the extension profiles and deformation contours to be changed drastically. It is observed that having higher values of P corresponds to more longitudinal extension in the X direction, which is justified with the conservation of mass theorem. Additionally, the second figure compares the effects of E on the deformation profile. A higher value of E can be inferred as the stiffer matrix in the X direction, and consequently, less extension in parallel to this axis.

A significant measure to determine the accuracy of the numerical model is making use of the stress-strain figure, and comparing the finite element results with the experimental dataset as presented in Figure 4.4, and Figure 4.5.

NSP-8020 and NSP-8515 are the hyper elastic materials that were used in the bias-extension test.

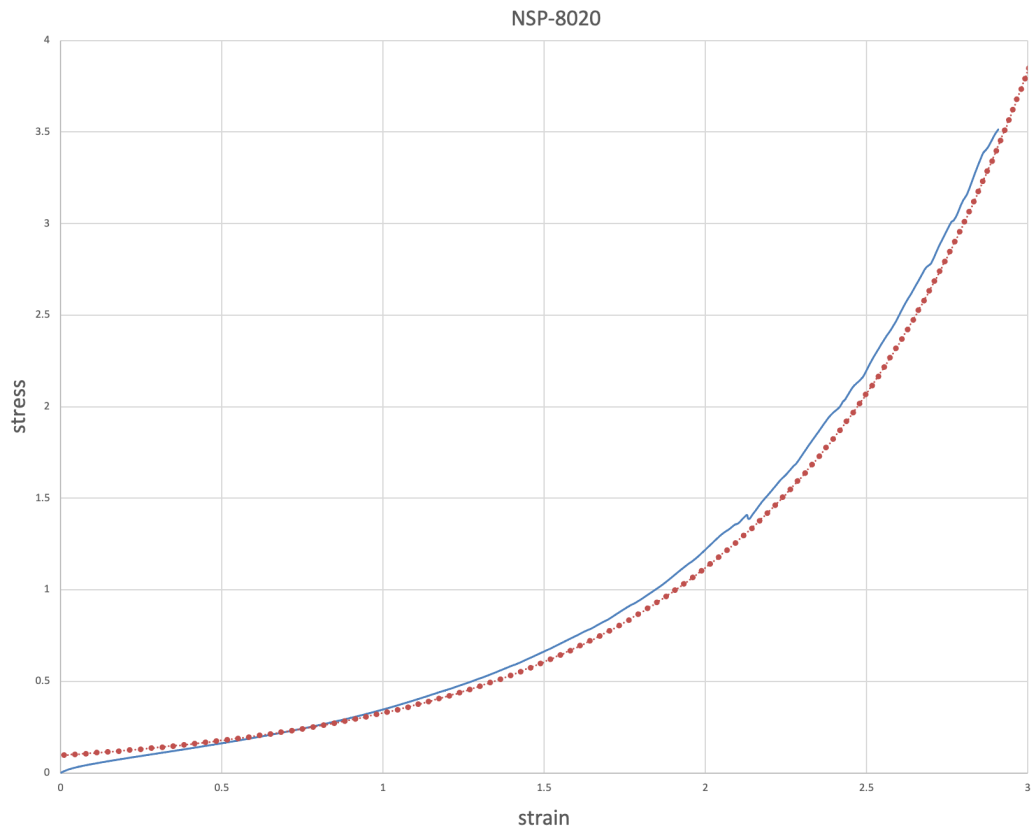


Figure 4.4: Comparison of stress-strain curves for NSP-8020, theoretical prediction (red), and experiment (blue).

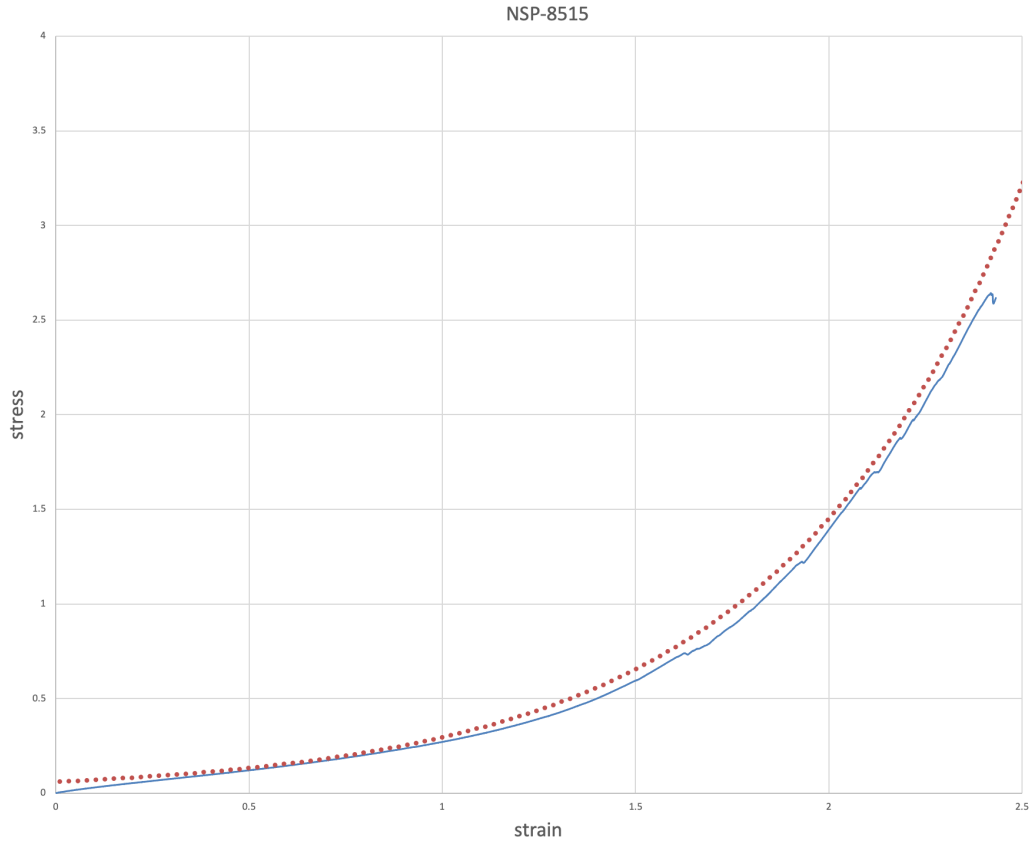


Figure 4.5: Comparison of stress-strain curves for NSP-8515, theoretical prediction(red), and experiment(blue).

As is inferred from the figures above, there is a reasonable agreement between the predictions of the theoretical model and experimental results. Basically, we find the exponential coefficients A , and B by trial and error to fit the stress-strain curve obtained from FEM to the experimental results. It should be noted that, A , and B play a vital role in determining the mechanical properties of hyper-elastic material. Values of A , and B that present the best fit are 0.06, 0.4 for NSP-8020, and 0.1, 0.145 for NSP-8515.

Changing A , and B as the exponential coefficients would result in considerable adjustments in the stress-strain contour. Some experiments regarding this matter have been done in the case of NSP-8020, and they are presented in Figure 4.6, and Figure 4.7.

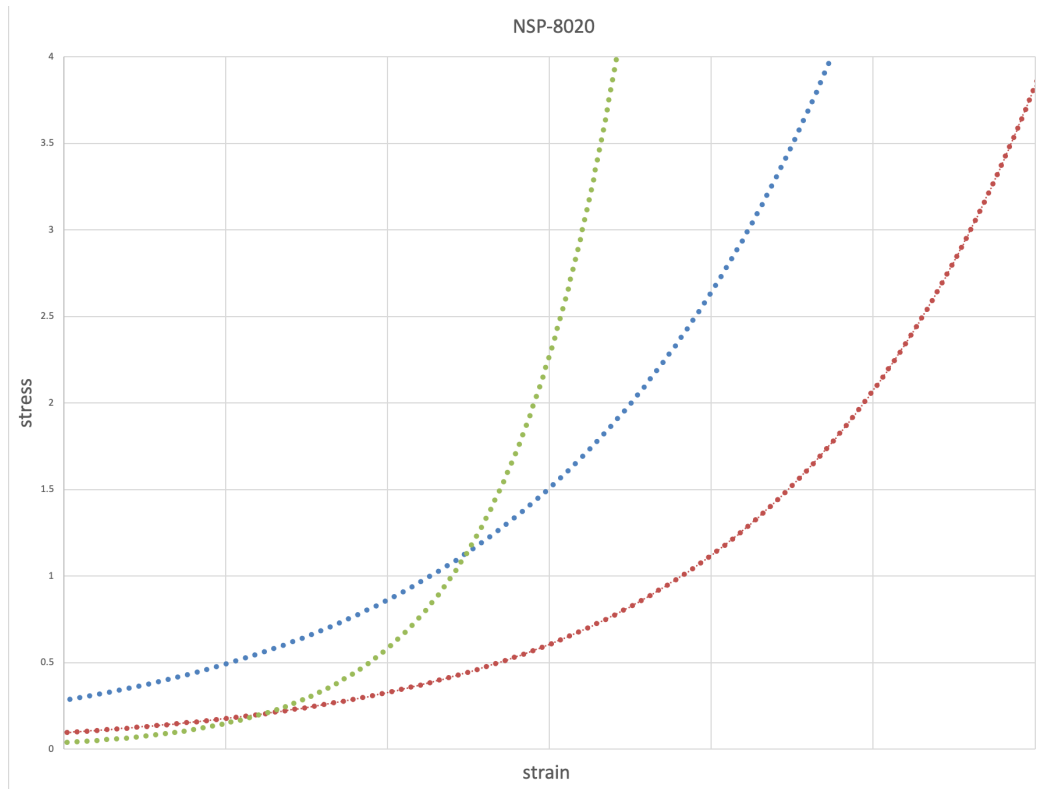


Figure 4.6: Stress-strain curves comparison while B is constant: $A = 0.06$ (red), $A = 0.05$ (green), $A = 0.04$ (blue).

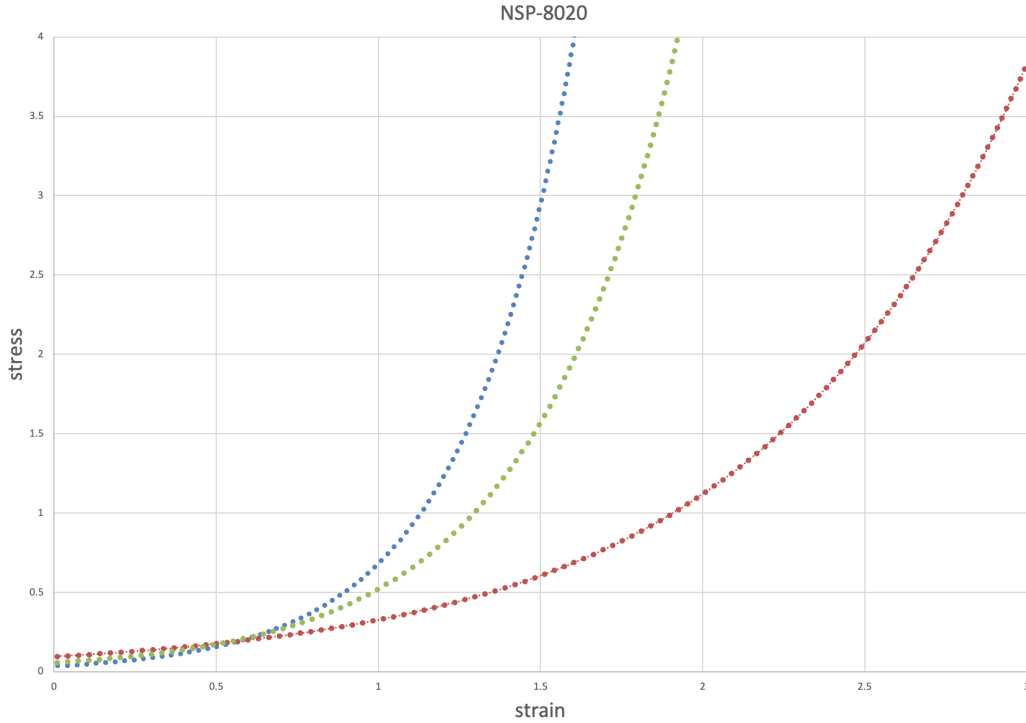


Figure 4.7: Stress-strain curves comparison while A is constant: $B = 0.3$ (blue), $B = 0.35$ (green), $B = 0.4$ (red).

The main focus of this research is predicting the behavior of composite materials subject to the various mechanical loads. In this chapter, we would try to estimate the behavior of the composite material based on the properties that we have gathered from the raw fiber data. Notably, it can be applied to the industries, and it would help the manufacturer to have a very clear idea of the mechanical characteristics of the reinforced composites before the production stage. For this purpose, we can fit the strain-stress predictions obtained from the finite element model to the raw fiber data that is resulted from the experiments by changing the values of exponential components. It should be considered that, finding the appropriate A , and B to reduce the error between the predictions and experiments is a trial and error procedure. Using the specific coefficients that we acquired from the previous step, we can acquire Figures 4.8 -4.11.

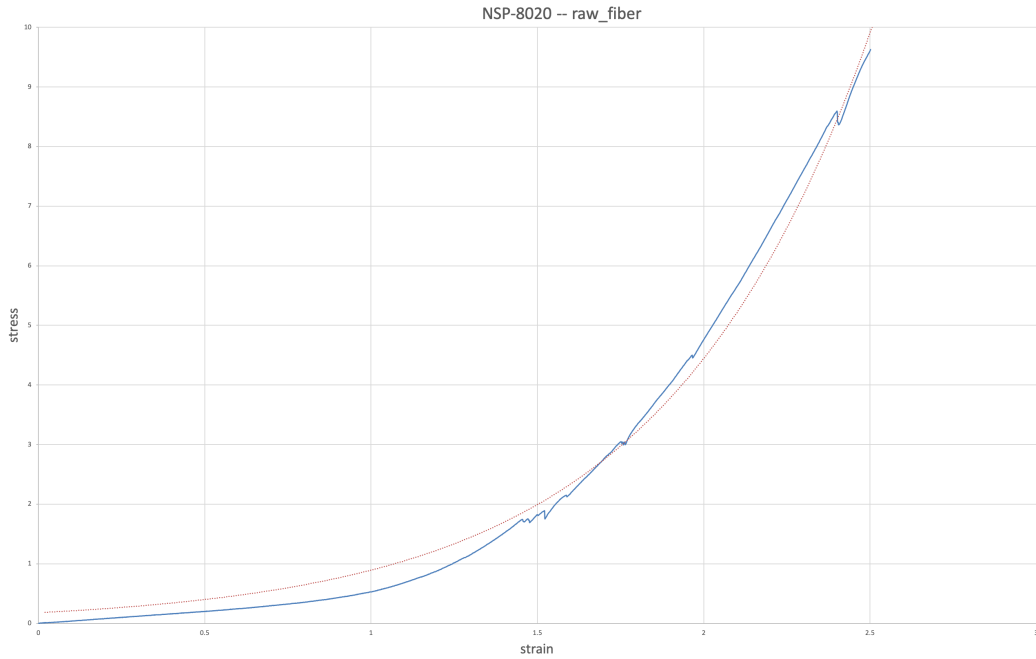


Figure 4.8: Comparison of stress-strain curves for NSP-8020 raw fiber material, theoretical prediction(red), and experiment(blue).

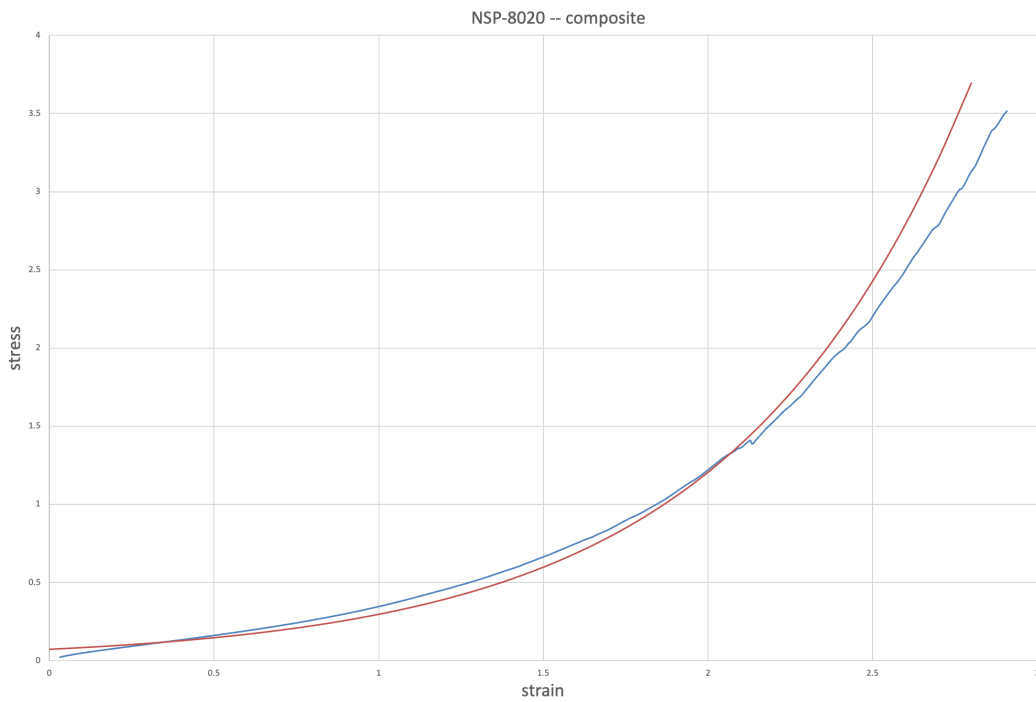


Figure 4.9: Comparison of stress-strain curves for NSP-8020 composite, theoretical prediction based on the raw fiber(red), and experiment(blue).

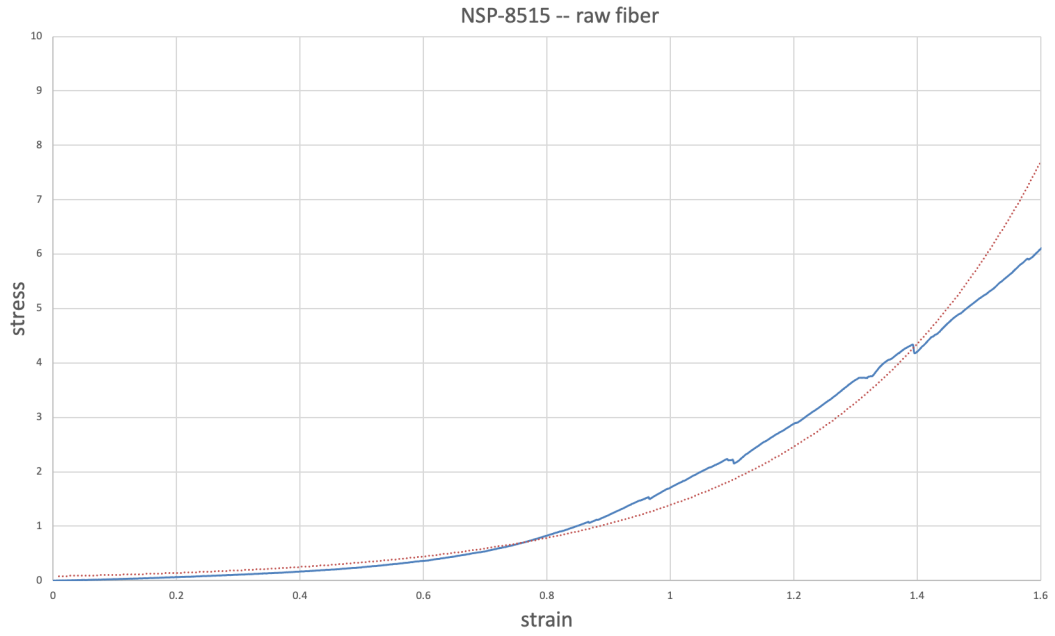


Figure 4.10: Comparison of stress-strain curves for NSP-8515 raw fiber material, theoretical prediction(red), and experiment(blue).

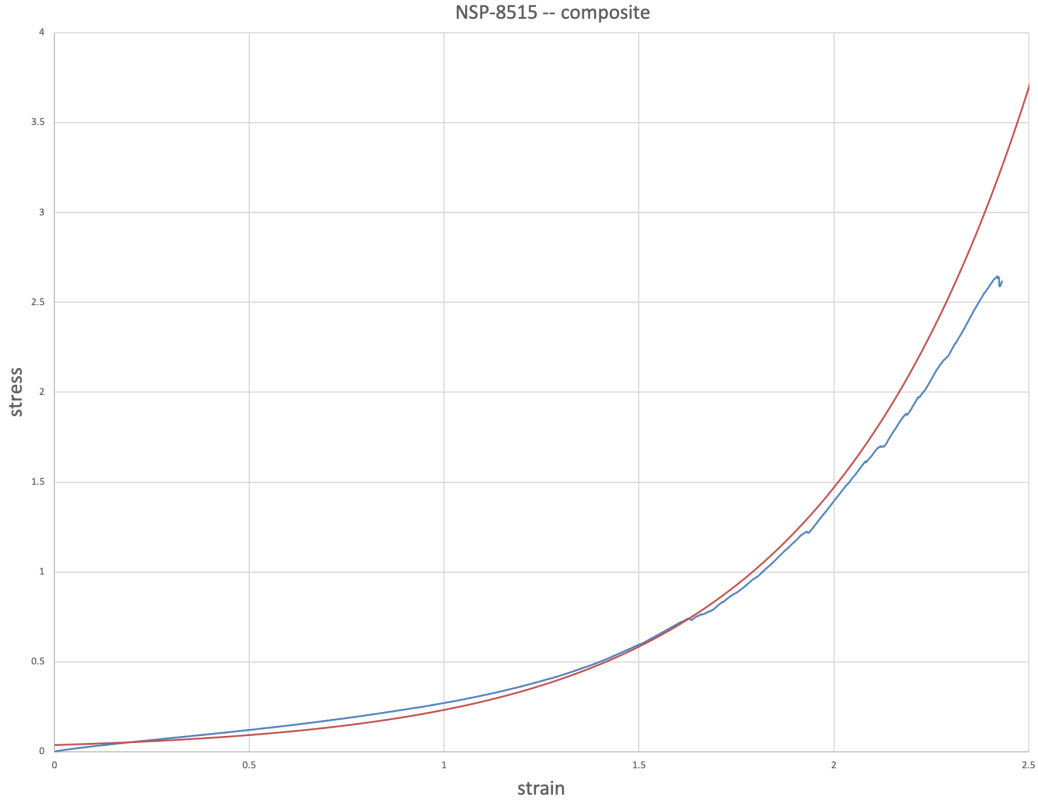


Figure 4.11: Comparison of stress-strain curves for NSP-8515 composite, theoretical prediction based on the raw fiber (red), and experiment (blue).

As inferred from the figures above, there seems to be a rational closure between the predictions of the finite element model and the experimental dataset. Values of A , and B that present the best fit are 0.0733, 1.4 for NSP-8020, and 0.0369, 1.8423 for NSP-8515. It should be noted that a cofactor has been used for the exponent of exponential function B that stands for the transformation of raw fiber to the composite, for each specific material.

4.5 Denouement

In this study, we present a second-order gradient method augmented with exponential energy function. This model has been designed to predict the non-linearity arose while the hyper-elastic composite is subjected to a tensile force. The principles of continuum mechanics and equilibrium equations have been used to derive a system of partial differential equations to describe the

composite material's mechanical response. Numerical analysis is based on the conventional finite element methods. Correspondingly, the weak form of the partial differential equations was derived and fed to the newton solver. Results for different values of exponential components represent an acceptable agreement with the experimental set obtained from NSP-8020 and NSP-8515 composite material. In conclusion, the values for A and B play a deterministic role in predicting the mechanical response of fiber-reinforced material. Factually, we can predict the behavior of fiber-reinforced hyper-elastic solids using the obtained coefficients from the raw fiber material.

Chapter 5

Conclusion and Future works

5.1 Conclusion

During recent years, Many efforts have been made by researchers to determine solutions to analyze the response of composite materials subjected to different types of mechanical loads [8], [9]. In this thesis, continuum-based mathematical frameworks have been employed to predict the behavior of fiber-reinforced composite materials.

In the first two chapters, the main objective is to derive an analytical expression that determines the mechanical response of composites subjected to flexural and tensile loads. In point of fact, determining equilibrium deformations of the fiber-reinforced solid flexed or extended at the boundaries can be resembled and correspondingly replaced by the problem of minimizing the potential energy. Small incremental deformation respect to the initial configuration was served as the baseline to acquire the linearized Euler equation. Elastic Neo-Hookean solid reinforced with unidirectional fiber is the structure that has been investigated to examine the continuum-based theory. Several measures, such as deformation contour, shear angle, and shear strain, have been included to validate the higher-order gradient model's accuracy. The obtained deformation contours are sensitive to both the double stress and triple stress parameters. For instance, we would see a gradual reduction in the deformed configuration by increasing the value of double stress caused by having stiffer material under the same load. To investigate the effects of third-order gradient parameter shear strain and shear angle contours have been computed.

It has been demonstrated that there are no sharp variations of the gradient in the acquired 3rd-order gradient shear strain contours, unlike the first and second-order methods. These dilatational contours have resulted from the smooth transitions in the corresponding shear gradient areas sustained by the third gradient continua. Moreover, the deformation profiles generated from the analytical model have been compared to the experimental results obtained from rubber composites. The relative error has been computed for the numerical predictions and the experimental data. A reasonable agreement can be concluded based on the value of the error. Finally, the 3rd-order gradient model seems to capture the behavior of fiber-reinforced solid accurately.

In the third chapter, a second gradient approach using the exponential fiber potential has been considered to describe the response of soft-material composites subjected to tensile load. Likewise, the continuum-based analysis starts with deriving the weak form of equilibrium equation to achieve the partial differential equations describing the behavior of fiber-reinforced material. Although, this chapter focuses on finding the finite element solution for the corresponding system of PDEs. The order of each equation has been decreased using a change of variables approach. Consequently, the Newton finite element solver is the primary solver that has been used to obtain the solution. Newton solver has been implemented in the FEniCS project, which is an open-source finite element solver in python. The main focus is on finding the exponential components of the energy function. These components are deterministic in the prediction of deformation contour. NSP-8020 and NSP-8515 are considered to be the solids that are investigated in the case of hyperelastic material. Exponential function properties are specified in such a way to fit the raw fiber data since the deformation contour is sensitive to any change in previously mentioned parameters. After acquiring the fitting process coefficients, I used them to approximate the composite deformation curve. Results have been presented with acceptable compliance between NSP-8020 AND NSP-8515 deformation curves and predictions from the FEM model. Overall, the previously mentioned parameters play a vital role in regulating the mechanical properties of hyper-elastic material. It should be noted, a rough estimation of composite

material response before going to the production stage in industries is very beneficial, and correspondingly having substantial information from the theoretical model would save manufacturers time and money.

5.2 Future Works

Extending the previously mentioned models by adding higher-order terms would be beneficial to predict the intrinsic properties of fiber-composites. Indeed, microstructure analysis of fiber-composite material needs to be investigated in every comprehensive framework due to its complication in the mathematical formulations. Using higher-order terms is beneficial in producing more accurate and reliable results. As a matter of fact, the microstructural properties of materials are entangled with the gradients of deformation in the case of fiber-reinforced composites

Moreover, the finite element analysis of the continuum mechanics formulations, followed by the corresponding weak forms of partial differential equations, is a rational alternative to investigate the effects of loads on the mechanical response of the fiber-reinforced materials. Indeed, a finite element framework can replace the analytical solution that has been derived in the first and second chapters. However, according to the complexity that arose from higher-order gradients, the convergence criterion is very sensitive in such cases.

Lastly, Utilizing an additional term as a complementary factor in the energy expression, such as polynomial or exponential functions, can impact our predictions tremendously. In this fashion, we can explore the behavior of raw fiber to obtain the necessary information similar to the exponent of exponential functions or the order of the polynomial to foresee the properties of fiber elastic composite before production. It is necessary to point out; within the third chapter of this thesis, the main focus is on soft rubber-like materials. However, other types of materials, such as viscoelastic materials, can be analyzed in a similar mathematical framework with different fiber potential functions.

References

- [1] Mischa, *The science and technology of composite materials*, Sep. 2017. [Online]. Available: <https://www.science.org.au/curious/technology-future/composite-materials>.
- [2] *Composite material*, Jul. 2020. [Online]. Available: https://en.wikipedia.org/wiki/Composite_material#:~:text=Composite%20materials%20are%20generally%20used,cultured%20marble%20sinks%20and%20countertops..
- [3] C. Zweben, “Composite materials,” in *Mechanical Engineers’ Handbook*. American Cancer Society, 2015, ch. 10, pp. 1–37, ISBN: 9781118985. DOI: 10.1002/9781118985960.meh110. eprint: <https://onlinelibrary.wiley.com/doi/pdf/10.1002/9781118985960.meh110>. [Online]. Available: <https://onlinelibrary.wiley.com/doi/abs/10.1002/9781118985960.meh110>.
- [4] D. Hull and T. W. Clyne, *An Introduction to Composite Materials*, 2nd ed., ser. Cambridge Solid State Science Series. Cambridge University Press, 1996. DOI: 10.1017/CB09781139170130.
- [5] S. Pal and B. C. Ray, *Molecular Dynamics Simulation of Nanostructured Materials: An Understanding of Mechanical Behavior*. CRC Press, 2020.
- [6] H. Alhashmy, “Fabrication of aluminium matrix composites (amcs) by squeeze casting technique using carbon fiber as reinforcement,” PhD thesis, Université d’Ottawa/University of Ottawa, 2012.
- [7] [Online]. Available: <https://www.nj-mkt.com/news/932.html>.
- [8] D. J. Steigmann and F. Dell’Isola, “Mechanical response of fabric sheets to three-dimensional bending, twisting, and stretching,” *Acta Mechanica Sinica*, vol. 31, no. 3, pp. 373–382, 2015.
- [9] M. Zeidi and C. I. Kim, “Mechanics of fiber composites with fibers resistant to extension and flexure,” *Mathematics and Mechanics of Solids*, vol. 24, no. 1, pp. 3–17, 2019.
- [10] S. E. Seyed Bolouri, C. I. Kim, and S. Yang, “Linear theory for the mechanics of third-gradient continua reinforced with fibers resistance to flexure,” *Mathematics and Mechanics of Solids*, vol. 25, no. 4, pp. 937–960, 2020.

- [11] A. Battista, L. Rosa, R. dell’Erba, and L. Greco, “Numerical investigation of a particle system compared with first and second gradient continua: Deformation and fracture phenomena,” *Mathematics and Mechanics of Solids*, vol. 22, no. 11, pp. 2120–2134, 2017.
- [12] M. Cuomo, F. Dell’Isola, L. Greco, and N. Rizzi, “First versus second gradient energies for planar sheets with two families of inextensible fibres: Investigation on deformation boundary layers, discontinuities and geometrical instabilities,” *Composites Part B: Engineering*, vol. 115, pp. 423–448, 2017.
- [13] A. C. Pipkin and T. G. Rogers, “Plane Deformations of Incompressible Fiber-Reinforced Materials,” *Journal of Applied Mechanics*, vol. 38, no. 3, pp. 634–640, Sep. 1971, ISSN: 0021-8936. DOI: 10.1115/1.3408866. eprint: <https://asmedigitalcollection.asme.org/appliedmechanics/article-pdf/38/3/634/5451296/634\1.pdf>. [Online]. Available: <https://doi.org/10.1115/1.3408866>.
- [14] M. Arndt and M. Griebel, “Derivation of higher order gradient continuum models from atomistic models for crystalline solids,” *Multiscale Modeling & Simulation*, vol. 4, no. 2, pp. 531–562, 2005.
- [15] N. Triantafyllidis and S. Bardenhagen, “On higher order gradient continuum theories in 1-d nonlinear elasticity. derivation from and comparison to the corresponding discrete models,” *Journal of Elasticity*, vol. 33, no. 3, pp. 259–293, 1993.
- [16] J. Mulhern, T. Rogers, and A. Spencer, “A continuum theory of a plastic-elastic fibre-reinforced material,” *International Journal of Engineering Science*, vol. 7, no. 2, pp. 129–152, 1969. DOI: 10.1016/0020-7225(69)90053-6.
- [17] A. H. England, “Plane problems for fibre-reinforced linearly elastic solids,” *Continuum Theory of the Mechanics of Fibre-Reinforced Composites*, pp. 73–121, 1984. DOI: 10.1007/978-3-7091-4336-0_3.
- [18] C. Boutin, “Microstructural effects in elastic composites,” *International Journal of Solids and Structures*, vol. 33, no. 7, pp. 1023–1051, 1996. DOI: 10.1016/0020-7683(95)00089-5.
- [19] X.-F. Wu and Y. A. Dzenis, “Elasticity of planar fiber networks,” *Journal of Applied Physics*, vol. 98, no. 9, p. 093 501, 2005.
- [20] S. Alieldin, A. Alshorbagy, and M. Shaat, “A first-order shear deformation finite element model for elastostatic analysis of laminated composite plates and the equivalent functionally graded plates,” *Ain Shams Engineering Journal*, vol. 2, no. 1, pp. 53–62, 2011.
- [21] M. M. Dawoud and H. M. Saleh, “Introductory chapter: Background on composite materials,” in *Characterizations of Some Composite Materials*, IntechOpen, 2018.

- [22] Z. Hashin, “Analysis of composite materials—a survey,” 1983.
- [23] D. B. Miracle, S. L. Donaldson, *et al.*, “Introduction to composites,” *ASM handbook*, vol. 21, pp. 3–17, 2001.
- [24] *Fiber-reinforced composite*, Jun. 2020. [Online]. Available: https://en.wikipedia.org/wiki/Fiber-reinforced_composite.
- [25] W. J. Cantwell and J. Morton, “The impact resistance of composite materials—a review,” *composites*, vol. 22, no. 5, pp. 347–362, 1991.
- [26] F. C. Campbell, *Structural composite materials*, 2010. [Online]. Available: <https://www.amazon.com/Structural-Composite-Materials-F-Campbell/dp/1615030379>.
- [27] M. Shahzad, A. Kamran, M. Z. Siddiqui, and M. Farhan, “Mechanical characterization and fe modelling of a hyperelastic material,” *Materials Research*, vol. 18, no. 5, pp. 918–924, 2015.
- [28] R. W. Ogden, *Non-linear elastic deformations*. Courier Corporation, 1997, pp. 100–200.
- [29] Y. Başar and D. Weichert, “Constitutive modelling,” in *Nonlinear Continuum Mechanics of Solids*, Springer, 2000, pp. 139–174.
- [30] R. S. Rivlin and D. Saunders, “Large elastic deformations of isotropic materials vii. experiments on the deformation of rubber,” *Philosophical Transactions of the Royal Society of London. Series A, Mathematical and Physical Sciences*, vol. 243, no. 865, pp. 251–288, 1951.
- [31] A. E. Green and R. S. Rivlin, “The mechanics of non-linear materials with memory,” *Archive for Rational Mechanics and Analysis*, vol. 1, no. 1, pp. 1–21, 1957.
- [32] T. J. Pence and K. Gou, “On compressible versions of the incompressible neo-hookean material,” *Mathematics and Mechanics of Solids*, vol. 20, no. 2, pp. 157–182, 2015.
- [33] *Neo-hookean solid*, Mar. 2020. [Online]. Available: https://en.wikipedia.org/wiki/Neo-Hookean_solid.
- [34] P. Boulanger and M. Hayes, “Finite-amplitude waves in mooney-rivlin and hadamard materials,” in *Topics in finite elasticity*, Springer, 2001, pp. 131–167.
- [35] M. Destrade and G. Saccomandi, “Finite-amplitude inhomogeneous waves in mooney–rivlin viscoelastic solids,” *Wave Motion*, vol. 40, no. 3, pp. 251–262, 2004.
- [36] C.-H. Chen and Y.-C. Wang, “An extended nonlinear mechanical model for solid-filled mooney-rivlin rubber composites,” *Polymer*, vol. 38, no. 3, pp. 571–576, 1997.
- [37] J. Bonet and R. D. Wood, *Nonlinear continuum mechanics for finite element analysis*. Cambridge university press, 1997.

- [38] *Stress measures*, Feb. 2020. [Online]. Available: https://en.wikipedia.org/wiki/Stress_measures.
- [39] *Stress measures*, Jun. 2020. [Online]. Available: <https://abaqus-docs.mit.edu/2017/English/SIMACAETHERefMap/simathe-c-stressmeas.htm>.
- [40] R. M. Hackett, “Stress measures,” in *Hyperelasticity Primer*, Springer, 2018, pp. 29–48.
- [41] A. Spencer and K. Soldatos, “Finite deformations of fibre-reinforced elastic solids with fibre bending stiffness,” *International Journal of Non-Linear Mechanics*, vol. 42, no. 2, pp. 355–368, 2007.
- [42] K. Friedrich, “Microstructural efficiency and fracture toughness of short fiber/thermoplastic matrix composites,” *Composites Science and Technology*, vol. 22, no. 1, pp. 43–74, 1985.
- [43] Y. Yang, W. Ching, and A. Misra, “Higher-order continuum theory applied to fracture simulation of nanoscale intergranular glassy film,” *Journal of Nanomechanics and Micromechanics*, vol. 1, no. 2, pp. 60–71, 2011.
- [44] R. K. A. Al-Rub, M. Eftehad, and A. N. Palazotto, “Microstructural modeling of dual phase steel using a higher-order gradient plasticity–damage model,” *International Journal of Solids and Structures*, vol. 58, pp. 178–189, 2015.
- [45] M. Eltaher, M. Hamed, A. Sadoun, and A. Mansour, “Mechanical analysis of higher order gradient nanobeams,” *Applied Mathematics and Computation*, vol. 229, pp. 260–272, 2014.
- [46] P. Jakubczak, J. Bieniaś, K. Majerski, M. Ostapiuk, and B. Surowska, “Methods of ultrasonic testing, as an effective way of estimating durability and diagnosing operational capability of composite laminates used in aerospace industry,” *Eksploatacja i Niezawodność - Maintenance and Reliability*, vol. 3, pp. 284–289, Jan. 2013.
- [47] C. I. Kim and M. Zeidi, “Gradient elasticity theory for fiber composites with fibers resistant to extension and flexure,” *International Journal of Engineering Science*, vol. 131, pp. 80–99, 2018.
- [48] M. Zeidi and C. I. Kim, “Mechanics of an elastic solid reinforced with bidirectional fiber in finite plane elastostatics: Complete analysis,” *Continuum Mechanics and Thermodynamics*, vol. 30, no. 3, pp. 573–592, 2018.
- [49] Z. Liu and C.-i. Kim, “Deformation analysis of lipid membranes subjected to general forms of intra-membrane viscous flow and interactions with an elliptical-cross-section substrate,” *Scientific Reports*, vol. 10, no. 1, pp. 1–19, 2020.

- [50] C. I. Kim and Z. Liu, “Mechanics of lipid membranes under the influence of intramembrane viscosity,” *Mathematical Problems in Engineering*, vol. 2019, 2019.
- [51] M. Zeidi and C. I. Kim, “Notes on superposed incremental deformations in the mechanics of lipid membranes,” *Mathematics and Mechanics of Solids*, vol. 24, no. 1, pp. 181–194, 2019.
- [52] R. A. Toupin, “Theories of elasticity with couple-stress,” 1964.
- [53] M. Zeidi, “Gradient elasticity modelling and analysis for the mechanics of unidirectional and bidirectional fiber reinforced composites,” 2018.
- [54] [Online]. Available: <http://silver.neep.wisc.edu/~lakes/Coss.html>.
- [55] H. Ramézani, J. Jeong, and Z.-Q. Feng, “On parallel simulation of a new linear cosserat elasticity model with grid framework model assumptions,” *Applied mathematical modelling*, vol. 35, no. 10, pp. 4738–4758, 2011.
- [56] [Online]. Available: <http://homepages.cae.wisc.edu/~lakes/CossWaves.html>.
- [57] [Online]. Available: [http://silver.neep.wisc.edu/~lakes/Coss.html#:~:text=The%20Cosserat%20theory%20of%20elasticity,well%20as%20the%20force%20stress%20\(](http://silver.neep.wisc.edu/~lakes/Coss.html#:~:text=The%20Cosserat%20theory%20of%20elasticity,well%20as%20the%20force%20stress%20()
- [58] E. Papamichos, “Continua with microstructure: Cosserat theory,” *European journal of environmental and civil engineering*, vol. 14, no. 8-9, pp. 1011–1029, 2010.
- [59] *Cosserat continuum*. [Online]. Available: <https://www.sciencedirect.com/topics/engineering/cosserat-continuum>.
- [60] V. A. Lubarda, “Constitutive theories based on the multiplicative decomposition of deformation gradient: Thermoelasticity, elastoplasticity, and biomechanics,” *Appl. Mech. Rev.*, vol. 57, no. 2, pp. 95–108, 2004.
- [61] J. Hron and S. Turek, “A monolithic fem/multigrid solver for an ale formulation of fluid-structure interaction with applications in biomechanics,” in *Fluid-structure interaction*, Springer, 2006, pp. 146–170.
- [62] *Composites industry overview - composites 101*. [Online]. Available: <http://compositeslab.com/composites-101/composites-industry-overview/>.
- [63] *Global composite materials market size, trends: Industry report, 2025*. [Online]. Available: <https://www.grandviewresearch.com/industry-analysis/composite-materials-market>.
- [64] *Composites market*. [Online]. Available: <https://www.marketsandmarkets.com/Market-Reports/composite-market-200051282.html>.

- [65] Boundless, *Boundless anatomy and physiology*. [Online]. Available: <https://courses.lumenlearning.com/boundless-ap/chapter/introduction-to-tissues/>.
- [66] S. Federico and T. C. Gasser, “Nonlinear elasticity of biological tissues with statistical fibre orientation,” *Journal of the Royal Society Interface*, vol. 7, no. 47, pp. 955–966, 2010.
- [67] S. C. Cowin, “Bone poroelasticity,” *Journal of biomechanics*, vol. 32, no. 3, pp. 217–238, 1999.
- [68] S. T. Rolfe and J. M. Barsom, “Fracture and fatigue control in structures: Applications of fracture mechanics(book),” *Englewood Cliffs, N. J., Prentice-Hall, Inc., 1977. 574 p*, 1977.
- [69] C.-H. Chen, E. Bouchbinder, and A. Karma, “Instability in dynamic fracture and the failure of the classical theory of cracks,” *Nature Physics*, vol. 13, no. 12, pp. 1186–1190, 2017.
- [70] L. B. Godefroid, G. L. d. Faria, L. C. Cândido, and S. Araujo, “Fatigue failure of a welded automotive component,” *Procedia materials science*, vol. 3, pp. 1902–1907, 2014.
- [71] T. G. Boué, G. Cohen, and J. Fineberg, “Origin of the microbranching instability in rapid cracks,” *Physical Review Letters*, vol. 114, no. 5, p. 054301, 2015.
- [72] R. Peerlings, R. De Borst, W. Brekelmans, and M. Geers, “Gradient-enhanced damage modelling of concrete fracture,” *Mechanics of Cohesive-frictional Materials: An International Journal on Experiments, Modelling and Computation of Materials and Structures*, vol. 3, no. 4, pp. 323–342, 1998.
- [73] M. Zeidi and C. I. Kim, “Finite plane deformations of elastic solids reinforced with fibers resistant to flexure: Complete solution,” *Archive of Applied Mechanics*, vol. 88, no. 5, pp. 819–835, 2018.
- [74] F. Dell’Isola and D. Steigmann, “A two-dimensional gradient-elasticity theory for woven fabrics,” *Journal of Elasticity*, vol. 118, no. 1, pp. 113–125, 2015.
- [75] E. Fried and M. E. Gurtin, “Gradient nanoscale polycrystalline elasticity: Intergrain interactions and triple-junction conditions,” *Journal of the Mechanics and Physics of Solids*, vol. 57, no. 10, pp. 1749–1779, 2009.
- [76] D. J. Steigmann, “Theory of elastic solids reinforced with fibers resistant to extension, flexure and twist,” *International Journal of Non-Linear Mechanics*, vol. 47, no. 7, pp. 734–742, 2012.
- [77] D. Steigmann, *Finite elasticity theory*, 2017. [Online]. Available: <https://www.amazon.com/Finite-Elasticity-Theory-David-Steigmann/dp/0198567782>.

- [78] W. Koiter, “Couple-stresses in the theory of elasticity, i & ii,” pp. 139–174, 1969.
- [79] P. Germain, “The method of virtual power in continuum mechanics. part 2: Microstructure,” *SIAM Journal on Applied Mathematics*, vol. 25, no. 3, pp. 556–575, 1973.
- [80] F. Dell’Isola, P. Seppecher, and A. Madeo, “How contact interactions may depend on the shape of cauchy cuts in nth gradient continua: Approach “à la d’alembert”,” *Zeitschrift für angewandte Mathematik und Physik*, vol. 63, no. 6, pp. 1119–1141, 2012.
- [81] H. Askes, A. Suiker, and L. Sluys, “A classification of higher-order strain-gradient models—linear analysis,” *Archive of Applied Mechanics*, vol. 72, no. 2-3, pp. 171–188, 2002.
- [82] F. Dell’Isola, A. D. Corte, and I. Giorgio, “Higher-gradient continua: The legacy of piola, mindlin, sedov and toupin and some future research perspectives,” *Mathematics and Mechanics of Solids*, vol. 22, no. 4, pp. 852–872, 2017.
- [83] F. Dell’Isola, A. Della Corte, L. Greco, and A. Luongo, “Plane bias extension test for a continuum with two inextensible families of fibers: A variational treatment with lagrange multipliers and a perturbation solution,” *International Journal of Solids and Structures*, vol. 81, pp. 1–12, 2016.
- [84] E. Turco, K. Barcz, M. Pawlikowski, and N. L. Rizzi, “Non-standard coupled extensional and bending bias tests for planar pantographic lattices. part i: Numerical simulations,” *Zeitschrift für angewandte Mathematik und Physik*, vol. 67, no. 5, p. 122, 2016.
- [85] F. dell’Isola, I. Giorgio, M. Pawlikowski, and N. L. Rizzi, “Large deformations of planar extensible beams and pantographic lattices: Heuristic homogenization, experimental and numerical examples of equilibrium,” *Proceedings of the Royal Society A: Mathematical, Physical and Engineering Sciences*, vol. 472, no. 2185, p. 20 150 790, 2016.
- [86] H. Askes, A. Suiker, and L. Sluys, “A classification of higher-order strain-gradient models—linear analysis,” *Archive of Applied Mechanics*, vol. 72, no. 2-3, pp. 171–188, 2002.
- [87] F. Dell’Isola and P. Seppecher, “The relationship between edge contact forces, double forces and interstitial working allowed by the principle of virtual power,” 1995.
- [88] J.-J. Alibert, P. Seppecher, and F. Dell’Isola, “Truss modular beams with deformation energy depending on higher displacement gradients,” *Mathematics and Mechanics of Solids*, vol. 8, no. 1, pp. 51–73, 2003.
- [89] R. Mindlin and H. Tiersten, “Effects of couple-stresses in linear elasticity,” COLUMBIA UNIV NEW YORK, Tech. Rep., 1962.

- [90] R. Toupin, "Elastic materials with couple-stresses," 1962.
- [91] A. Javili, F. dell'Isola, and P. Steinmann, "Geometrically nonlinear higher-gradient elasticity with energetic boundaries," *Journal of the Mechanics and Physics of Solids*, vol. 61, no. 12, pp. 2381–2401, 2013.
- [92] H. Askes, A. Suiker, and L. Sluys, "A classification of higher-order strain-gradient models—linear analysis," *Archive of Applied Mechanics*, vol. 72, no. 2-3, pp. 171–188, 2002.
- [93] W. Read, "Series solutions for laplace's equation with nonhomogeneous mixed boundary conditions and irregular boundaries," *Mathematical and computer modelling*, vol. 17, no. 12, pp. 9–19, 1993.
- [94] Y. Huang and X.-J. Zhang, "General analytical solution of transverse vibration for orthotropic rectangular thin plates," *Journal of Marine Science and Application*, vol. 1, no. 2, pp. 78–82, 2002.
- [95] C. I. Kim, "Superposed incremental deformations of an elastic solid reinforced with fibers resistant to extension and flexure," *Advances in Materials Science and Engineering*, vol. 1, 2018.
- [96] C. I. Kim, "Strain-gradient elasticity theory for the mechanics of fiber composites subjected to finite plane deformations: Comprehensive analysis," *Multiscale Science and Engineering*, vol. 1, no. 2, pp. 150–160, 2019.